2013

A Comparison and Catalog of Intrinsic Tumor Growth Models

Elizabeth A. Sarapata
Harvey Mudd College

A Comparison and Catalog of Intrinsic Tumor Growth Models

Elizabeth Sarapata

Lisette de Pillis, Advisor

Ami Radunskaya, Reader

Department of Mathematics

May, 2013

Abstract

Determining the dynamics and parameter values that drive tumor growth is of great interest to mathematical modelers, experimentalists and practitioners alike. We provide a basis on which to estimate the growth dynamics of ten different tumors by fitting growth parameters to at least five sets of published experimental data per type of tumor. These timescale tumor growth data are also used to determine which of the most common tumor growth models (exponential, power law, logistic, Gompertz, or von Bertalanffy) provides the best fit for each type of tumor. In order to compute the best-fit parameters, we implemented a hybrid local-global least squares minimization algorithm based on a combination of Nelder-Mead simplex direct search and Monte Carlo Markov Chain methods.

Acknowledgments

To Dr. Lisette de Pillis and Dr. Radunskaya, who pointed me in all the right directions.

Contents

Abstract **iii**

Acknowledgments **v**

1 Introduction **1**
1.1 Introduction 1
1.2 Previous Research 2

2 Assumptions and Methods **5**
2.1 Experimental data 5
2.2 Unit normalization 5
2.3 ODE Tumor Growth Models 6
2.4 Parameter fitting algorithms 7
2.5 Biologically Motivated Assumptions 11
2.6 Fitting evaluation metrics 12
2.7 Parameter Sensitivity Analysis 12

3 Results **17**
3.1 Tumor Growth Parameter Values 17
3.2 Parameter Sensitivity Analysis 22

4 Discussion **27**
4.1 Parameter Fitting 27
4.2 Parameter Fitting Algorithms 28
4.3 Parameter Sensitivity Analysis 29
4.4 Usage of Least Squares Residuals versus BIC 30

5 Future Work **33**
5.1 ODE models for CD47 Treatment 33

A Supplemental Materials **37**
A.1 Sources of Data for Parameter Values 37
A.2 Results of Parameter Fittings 40

Bibliography **81**

List of Figures

3.1 Logistic Model of Control B16 Data from Agur 2011 23
3.2 Local Parameter Sensitivity Analysis for Five Models, Altering Parameters by 10% 24
3.3 Local Parameter Sensitivity Analysis for Five Models, Altering Parameters by 10% (with Power Law *a* results removed) 25

A.1 Parameter Fittings to *In Vitro* Bladder Cancer Trials 42
A.2 Parameter Fittings to Individual *In Vivo* Bladder Cancer Trials 43
A.3 Parameter Fitting to Combined *In Vivo* Bladder Cancer Trials 44
A.4 Parameter Fittings to Individual *In Vitro* Breast Cancer Trials 45
A.5 Parameter Fitting to Combined *In Vitro* Breast Cancer Trials 46
A.6 Parameter Fittings to Individual *In Vivo* Breast Cancer Trials 47
A.7 Parameter Fitting to Combined *In Vivo* Breast Cancer Trials . 48
A.8 Parameter Fittings to Individual *In Vitro* Colon Cancer Trials 49
A.9 Parameter Fitting to Combined *In Vitro* Colon Cancer Trials . 50
A.10 Parameter Fittings to Individual *In Vivo* Colon Cancer Trials 51
A.11 Parameter Fitting to Combined *In Vivo* Colon Cancer Trials . 52
A.12 Parameter Fittings to Individual *In Vitro* Head and Neck Squamous Cell Carcinoma Trials 53
A.13 Parameter Fitting to Combined *In Vitro* Head and Neck Squamous Cell Carcinoma Trials 54
A.14 Parameter Fittings to Individual *In Vivo* Head and Neck Squamous Cell Carcinoma Trials 55
A.15 Parameter Fitting to Combined *In Vivo* Head and Neck Squamous Cell Carcinoma Trials 56
A.16 Parameter Fittings to Individual *In Vitro* Hepatocellular Carcinoma Trials 57
A.17 Parameter Fitting to Combined *In Vitro* Hepatocellular Carcinoma Trials 58

A.18 Parameter Fittings to Individual *In Vivo* Hepatocellular Carcinoma Trials 59
A.19 Parameter Fitting to Combined *In Vivo* Hepatocellular Carcinoma Trials 60
A.20 Parameter Fittings to Individual *In Vitro* Lung Cancer Trials 61
A.21 Parameter Fitting to Combined *In Vitro* Lung Cancer Trials . 62
A.22 Parameter Fittings to Individual *In Vivo* Lung Cancer Trials . 63
A.23 Parameter Fitting to Combined *In Vivo* Lung Cancer Trials . 64
A.24 Parameter Fittings to Individual *In Vitro* Melanoma Trials . . 65
A.25 Parameter Fitting to Combined *In Vitro* Melanoma Trials . . 66
A.26 Parameter Fittings to Individual *In Vivo* Melanoma Trials . . 67
A.27 Parameter Fitting to Combined *In Vivo* Melanoma Trials . . . 68
A.28 Parameter Fittings to Individual *In Vitro* Ovarian Cancer Trials 69
A.29 Parameter Fitting to Combined *In Vitro* Ovarian Cancer Trials 70
A.30 Parameter Fittings to Individual *In Vivo* Ovarian Cancer Trials 71
A.31 Parameter Fitting to Combined *In Vivo* Ovarian Cancer Trials 72
A.32 Parameter Fittings to *In Vitro* Pancreatic Cancer Trials 73
A.33 Parameter Fittings to Individual *In Vivo* Pancreatic Cancer Trials 74
A.34 Parameter Fitting to Combined *In Vivo* Pancreatic Cancer Trials 75
A.35 Parameter Fittings to Individual *In Vitro* Renal Cell Carcinoma Trials 76
A.36 Parameter Fitting to Combined *In Vitro* Renal Cell Carcinoma Trials 77
A.37 Parameter Fittings to Individual *In Vivo* Renal Cell Carcinoma Trials 78
A.38 Parameter Fitting to Combined *In Vivo* Renal Cell Carcinoma Trials 79

List of Tables

3.1 Recommended Parameter Values and Ranges for Ten Different Types of Cancer and Five ODE Growth Laws 19
3.2 Model Evaluation Metrics for Combined Experimental Data Fittings 20
3.3 Model Fit Ranking According to Least Squares Residuals . . 21
3.4 Results of Partial Rank Correlation Coefficient Test for Two-Parameter Growth Models 26

A.1 Sources of Timescale Data by Type of Cancer and Cell Line . 37
A.1 Sources of Timescale Data by Type of Cancer and Cell Line . 38
A.1 Sources of Timescale Data by Type of Cancer and Cell Line . 39

Chapter 1

Introduction

1.1 Introduction

Mathematical models of tumor-immune system interactions are an especially useful class of dynamical systems model, utilizing a vast range of mathematical methods to model stochastic biological processes. Many researchers choose to represent tumor-immune system interaction by nonlinear systems of differential equations that account for various interacting cell populations or concentrations of chemicals (Sanga et al., 2006; de Pillis et al., 2013a; Jackson and Byrne, 2000; Robertson-Tessi et al., 2012; Hart et al., 1998; de Pillis and Radunskaya, 2006). If pharmaceuticals are also taken into account, these models allow both for an unlimited number of patient trials and the ability to vary dosages and combinations of medications such that the likelihood of eliminating the tumor is maximized.

Although many facets of these models change—underlying assumptions, the specific cell populations being modeled, the functions used to approximate biological phenomena—they all must have a function that approximates tumor growth. Many researchers make this estimation by either citing an earlier paper or performing a fitting to one or two experimental data sets (Sanga et al., 2006; de Pillis et al., 2013a; Jackson and Byrne, 2000; Robertson-Tessi et al., 2012; Hart et al., 1998; de Pillis and Radunskaya, 2006). It may save a great deal of work and provide a stronger basis for tumor growth models to have an easily accessible catalog of tumor growth functions in one place, especially one that provides a range of possible values and uses a large number of different experimental data sources for the fittings. We have created such a catalog and encourage its use by mathematical researchers. Our catalog accounts for tumors originating from ten

different organs, each with a minimum of seven data sets from a minimum of five different papers each.

In addition to improving the fit with a large amount of published experimental data, we also test five different tumor growth functions. There are five widely used growth functions in the field of dynamical systems tumor models: exponential growth functions, power law functions, logistic growth functions, Von Bertalanffy growth functions, and Gompertz growth functions (de Pillis and Radunskaya, 2006; Hart et al., 1998). For each of the ten types of tumor, we fit the experimental data to each of these growth functions and report several metrics to evaluate the fitting. This information will not only suggest which function is best suited to model the growth of each tumor type, but will provide an experimental basis for determining whether each individual function truly captures the dynamics of tumor growth as well.

With access to a large catalog of tumor growth data, we are uniquely able to implement a series of comparative models using CD47 treatment, a relatively new form of cancer treatment (Willingham, Stephen B. et al., 2012; B. Edris et al., 2012; Chen et al., 2005). Researchers have isolated a protein, CD47, which can be targeted on many different types of tumor for effective treatment. This is especially significant because cancer treatments are usually tailored according to the organ of origin and nature of the tumor. Current data on CD47 treatment record its effects on eight of the ten different types of tumor. We propose a preliminary model that can be used to explore tumor-specific dynamics with CD47 treatment. In future work we will take advantage of the data fittings we have made available, and using the high and low ranges of the tumor growth parameters with the best-fit tumor growth function we have determined, we will further develop and test our proposed CD47 treatment model.

1.2 Previous Research

Four of the different tumor growth functions have been studied side-by-side by de Pillis for human melanoma grown in mice (de Pillis and Radunskaya, 2006). By a least-squares residual comparison, this study determined that Von Bertalanffy and logistic growth models provided the best fits for the experimental data. Only one set of experimental trials from one source was used to determine this result.

An earlier study by Hart et al. compared Gompertz, logistic, exponential and power growth law models in breast cancer (Hart et al., 1998). This

study concluded that power law growth was the best candidate for the function governing the growth of breast cancer. However, in a later model developed in part by Zvia Agur, who worked on the previous paper, logistic growth instead of power law growth was used to represent the tumor growth equation (Elishmereni et al., 2011).

One of the earliest works comparing different tumor growth functions was published in 1973, and focuses on fitting tumor growth data to the Gompertz and logistic models (Aroesty et al., 1973). Rather than determining which growth function is the better fit to the data using fitting evaluation metrics, Aroesty's paper mentions the theoretical similarities between the Gompertz and logistic models. However, no direct comparisons of the fitting results are provided.

Similar studies have also been performed for comparing bacterial growth rates (López, S. et al., 2004). Lòpez 2004 used two data sets and nine different growth functions as opposed to four or five, and found that the most effective models for bacterial population growth were Baranyi, three-phase-linear, Richards and Weibull growth models. The fact that no direct comparisons of the fitting results are made demonstrates that large-scale comparison projects of this character are a relatively recent ordeal.

Chapter 2

Assumptions and Methods

2.1 Experimental data

We curated a database of timescale tumor growth data sets for bladder cancer, breast cancer, colon cancer, head and neck squamous cell carcinoma, hepatocellular carcinoma, lung cancer, melanoma, ovarian cancer, pancreatic cancer, and renal cell carcinoma. Each group of data sets was collected from at least five peer-reviewed publications, with the smallest-sized group containing seven data sets and the largest containing 17. In addition, at least one data set collected for each type of cancer was obtained from *in vitro* trials and at least one data set is composed of data collected from *in vivo* trials. Along with *in vitro* trials, the range of target organisms includes SCID mice, nude mice, normal mice, hamsters and humans. Table A.1 shows all sources for each timescale data set included in the study, as well as the cell lines for each trial.

2.2 Unit normalization

Of the papers which reported timescale tumor growth, the units and methods of measurement varied greatly. At least one paper per type of tumor was an *in vitro* trial that reported tumor size as a cell number, the preferred unit for our purposes, but all data from *in vivo* and *in situ* trials were presented in units of mm^3, mm^2, mm, cm^3, or relative volume. In addition, instead of assuming a spherical tumor, volume was reported in a majority of papers as the product of the height, length and width of the tumor, overestimating the volume. However, we will also assume that no individual tumor cells are compressed, which will underestimate the number of tu-

mor cells. The combination of these two assumptions is presumed to bring the estimated cell number within reasonable error of the real cell number.

In many cases, we were able to obtain an estimate of the number of tumor cells in a given volume from murine data sets which reported an initial cell count along with an initial volume measurement. We then divided the volume by the cell number, allowing for an estimate of the volume of a single tumor cell. We used this same estimate for data sets on tumor growth for tumors originating from the same organ. The most accurate conversion estimate, requiring the fewest conversions from the original data, was an estimate of 2.85×10^3 cells$/\mu$m^3 for pancreatic cancer (Kisfalvi et al., 2009). For types of tumor which did not have a conversion data set available, we estimated the conversion ratio at approximately 1.82×10^3 cells$/\mu$m^3 (de Pillis et al., 2013a). Although these two estimates were obtained from different sources and for different cells, it should be noted that they are the same order of magnitude despite the high variability of cell size.

This volume estimate of a tumor cell provides a method with which to convert volume, area or distance measurements to cell number. For those data sets which reported growth in volume, we normalized each datum by $\frac{1}{\mu_T}$ where μ_T is the tumor cell volume calculated as above. The papers that reported an area measurement all obtained the values by multiplying the minor axis of the tumor by the major axis (Ricker et al., 2004; Sunwoo et al., 2001; Boukerche et al., 1989; Juhl et al., 1997). In this case, we assumed a cubic tumor with a volume of $a\sqrt{a}$ where a is the reported area measurement. This allows us to calculate cell number from volume as before. Another set of papers reported only the major axis of the tumor (Murgo, 1985; Burke et al., 1997; Fujimoto et al., 1995). Here, we assumed a spherical tumor with the radius being one-half the major axis, using the volume of the sphere to estimate the cell number. For those papers that reported relative volume, we converted the data to cell number using the information in the supplemental material sections of each paper (Okegawa et al., 2001; Fujiwara et al., 1993; Ahonen et al., 2000).

2.3 ODE Tumor Growth Models

We compare fittings of tumor data for five different ODE growth models; exponential, power law, logistic, Gompertz, and Von Bertalanffy. Let P represent an arbitrary population and let t represent time. Exponential growth

models are the simplest ODE growth model, described by

$$\frac{dP}{dt} = CP \tag{2.1}$$

for some constant C. It is a special case of power law growth,

$$\frac{dP}{dt} = CP^a, \tag{2.2}$$

where both C and a are parameters that must be fit to the data. Logistic growth, which incorporates a carrying capacity, is given by

$$\frac{dP}{dt} = rP\left(1 - \frac{P}{K}\right) \tag{2.3}$$

where r represents the intrinsic growth rate and K represents the carrying capacity. Von Bertalanffy growth is the least complex growth model that incorporates a carrying capacity, given by

$$\frac{dP}{dt} = r(K - P). \tag{2.4}$$

The final commonly used tumor growth model is Gompertz growth,

$$\frac{dP}{dt} = r\log\left(\frac{K}{P}\right)P. \tag{2.5}$$

Of these models, we expect logistic growth to provide the best estimation of experimental data, since it approximates exponential growth at low populations while accounting for the resource-limited growth behavior at high populations. Unfortunately, very few data sets exist that allow tumors to grow large enough in order to get a proper estimate of the carrying capacity. We specifically sought out data sets that included data for large populations in order to properly compare the former two models with the latter three (Fujiwara et al., 1993; Takahashi et al., 1992; Murgo, 1985; Richmond et al., 1983; Kisfalvi et al., 2009; Reinmuth et al., 2002; Nakata et al., 1998; Caltagirone et al., 2000; Ricker et al., 2004).

2.4 Parameter fitting algorithms

All fitting results were obtained by minimizing the non-weighted least squares distance. We refer to the least-squares distance by the quantity d, where

$$d(p) = \sqrt{(q_1 - f(p, t_1))^2 + \cdots + (q_n - f(p, t_n))^2}$$

for each t_n representing a time value at which data are collected, q_n representing the experimentally determined data point at t_n and $f(p,t)$ representing the fitting given parameter p and time t. We say that ϕ is a best-fit parameter if ϕ minimizes $d(p)$.

The parameters for each tumor growth model were estimated using at least two least-squares distance minimization algorithms. For each ODE model, the ODE with parameters was solved numerically using MATLAB's `ode45` function, implementing a 4th and 5th order Runge-Kutta solver. We then minimized a least squares distance function between this solution and a target set of data using either MATLAB's built-in `fminsearch` function or a Markov chain fitting with simulated annealing. MATLAB's `fminsearch` is a Nelder-Mead simplex direct search function. Nelder-Mead is one of a class of local-search algorithms, which require that one choose a very good initial guess, or the method will not converge to a global minimum but instead iterate toward a nearby local minimum. The local minimum found may not produce the best fit (Lagarias et al., 1998). This necessitates the use of an alternate, global, data-fitting method. In the next sections we provide more detail describing both the local Nelder-Mead algorithm and a global minimization algorithm that implements a Markov chain fitting with simulated annealing.

2.4.1 The Nelder-Mead simplex direct search

The Nelder-Mead simplex direct search algorithm implemented in MATLAB's `fminsearch` and described in New Computing Environments: Microcomputers in Large-Scale Computing (Dennis and Woods, 1987), goes through k iterations. It begins by sampling $n+1$ time values, which we will refer to as $x_1, x_2, \cdots, x_{n+1}$. These values are sorted in increasing order of their image under the target function $f(x)$, that is,

$$f(x_1) \leq f(x_2) \leq \cdots \leq f(x_{n+1}).$$

The point with the i^{th} lowest image at the k^{th} iteration will be referred to as x_i^k. We then define a simplex S_k with vertices $x_1, x_2, \cdots x_n$, denoted by $S_k =< x_1, x_2, \cdots, x_{n+1} >$. This simplex is then modified by reflection, expansion, contraction, or shrinkage, in that order, until a new simplex S_{k+1} which converges more closely to the local minimum is determined. The first step reflects the largest vertex, x_{n+1}, through the centroid of the vertices $x_1, \cdots, x_n$. The new reflected vertex, x_r, is calculated by

$$x_r = (1+\alpha)\overline{x} - \alpha x_{n+1}$$

such that $\alpha = 1$ and $\overline{x}$ is the centroid:

$$\overline{x} = \frac{1}{n}\sum_{i=1}^{n} x_i.$$

If $f(x_1) \leq f(x_r) < f(x_n)$, we move to the next iteration of the search with $S_{k+1} =< x_1, x_2, \cdots, x_n, x_r >$. The fact that x_r is not in order with the rest of the vertices is intentional. However, if $f(x_r) < f(x_1)$, implying that $f(x_r)$ is now the closest point to the local minimum, we continue the step by producing an expansion vertex

$$x_e = \gamma x_r + (1 - \gamma)\overline{x}$$

where $\gamma = 2$. We choose the expansion vertex if $f(x_e) < f(x_1)$ and the reflected vertex elsewise. If neither the reflected or expanded vertices are accepted, which corresponds to the case where $f(x_n) \leq f(x_r)$, we compute a contracted vertex. This contraction vertex is calculated as

$$x_c = \beta x_{r'} + (1 - \beta)\overline{x}$$

where $\beta = \frac{1}{2}$ and $x_{r'} = \min(x_{n+1}, x_r)$. This new vertex becomes part of the new simplex if $f(x_c) < f(x_n)$, and a new iteration begins. However, if $f(x_n) \leq f(c)$, we move to shrink the simplex by replacing each x_i with the midpoint of the line segment connecting x_1 and x_i, or

$$x_{i(new)} = \frac{x_1 + x_i}{2}.$$

The new simplex S_{k+1} is created by rearranging the new x_i according to their images under $f(x)$. This algorithm produces a simplex that moves toward a local minimum and shrinks if it is unable to locate a deeper local minimum. Although there are several stopping criteria for this algorithm, MATLAB stops `fminsearch` when the distance traveled in parameter space during the last iteration is under a pre-set tolerance.

2.4.2 Markov Chain fitting with Simulated Annealing

We use a Markov chain Monte Carlo (MCMC) fitting with simulated annealing. The MCMC fitting is non-deterministic alternative and tests a wider range of values in parameter space than `fminsearch`, causing it to be more capable of locating sinks that contain global minima (Winkler, 2003; Gilks et al., 1996; Brooks et al., 2011). Markov chain fitting itself starts by

choosing an initial condition, a point in parameter space, denoted by $\mathbf{p}_0$. On the i^{th} iteration of the fitting, a vector $\mathbf{v}$ of random magnitude and direction is determined from a set of uniformly distributed values over a closed disk of radius r, generating a new set of parameters $\mathbf{p}_{new} = \mathbf{p}_i + \mathbf{v}$. For a minimization function $d'(p)$ (usually the least-squares distance,) we determine the output of this step by comparing $d'(p_i)$ and $d'(p_{new})$. If $d'(p_{new}) \leq d'(p_i)$, we let $\mathbf{p}_{n+1} = \mathbf{p}_{new}$ with probability 1. However, if $d'(p_{new}) > d'(p_i)$, i.e., the least-squares distance is smaller with the older parameters, we move to the new parameters with probability

$$\frac{d'(\mathbf{p}_i)}{d'(\mathbf{p}_{new})}.$$

Although this method seems counterintuitive, the action of moving away from local minima ensures that the Markov chain fitting function is more likely to locate global minima. This serves two purposes—to escape more easily from a local minimum that is not a global minimum, and to allow repeated iterations of the same algorithm to increase the accuracy of the results. The stochasticity in the algorithm allows for different outcomes even among trials with the same initial conditions (Winkler, 2003; Gilks et al., 1996; Brooks et al., 2011). This process is repeated n times— where n is an arbitrary number chosen by the user—before stopping. This algorithm has no standard stopping condition. In our case, we chose $n = 200$. This number of runs allowed us to achieve relatively good fits while keeping computational running times reasonable. Implementing this algorithm with a larger n would increase the chance that a global minimum is located.

Simulated annealing is the process of fitting not to the distance function, but the distance function raised to successive powers from 0 to 1, where the result of each fitting is used as the initial condition for the next fitting. This algorithm reduces the chances that a minimization function will converge to a local minimum instead of a global minimum, since the act of raising the distance function to a power less than 1 reduces the prominence of local minima (Winkler, 2003). In this case, we ran 10 trials with simulated annealing, corresponding to ten iterations. The n^{th} iteration uses the Markov chain fitting algorithm to minimize the function $(d(p))^{\beta_n}$ for $\beta_n = 0.1n$. The fitting for $\beta_n = 1$, *i.e.*, the parameter values for $n = 10$, are accepted as the final parameters for this iteration of the fitting.

2.4.3 Hybrid Minimization Algorithm

Note that part of the difference in usage and performance between these two algorithms arises from the fact that Nelder-Mead simplex direct search, *i.e.* `fminsearch`, finds local function-minimizing parameters, but MCMC and Markov chain methods are more likely to find global function-minimizing parameters (Ashyraliyev et al., 2009). That is, while `fminsearch` will return the parameter values that produce the lowest least-squares fitting within a bounded neighborhood of the initial parameters, all Markov chain methods return the parameter values that produce the lowest least-squares fitting over a finite number of arbitrary parameters from anywhere in the parameter space (Ashyraliyev et al., 2009). This difference in the domain of each algorithm leads to defining behaviors that either help or hinder the goodness of fit. Since `fminsearch` is a local minimizer of the least squares distance, it is excellent at converging to local minima, but is known to ignore global minima that may produce a better fit. Likewise, MCMC and Markov chain methods have the ability to locate other minima that may be far removed from the initial conditions, but are less likely to hone in on the exact minimum in a local sink.

In order to address the respective shortcomings of global and local parameter fitting algorithms, we used a hybrid of Nelder-Mead simplex direct search and Markov chain fitting with simulated annealing. We started with one round of `fminsearch` fitting, and the resulting parameters were passed as initial conditions to the Markov chain algorithm. If the resulting parameters did not meet visual standards or had singularities, the parameters underwent another round of Markov chain fitting. Next, since Markov chain fitting is effective at breaking out of local minima but less effective at converging to minima, a second round of `fminsearch` was performed using the results of the Markov chain fitting as initial conditions to ensure convergence to the deepest local minimum. All parameters reported in the Results section were determined by this sequence of fitting algorithms.

2.5 Biologically Motivated Assumptions

To determine the recommended parameters for each model, we recorded the parameters of the function that best represented all trials with the same model organism at once. However, in order to determine the full range of parameters, we performed fittings to each data set individually and recorded the extrema of each set of parameters. It is also assumed that

in vitro trials are better indicators of intrinsic tumor growth rates, due to the lack of an immune system in the growth environment; and that *in vivo* trials are better indicators of animal carrying capacity, since the growth media are closer to conditions the tumor would encounter in a living organism. Thus, when relevant, intrinsic growth rates are determined from *in vitro* trials only and carrying capacities are determined from *in vivo* trials only. In cases where no carrying capacity is given, *i.e.*, the exponential and power law growth models, only *in vitro* trials are used to determine the growth rate, and the *in vitro* trials are also used to determine the exponent for the power law model.

2.6 Fitting evaluation metrics

We can compare the goodness-of-fit between the output of `fminsearch` and MCMC by noting the least-squares residuals for each data set. Using this metric, lower residuals will suggest a better fitting. We also use the least-squares residuals to calculate the Bayesian Information Criterion (BIC) for each fitting, which accounts for goodness-of-fit as well as the number of parameters to guard against over-fitting. The particular formula that we use is

$$BIC = n \cdot \ln\left(\frac{1}{n-1} d(p)\right) + k \cdot \ln(n).$$

where x represents the experimental data, n is the number of data points in x, and k is the number of parameters which are being estimated in the model (Priestley, 1981). For our purposes, $k = 1$ for the exponential model and $k = 2$ for the four other models. Note the inclusion of the least-squares residuals. The primary reason for using BIC in conjunction with least-squares residuals in model evaluation is to determine the effects of using more parameters than necessary. The Bayesian Information Criterion incorporates slightly more information than the least squares residuals, penalizing models for using a larger number of parameters.

2.7 Parameter Sensitivity Analysis

We use two separate parameter sensitivity analysis techniques: a localized parameter sensitivity algorithm, and the Partial Rank Correlation Coefficient (PRCC) test using Latin Hypercube Sampling (LHS). These techniques account for the effects of slight parameter modifications on the overall function and accuracy of the model.

The local parameter sensitivity analysis is used to determine how altering the value of a single parameter affects the behavior of the overall model Mummert (2010). In order to perform a local parameter sensitivity analysis, we start with an initial set of parameters $\mathbf{p}$, then choose a percentage $0 < p < 1$, an initial condition y_0 for the ODE model, and a time $t > 0$. Then, where p_j represents the j^{th} parameter, we let y_t be the value at t of the ODE model with parameters $\mathbf{p}$ starting at y_0, let y_+ be the value at t of the ODE model with parameters $(p_1, \cdots, p_j(1+p), \cdots, p_n)$ starting at y_0, and let y_- be the value at t of the ODE model with parameters $(p_1, \cdots, p_j(1-p), \cdots, p_n)$ starting at y_0. We then calculate the percentages of change, $C_{\%+}$ and $C_{\%-}$, from the previous model output to the new model output as

$$C_{\%+} = \frac{y_+ - y_t}{y_t} \times 100,$$
$$C_{\%-} = \frac{y_- - y_t}{y_t} \times 100.$$

If the model value and the value of an individual parameter are positively correlated, we expect $C_{\%+}$ to be positive and $C_{\%-}$ to be negative. Similarly, if the model value and the value of an individual parameter are negatively correlated, we expect $C_{\%+}$ to be negative and $C_{\%-}$ to be positive. In addition, a larger $C_{\%+}$ or $C_{\%-}$ value indicates that the parameter p_j has a more significant effect on the behavior of the model.

One of the issues with only using local parameter sensitivity analysis is that it does not account for interactions between parameters. This is why we use a second parameter sensitivity analysis technique, the Partial Rank Correlation Coefficient (PRCC). We begin by using Latin Hypercube Sampling (LHS) to generate a sampling of random vectors in parameter space. Contrast this with the local parameter sensitivity analysis, which can only evaluate the model along the axes of parameter space. For some integer $N > 0$, LHS attempts to cover parameter space by separating a bounded subset of parameter space into N sections and choosing a random value in each section from a uniform distribution Mummert (2010). MATLAB has a built-in function for performing LHS: `lhsdesign`. This function returns a matrix of parameter values between 0 and 1. Since these values are not viable to use as carrying capacities, we multiplied each set of carrying capacity parameters by 10^9. We let M be the matrix returned by `lhsdesign`.

From the results of the LHS, we generate an output vector, $\mathbf{y}$, where y_j is the model value at time t using the parameters given by the j^{th} row

of M. The first step to implementing the PRCC test is to rank transform the matrices, which takes M and $\mathbf{y}$ as input and returns a matrix of the same dimensions, called $\underline{M}$ and $\underline{\mathbf{y}}$, where each column contains all of the integer values from 1 to N. The ordering of these integers corresponds to the ordering of values in the original matrices, where a 1 in the k^{th} column of $\underline{M}$ corresponds to the position of the lowest value in the k^{th} column of M and N corresponds to the highest value.

We then use the rank transformed matrices to calculate the linear regression models for each parameter, $\overline{p_k}$, which expresses the target parameter p_k as a linear combination of all of the other parameters. The equation

$$\overline{p_k} = c_0 + c_1 p_1 + \cdots + c_{k-1} p_{k-1} + c_{k+1} p_{k+1} + \cdots c_n p_n$$

is solved by

$$\underline{c} = (X^T X)^{-1}(X^T \underline{p_k}); \qquad \underline{c} = \begin{bmatrix} c_0 \\ \vdots \\ c_n \end{bmatrix} \text{ and } X = [1, p_1, \cdots p_{k-1}, p_{k+1}, \cdots p_n].$$

In a similar manner, we define

$$\overline{y_{p_k}} = a_0 + a_1 p_1 + \cdots + a_{k-1} p_{k-1} + a_{k+1} p_{k+1} + \cdots a_n p_n,$$

which is solved by

$$\underline{a} = (X^T X)^{-1}(X^T \underline{y}); \qquad \underline{a} = \begin{bmatrix} a_0 \\ \vdots \\ a_n \end{bmatrix} \text{ and } X = [1, p_1, \cdots p_{k-1}, p_{k+1}, \cdots p_n].$$

This allows us to define two sets of residuals; $\text{res}(p_k) = \underline{p_k} - \overline{p_k}$ and $\text{res}(y_{p_k}) = \underline{y} - \overline{y_{p_k}}$. We finalize the PRCC algorithm using the MATLAB function `corrcoef` to determine the correlation coefficient between $\text{res}(p_k)$ and $\text{res}(y_{p_k})$. These correlation coefficients are the final result of the PRCC test, and they give a measure for the strength of the relationship between two parameters. A correlation coefficient of 1 between two parameters implies a strong positive linear relationship between the parameters, while a correlation coefficient of -1 between two parameters suggests a strong negative relationship.

If the correlation coefficient is between -0.5 and 0.5, the parameters do not have a linear relationship.

It should also be noted that PRCC can only be used on models that have a monotonic relationship on the model output, which is true of all parameters in our case, and the model must have two or more parameters in order to perform the test. This excludes the exponential model from PRCC analysis, as it only needs one parameter.

Chapter 3

Results

3.1 Tumor Growth Parameter Values

In order to determine a set of recommended parameters and appropriate range for each type of cancer and growth model, we fit the parameters of each growth equation to a minimum of five data sets per type of cancer. These parameters fall into three different classes: intrinsic growth rates (denoted r), exponents (denoted a) and carrying capacities (denoted K.) It is assumed that intrinsic growth rates and exponents could be determined more accurately from *in vitro* and SCID mouse trials, *i.e.*, due to the lack of an immune system interfering with growth; and that carrying capacities for humans are closer to the carrying capacities from *in vivo* trials, given that carrying capacities are highly dependent on the organ of origin belonging to each type of cancer. Therefore, for all models except the Power Law model, the intrinsic growth rate is determined from *in vitro* trials and the carrying capacity, if it exists, is determined from *in vivo* trials only. The Power Law is a special case which is addressed in the discussion section.

To fit the parameters, we used a hybrid of Monte Carlo fitting with simulated annealing and Nelder-Mead simplex direct search. Nelder-Mead, in the form of MATLAB's `fminsearch` function, was used to initialize parameters for the Monte Carlo fitting, which was performed to nudge the results of `fminsearch` out of local minima, then a second round of Nelder-Mead is used to lower the least squares residuals to the closest local minimum. In addition, two different types of fittings were performed on each set of related data sets. The *in vitro* trials for each type of cancer were fitted separately for the best fit parameters to determine an acceptable parameter range, then together with different initial conditions to determine the sug-

gested parameter values.

As a result of the parameter fitting, a catalog of suggested values and ranges was found for ten types of cancer and five models, in Table 2.1. The least squares residuals and BIC values for the combined fittings can be found in Table 2.2. In order to highlight the best fittings and the relationship between least squares residuals and BIC values, the lowest least squares residuals values and BIC values in each row have been highlighted in purple and blue, respectively. Graphs for each individual fitting and combined fittings, as well as the residuals, parameters and sources for all fittings, can be found in the Supplemental Data section. We were also able to determine a ranking of model fit for each cancer type from the evaluation metrics, displayed in Table 2.3. This ranking was determined by comparing the sum of the least squares residuals for all individual and combined trials for each type of cancer.

Cancer		Exponential	Power Law	Logistic	Gompertz	Von Bertalanffy
Bladder	r	0.0165:(0.0942):0.1919	0.0033:(5.5976):51.2297	0.1378:(1.3454):9.0473	0.0075:(0.2893):0.2893	3.6E−4:(0.0392):0.0037
	a, K		0.6839:(0.8582):1.1552	5.36E4:(1.24E9):1.91E10	3.07E5:(8.10E6):9.01E11	1.5E4:(1.5E4):1.11E11
Breast	r	0.183:(0.4593):1.3311	0.0456:(5.3077):3988.3	0.183:(1.4808):1.5488	0.0095:(0.4834):0.4834	6.17E−5:(2.95E−4):0.0062
	a, K		0.3151:(0.8299):1.122	9.45E5:(2.46E9):2.73E9	1.92E6:(1.53E10):4.24E13	3.95E8:(1.06E10):5.2E11
Colon	r	0.4555:(0.4816):0.5533	1.606:(1.606):35.339	0.5521:(0.5775):0.8401	0.0608:(0.0608):0.2405	1.8E−4:(1.8E−4):2.6E4
	a, K		0.5521:(0.8819):0.8819	2.32E8:(8.02E8):3.65E51.47E9	3.78E8:(9.90E8):1.44E12	1.65E9:(4.49E10):2.04E11
HNSCC	r	0.0277:(0.0286):0.5014	0.0728:(0.6353):42.0098	0.0309:(0.0328):0.576	0.0017:(0.0044):0.1218	1.19E−5:(1.19E−5):1.51E−4
	a, K		0.7384:(0.8376):0.9597	5.17E6:(1.37E7):1.37E7	1.11E7:(1.17E12):7.01E14	7.66E8:(2.94E10):2.94E10
Liver	r	0.1749:(0.1754):0.5307	:2.8332(278.3617):738.1756	0.2402:(0.2421):0.5982	0.0637:(0.0670):0.0730	6.99E−5:(6.99E−5):2.53E−4
	a, K		0.5685:(0.619):0.8589	1.34E6:(4.85E8):2.44E9	3.04E8:(4.96R8):1.60E13	2.51E7:(5.01E8):3.55E10
Lung	r	0.0804:(0.3358):0.6501	0.0026:(0.2814):2.15E6	0.35:(0.381):1.3577	0.004:(0.0049):0.658	2.93E−5:(2.93E−5):0.1143
	a, K		-0.0806:(0.995):1.3872	3.77E7:(1.36E12):1.36E12	3.85E7:(2.84E21):2.84E21	4.02E7:(9.70E11):2.07E12
Melanoma	r	0.0908:(0.1502):0.2414	0.0081:(0.0081):299.271	0.1061:(0.1502):0.4766	0.0043:(0.0043):0.2872	0.0015:(0.5303):0.5303
	a, K		0.5442:(1.1596):1.1596	4.87E7:(7.36E8):2.36E9	7.93E7:(5.02E8):3.48E9	9.48E7:(4.06E8):3.49E11
Ovarian	r	0.5087:(0.6765):0.7634	1.42E−4:(2.3356):3.58E7	0.5087:(0.823):2.4545	0.0193:(0.0815):1.4489	3.35E−4:(4.96E−4):0.7245
	a, K		-0.4252:(0.8963):1.7012	8.08E8:(3.07E12):3.07E12	2.06E9:(9.41E19):9.41E19	9.32E10:(1.20E13):1.20E13
Pancreatic	r	0.0541:(0.3093):0.4122	2.84E−5:(0.668):13.216	0.0541:(0.348):0.4645	0.0023:(0.0524):0.1566	1.92E−5:(0.0055):0.0055
	a, K		0.7126:(0.9102):1.493	5.69E7:(5.69E7):7.62E8	7.09E7:(7.09E7):5.81E15	1.79E9:(6.28E9):2.81E11
RCC	r	0.3674:(0.4504):0.5568	0.6554:(44.7253):172.3193	0.3884:(0.5719):1.365	0.0342:(0.0773):0.8647	3.5E−6:(3.5E−6):0.4437
	a, K		0.2805:(0.6182):0.9473	2.49E8:(8.91E8):1.41E9	3.02E8:(3.02E8):4.19E11	2.95E8:(2.95E8):1.46E11

Table 3.1 Recommended Parameter Values and Ranges for Ten Different Types of Cancer and Five ODE Growth Laws

Trial	Exponential		Power Law		Logistic		Gompertz		Von Bertalanffy	
	Residuals	BIC	Residuals	BIC	Residuals	BIC	Residuals	BIC	Residuals	BIC
Bladder *in vitro*	7.43E10	97.117	4.22E10	96.241	3.00E10	94.876	3.30E8	76.837	2.40E11	103.194
Bladder *in vivo*	7.43E10	2363.3	4.22E10	2339.9	3.00E10	2353.2	2.21E17	2329.9	1.09E18	2337.0
Breast *in vitro*	5.70E12	506.07	2.04E12	489.52	2.28E12	491.59	2.08E12	489.87	2.39E12	492.55
Breast *in vivo*	2.10E18	749.61	1.40E18	744.80	6.02E17	728.80	1.01E18	738.68	8.92E18	780.03
Colon *in vitro*	1.72E9	228.87	1.18E9	226.87	1.18E9	226.88	1.18E9	226.83	1.03E10	252.80
Colon *in vivo*	1.79E18	1799.3	8.71E17	1769.3	1.33E18	1789.1	1.12E18	1781.1	8.60E17	1768.6
HNSCC *in vitro*	6.02E17	1531.0	5.00E17	1527.0	5.57E17	1532.4	5.09E17	1527.8	1.17E18	1562.1
HNSCC *in vivo*	5.03E13	519.78	3.07E13	513.78	3.77E13	517.48	5.13E13	523.02	2.30E14	550.03
Liver *in vitro*	1.51E17	770.77	2.15E16	732.92	9.64E15	716.08	1.59E16	726.60	3.60E17	792.09
Liver *in vivo*	1.17E19	1809.5	8.60E18	1799.3	7.51E18	1793.2	7.56E18	1793.4	7.83E18	1795.0
Lung *in vitro*	1.75E22	4201.0	1.74E22	4214.2	1.29E22	4187.3	2.14E22	4232.6	1.75E22	4214.6
Lung *in vivo*	1.86E18	861.64	1.64E18	861.85	1.86E18	864.73	1.90E18	865.11	2.86E18	874.11
Melanoma *in vitro*	5.25E18	688.49	1.26E18	667.04	5.25E18	691.32	5.67E18	692.62	7.99E18	698.45
Melanoma *in vivo*	7.20E18	1903.2	2.42E18	1854.8	6.48E18	1902.0	7.67E18	1910.1	8.34E18	1914.2
Ovarian *in vitro*	1.60E11	372.25	1.58E11	374.82	1.56E11	374.55	1.58E11	374.80	2.20E11	380.09
Ovarian *in vivo*	3.27E18	758.01	2.88E18	758.54	3.27E18	760.95	7.45E18	788.85	3.44E20	849.44
Pancreatic *in vitro*	5.87E5	61.088	5.86E5	62.534	5.48E5	62.359	5.79E5	62.630	2.09E6	69.045
Pancreatic *in vivo*	5.79E16	1401.1	3.83E16	1388.2	4.50E16	1394.7	4.15E16	1391.4	3.83E16	1388.2
RCC *in vitro*	6.90E11	1140.5	6.40E11	1138.9	4.71E11	1131.3	4.92E11	668.17	1.12E12	691.14
RCC *in vivo*	1.59E18	2052.6	1.51E18	2054.0	1.59E18	2056.6	1.80E18	2063.5	1.83E18	2064.4

Table 3.2 Model Evaluation Metrics for Combined Experimental Data Fittings

Cancer	**Model Ranking**				
	1	2	3	4	5
Bladder	Power Law	Gompertz	Logistic	Exponential	Von Bertalanffy
Breast	Logistic	Gompertz	Power Law	Exponential	Von Bertalanffy
Colon	Power Law	Von Bertalanffy	Gompertz	Logistic	Exponential
HNSCC	Gompertz	Power Law	Exponential	Logistic	Von Bertalanffy
Liver	Logistic	Gompertz	Power Law	Von Bertalanffy	Exponential
Lung	Logistic	Power Law	Gompertz	Von Bertalanffy	Exponential
Melanoma	Power Law	Logistic	Exponential	Gompertz	Von Bertalanffy
Ovarian	Power Law	Exponential	Gompertz	Logistic	Von Bertalanffy
Pancreatic	Power Law	Gompertz	Logistic	Exponential	Von Bertalanffy
RCC	Power Law	Logistic	Exponential	Gompertz	Von Bertalanffy

Table 3.3 Model Fit Ranking According to Least Squares Residuals

In addition to building a new catalogue, we have tested our methods on established results as well. Agur *et al.* 2011 estimates logistic tumor growth parameters from expermiental data regarding B16 growth, some of which is reported (Elishmereni et al., 2011). When applied to the given control B16 data in Agur 2011, our parameter fitting algorithm returned an intrinsic growth rate of $r = 0.5392$ and a carrying capacity of $7.4944E8$ with least squares residuals of $8.60E14$ for the logistic fit. Agur *et al.*'s original result was $r = 0.0014$ and $1.5E9$ (Elishmereni et al., 2011). As their least-squares residuals and exact data sets used for parameter estimation were not reported, we were unable to perform a suitable comparison to their parameters.

3.2 Parameter Sensitivity Analysis

Two types of parameter sensitivity analysis were performed on the individual tumor growth models. The local parameter sensitivity analysis is performed to measure what the effect on the model would be if a parameter were increased or decreased by some percentage of its value, while the Partial Rank Correlation Coefficient test, commonly referred to as the PRCC, is intended to measure the statistical influence on the model output of parameters that have monotonic but nonlinear behavior Gomero (2012). As it is impossible to determine PRCC values from a model that has only one parameter, the exponential model is excluded from PRCC analysis.

We perform a local parameter sensitivity analysis altering each parameter by 10%, with an initial condition of 1×10^4 tumor cells, running the model for 10 days, and starting with the parameters from the individually determined *in vitro* colon trials. The results are presented in Figure 3.2 and Figure 3.3 (where Figure 3.3 has the power law exponent removed to increase readability of the percent changes associated with the other parameters.) We also provide a PRCC analysis over 1000 randomized parameter values using Latin hypercube sampling, which is presented in Table 3.4.

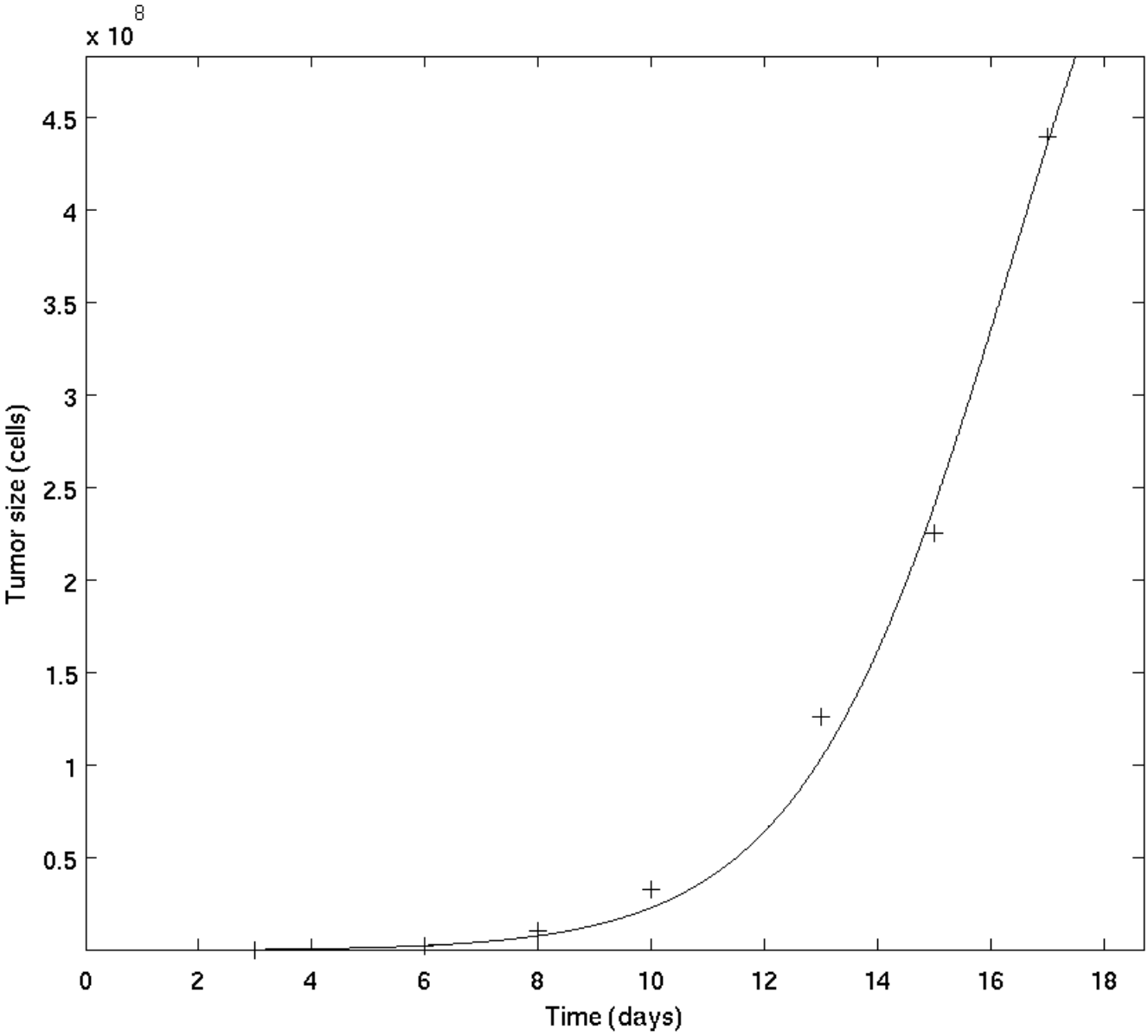

Figure 3.1 Logistic Model of Control B16 Data from Agur 2011

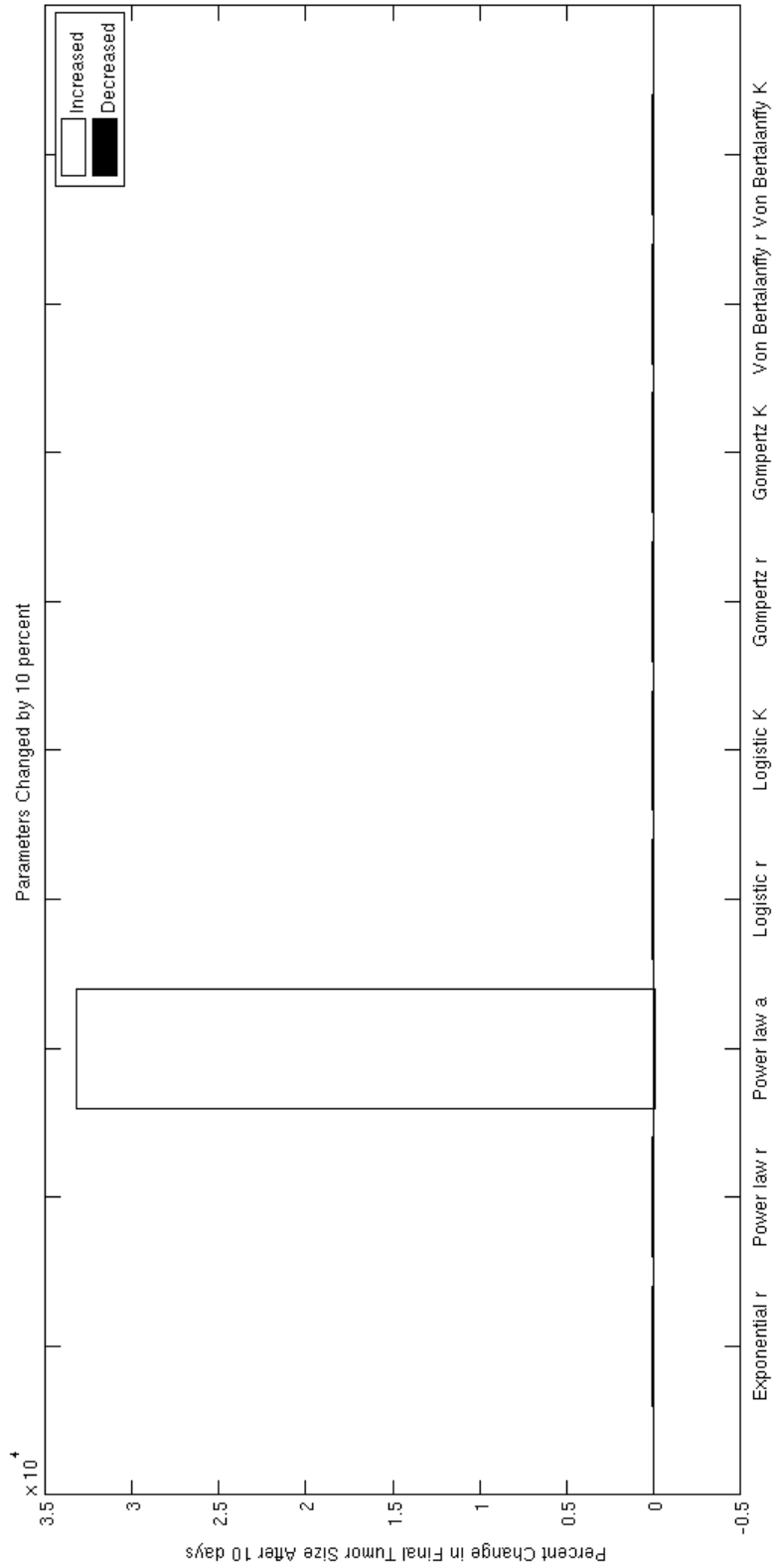

Figure 3.2 Local Parameter Sensitivity Analysis for Five Models, Altering Parameters by 10%

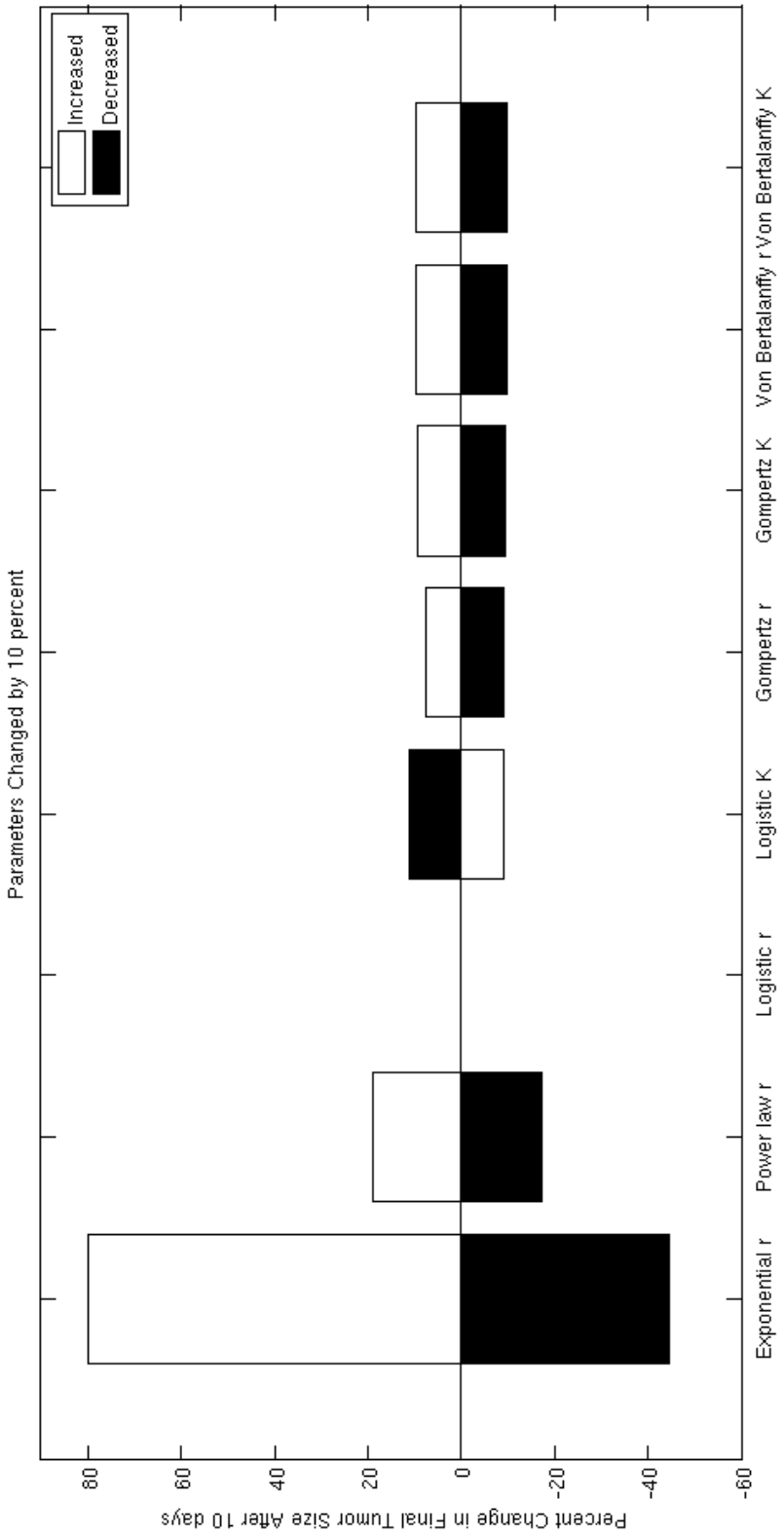

Figure 3.3 Local Parameter Sensitivity Analysis for Five Models, Altering Parameters by 10% (with Power Law a results removed)

Parameter	PRCC
Power law r	0.0412
Power law a	0
Logistic r	0
Logistic K	0
Gompertz K	0.0292
Gompertz K	0
Von Bertalanffy K	- 0.0104
Von Bertalanffy K	0

Table 3.4 Results of Partial Rank Correlation Coefficient Test for Two-Parameter Growth Models

Chapter 4

Discussion

4.1 Parameter Fitting

In some cases, the results of the fitting algorithm are misleading. Logistic growth fittings sometimes ended with a carrying capacity with an order of magnitude much higher than comparable trials and the same intrinsic growth rate as the exponential fit to the same data. This occurs with *in vivo* trial 3 for breast cancer, *in vivo* trial 4 for head and neck squamous cell carcinoma; *in vitro* trials 1, 2, and 10 and *in vivo* trial 1 and the combined *in vivo* fit for lung cancer; and *in vitro* trials 1 and 3 for ovarian cancer. When this happens, we assume that the exponential fit is a better match to the data than the logistic fit, so the logistic growth function approximates exponential growth by raising the carrying capacity to a number high enough so that it does not affect the fitting. This theory is supported by the least squares residuals; the least squares residuals from the exponential fit and the residuals from the logistic fit are the same when this situation occurs.

Another result determined from the parameter fitting process is that it may not be justifiable to alter power law growth parameters, even within the range given by repeated fits. This is because the best fit power law parameters occasionally have uncharacteristically high intrinsic growth rates (e.g. *in vivo* breast cancer trials 1 and 2, the combined head and neck squamous cell carcinoma *in vivo* trial, *in vitro* lung trial 5) and exponents that are lower than the exponents in trials in the same cancer. These results suggest that power law fitting is highly sensitive, where the intrinsic growth rates rise unpredictably to accommodate lower exponents and vice versa. Therefore, although power law fits occasionally have lower residuals than the other growth laws, their unstable nature prevents researchers from being

able to justifiably change parameters within a certain range. For this reason, we discourage future tumor growth modelers from using the power law model.

One concern that must be addressed is whether the best-fit parameters are biologically accurate (Slezak et al., 2010). We note that the best-fit Von Bertalanffy parameters, which are expected to have intrinsic growth rates similar to all other models, consistently have intrinsic growth rates that are two or three orders of magnitude smaller. This is enough of an indication to doubt the biological veracity of the Von Bertalanffy parameters obtained by least-squares fitting. In addition, we have reason to question the biological relevance of the power law fittings for the same reasons as previously addressed.

4.2 Parameter Fitting Algorithms

To see that the hybrid fitting algorithm is more effective than either the Nelder-Mead simplex direct search or Markov Chain method with simulated annealing, we note that a set of parameters is only accepted if the least squares residuals are lower than they were in the previous fitting. Since `fminsearch` is used to provide initial values for the Markov Chain method, the residuals of a Nelder-Mead simplex direct search on a given data set bound the residuals of the hybrid search from above. Due to the nondeterministic nature of the Markov Chain method, the residuals are not necessarily always greater than those of the hybrid method, but it is true that the residuals returned by a specific iteration of the Markov Chain method will always be greater than the results of the hybrid algorithm using that specific iteration of the Markov Chain method. We have noted the inability of the Markov chain method to converge on global minima.

What is questionable, though, is the justification of using a much more complicated fitting algorithm than is necessary when `fminsearch` would have been sufficient. One issue with `fminsearch` is the inability to converge to a better minimum once a local minimum is detected by the algorithm, and to improve the fitting would necessitate changing parameters by hand. Since this project required 20 separate parameter fitting trials each to 70 data sets, not including the 90 combined fittings, manually altering parameters was not a viable option. Thus, even one instance of `fminsearch` converging to a non-global minimum would necessitate the use of a stronger parameter fitting algorithm. This hybrid method was adopted after repeated difficulties with `fminsearch` which would have remained unfixable otherwise.

As a side note, it is possible to fit the equations with carrying capacities

in two different ways: the first, defining the parameters to be estimated as r and K, and the second, defining the parameters to be estimated as r and $1/K$. Although theoretically equivalent, these two approaches can produce different outcomes depending on which fitting metric is used. For the logistic equation defined as

$$\frac{dP}{dt} = rP\left(1 - \frac{P}{K}\right), \tag{4.1}$$

it is possible that the fitting algorithm may be slower in converging to the best-fit K, because it is possible for the best-fit K to be several orders of magnitude higher than the initial condition. However, for the logistic equation defined as

$$\frac{dP}{dt} = rP\left(1 - bP\right) \tag{4.2}$$

where $b = \frac{1}{K}$, both the Nelder-Mead simplex direct search and the Markov Chain method occasionally produced results where the carrying capacity was negative. This is a result of the relative distance in parameter space from the negative real axis; 1×10^6 and -1×10^6 are much further apart than 1×10^{-6} and -1×10^{-6}, for example, thus the first condition makes it more difficult for either algorithm to reach negative values. We recommend using the first fitting method in order to avoid the fittings from producing a biologically inaccurate carrying capacity.

4.3 Parameter Sensitivity Analysis

While it may seem odd to perform a sensitivity analysis on a series of models that each have only one or two parameters, these techniques can be interpreted to compare the justifiability of tweaking parameters in each growth model. The PRCC values provide a measure of the strength of the relationship between two parameters, while the local parameter sensitivity analysis measures the effect of individual parameters on the model output. Therefore, while the local parameter sensitivity analysis can be used to estimate the effects of changing the value of a single parameter, the PRCC measure can tell us whether altering a single parameter while leaving the other constant is justifiable. If the local parameter sensitivity analysis reveals that altering a parameter by a small amount changes the output of the model by a significant amount, possibly 50% or greater, researchers should be warned against changing these parameters. Furthermore, if the PRCC

indicates that two parameters have a low correlation coefficient, it indicates that the parameters have a non-monotonic relationship Gomero (2012).

For our purposes, the sensitivity analyses can be used to provide a basis for our claim that the power law is not a viable model. Figure 3.2 suggests that a, the exponential component of the power law model, affects the model output at a much higher percentage than any other parameter in any other model. In fact, increasing a by only 10% caused the tumor to grow almost 35000% larger in only 10 days. This suggests that altering a individually would change the tumor growth behavior at a massive rate that has no biological justification. An alternative would be to alter a and r in conjunction, such that the relatively low least squares residuals for the fitting are preserved. However, as the PRCC results suggest, the relationship between a and r is highly nonlinear. This is not suggestive in and of itself—none of the other parameters had significant PRCC results—rather, we draw the conclusion in light of the results of the local parameter sensitivity analysis. In practice, a researcher seeking to lower the growth rate or raise the exponent of some of the less biologically sound power law fittings would have difficulty determining a relationship between a and r which allows the parameters to be altered while preserving the behavior of the original curve. This rigidity and extreme sensitivity is what makes the power law a less than ideal choice for a tumor growth model.

It should be noted in the local parameter sensitivity analysis that changing the logistic r appears to have no effect on parameter sensitivity. This occurs because with the chosen parameters, the model reaches its carrying capacity by $t = 10$ for all values in the sampled range of r, and a different percent growth would be obtained if the tumor growth were sampled at a different time.

4.4 Usage of Least Squares Residuals versus BIC

Although only using one model evaluation metric would not be thorough, it was necessary for the purpose of this project to choose one evaluation metric as the dominant one. The model performance ended up being ranked primarily by least squares residuals. Although the BIC can be seen as an extension of the least squares residual and incorporates more information, it was used as only a secondary evaluative tool for two reasons. Least squares residuals have the benefit of being easier to interpret and understand. More importantly, the strength of the BIC is that it penalizes models for having more parameters, even if more parameters produce a better fitting, because

increasing the number of parameters also decreases the probability that the parameters used are statistically accurate. This may be important for larger models, but, for our purposes, all models either had one or two parameters, making this feature redundant. It could also be argued that two parameters is the least that a biologically viable tumor growth model can have, given that tumor growth is limited by the amount of available nutrients in the local area, so a carrying capacity must always exist. This is why the ranked model evaluation takes the least squares residuals into account more strongly than the BIC values for each trial.

Another relation between the evaluation metrics to take into account is whether the models with the lowest least squares residuals also had the lowest BIC values. As demonstrated in Table 3.2, the trial with the lowest least squares residuals also had the lowest BIC values in 65% of the cases, while the two metrics disagreed on 35% of the cases. While this nontrivial behavior is expected, given that the function that generates BIC values is a nonlinear function over the least squares residuals of a model, this difference serves to highlight the fact that choosing a different model evaluation metric would produce a different ranked ordering of models.

Chapter 5

Future Work

5.1 ODE models for CD47 Treatment

To develop an ODE model accounting for CD47 treatment, we must first determine which components of the immune system are affected by CD47 suppressors. Willingham *et al.* reports that CD47 prevents phagocytosis of tumor cells by binding to SIRPα, a protein expressed on the surface of both macrophages and dendritic cells (Willingham, Stephen B. et al., 2012). Blocking the CD47 protein greatly increases the rate of phagocytosis of tumor cells by macrophages. In addition, anti-CD47 treatment increases the rate of activation by dendritic cells of tumor-specific cytotoxic lymphocytes (CTLs). Therefore, along with the usual cell types accounted for in tumor-immune system interaction models; natural killer (NK) cells, CTLs; we must also account for changes in the dendritic cell and macrophage populations. In addition, anti-CD47 treatment is a monoclonal antibody (MAB) treatment, requiring an additional term for treatment concentration.

We begin with a simplified model from de Pillis 2005, which accounts for tumor growth, NK cell populations, and CTL populations (de Pillis et al., 2005). Although future models published by the same authors have also included interleuken-2 (IL-2) dynamics, accounting for a chemical signal that affects CTL proliferation, there are many immunotherapies that affect the IL-2 concentration (de Pillis et al., 2013a, 2009, 2013b). In this model, because the particular immunotherapy we are studying affects IL-2 concentration only indirectly through the proliferation of other cell lines, we reference it only indirectly and remove the IL-2 equation. We let $T(t)$ represent the tumor population, $N(t)$ represent the NK cell population, and $L(t)$ represent the CTL population. The original model, from de Pillis 2005,

is given as

$$\frac{dT}{dt} = \gamma(T) - cNT - D \tag{5.1}$$
$$\frac{dN}{dt} = \sigma - fN + \frac{gT^2}{h+T^2}N - pNT \tag{5.2}$$
$$\frac{dL}{dt} = -mL + \frac{jD^2}{k+D^2}L - qLT + rNT \tag{5.3}$$

where

$$D = d\frac{(L/T)^\lambda}{s+(L/T)^\lambda}T$$

and $\gamma(T)$ is the ODE tumor growth equation which was determined to be the best-fit model for the target type of cancer by our previous parameter fittings. To account for dendritic cell dynamics, we can include a new dendritic cell paper with all of the compartments (de Pillis et al., 2013b). Our macrophage dynamics depend both on the total macrophage population, the localized macrophage population near the tumor cell, and the concentration of chemoattractant near the tumor cell. The macrophage population and chemoattracant concentration, denoted M and W, respectively, are based on a model from Byrne et al. 2004 (Byrne, H.M. and Cox, S.M. and Kelly, C.E., 2004):

$$\frac{dM}{dt} = (M* - M)\frac{aW}{1+bW} - uM(T+M+v) \tag{5.4}$$
$$\frac{dW}{dt} = wT - xW. \tag{5.5}$$

This is where we encounter a significant challenge, however, because Byrne et al. did not have sufficient data to determine biologically accurate parameters, making most of the macrophage-associated constants unusable for modeling purposes. While the decision to estimate parameters without experimental data did allow Byrne et al. to evaluate the macrophage model as a dynamical system, the current state of the model cannot be used to verify tumor-immune system behavior under the influence of various medicines. In addition, a thorough literature search revealed that experimental data relating directly to the macrophage parameters was either difficult to find or nonexistent. Therefore, producing a biologically motivated CD47 model would require large parts of the model to be built from scratch, which was not possible in the time period given for this project.

Despite the difficulty inherent in attempting this project, modeling tumor-immune system interaction with CD47 treatment is extremely attractive because the treatment acts in a way that is relatively novel to the field of cancer therapy, as previously stated. One of the implications of building a CD47 model is the inclusion of tumor types that are not normally associated with successful reactions to immunotherapies. Out of all of the cancer types, only renal cell carcinoma and melanoma have been shown to have success with CD8+ and interleuken-affecting immunotherapies; however, as CD47 treatment has been shown to affect ovarian, breast, colon, bladder, and prostate cancer, as well as glioblastoma and hepatocellular carcinoma, it is necessary for ODE model developers to produce tumor growth parameters for an ever-increasing number of tumor types (de Pillis et al., 2013a, 2009, 2013b; Willingham, Stephen B. et al., 2012). The results of this project make these efforts almost trivial, so that future dynamical systems researchers need only develop the parameters for macrophage and dendritic cell terms.

Appendix A

Supplemental Materials

A.1 Sources of Data for Parameter Values

A large number of individual studies were gathered in determining appropriate timescale tumor growth data sets to be used in the fitting process. Not only are the sources for each type of cancer listed, the individual cell lines used in each paper are included for posterity. Some papers, which used tissue samples from human subjects as the source of cancerous cells, did not specify a cell line.

Cancer and Cell Line	Sources
Bladder Cancer	
HT1376	Golshani et al. (2008)
UMUC-3	Kamada et al. (2007)
KoTCC-1	Miyake et al. (2001)
EJ-1	Ohnishi et al. (2003); Du and Hou (2003)
Breast Cancer	
MDA-MB-435BAG	Coopman et al. (2000)
MCF-7	Lu and Serrero (1999)
KPL-1	Nakagawa et al. (2001)
4T1-GFP-FL	Smith et al. (2004)
Colon Cancer	
KM12L4	Reinmuth et al. (2002)
Moser	Sarraf et al. (1998)
HCT116	Sarraf et al. (1998); Sheng et al. (1997)
CX-1	Sarraf et al. (1998)

Table A.1 Sources of Timescale Data by Type of Cancer and Cell Line

Cancer and Cell Line	Sources
HCA7	Sheng et al. (1997)
LS LiM6	Warren et al. (1995)
Unspecified	Todaro et al. (2007)
Head and Neck Squamous Cell Carcinoma	
UM-SCC-9	Duffey et al. (1999)
Tu-138	Liu et al. (1999)
Tu-167	Liu et al. (1999)
686LN	Liu et al. (1999)
CAL27	LoTempio et al. (2005)
UM-SCC-X	Ricker et al. (2004)
PAM-LY2	Sunwoo et al. (2001)
Hepatocellular Carcinoma	
HCC-26-1004	Huynh et al. (2008)
HCC-2-1318	Huynh et al. (2008)
SH-J1	Jung et al. (2006)
PLC	Liu et al. (2005)
Hep3B	Liu et al. (2005)
SMMC-7721	Wong et al. (2005)
Unspecified	Zender et al. (2008)
Lung Cancer	
SW-900	Esquela-Kerscher et al. (2008)
H226	Esquela-Kerscher et al. (2008)
A549	Esquela-Kerscher et al. (2008)
	Fabbri et al. (2005)
	Tsubouchi et al. (2000)
H460	Fabbri et al. (2005)
H1299	Fabbri et al. (2005)
U2020	Fabbri et al. (2005)
H322a	Fujiwara et al. (1993)
WT226b	Fujiwara et al. (1993)
NCI-H727	Moody et al. (1993)
3LL	Sharma et al. (1999)
NCI-H358	Takahashi et al. (1992)
H841	Tsubouchi et al. (2000)
pc14	Tsubouchi et al. (2000)
Melanoma	
M3Dau	Boukerche et al. (1989)

Table A.1 Sources of Timescale Data by Type of Cancer and Cell Line

Cancer and Cell Line	Sources
MIRW5	Bregman et al. (1986)
B16-BL6	Caltagirone et al. (2000); Murgo (1985)
A-375	Kunstfeld et al. (2003)
M21	Petitclerc et al. (1999)
Hs0294	Richmond et al. (1983)
Unspecified	Abe et al. (2004)
Ovarian Cancer	
SKOV-3	Juhl et al. (1997); Polato et al. (2005)
HRA	Nakata et al. (1998)
A2780	Polato et al. (2005)
IGROV-1	Polato et al. (2005)
HCT-116	Polato et al. (2005)
MA148	Yokoyama et al. (2000)
Pancreatic Cancer	
PC-1	Burke et al. (1997)
MIAPaCa-2	Ito et al. (1996); Kisfalvi et al. (2009)
PANC-1	Kisfalvi et al. (2009)
PancTu1	Vogler et al. (2009)
HPAC	Zervos et al. (1997)
Renal Cell Carcinoma	
786-O	Dhanabal et al. (1999); Lieubeau-Teillet et al. (1998)
ACHN	Huang et al. (2008)
A-498	Huang et al. (2008)
Caki-1	Inoue et al. (2001); Schirner et al. (1998) Shi and Siemann (2002)
SK-RC-29	Prewett et al. (1998)
Caki-2	Schirner et al. (1998)
Unspecified	Fujimoto et al. (1995)

Table A.1 Sources of Timescale Data by Type of Cancer and Cell Line

A.2 Results of Parameter Fittings

Individual data sets are labeled with the year and author, and given a unique identifier: either the label they were presented with in the figure from which the data originated, or the cell line that is used in the paper.

In some cases, the line representing the result of the parameter fitting is not visible. This happens for one of two reasons: a large difference between orders of magnitude in separate data sets, limiting the available space for data sets with smaller orders of magnitide; or because two or more data sets started with the same initial condition, causing the combined fitting result to produce the same curve. A complete list of all of the parameter fittings that are not visible, and the reason for why they cannot be seen, is given below:

- In the combined *in vitro* bladder cancer trials, the AS clustering and MM control trials of Miyake 2001 share an initial condition, hence only the MM control fitting is visible.
- In the combined *in vitro* breast cancer trials, the three Smith 2004 trials share the same initial condition, so the purple curve indicates the fitting to all three of these trials.
- In the combined *in vivo* breast cancer trials, the two Coopman 2000 trials share an initial condition, thus the green curve represents the fitting to both trials.
- In the combined *in vitro* colon cancer trials, the Moser and HCT116 trials have the same initial condition, so the green curve represents the combined fitting to both.
- In the combined *in vivo* colon cancer trials, two sets of trials have the same initial condition—the two Reinmuth 2002 trials and the two Warren 1995 trials. As a result, the orange curves account for both Reinmuth 2002 trials and the pink curves to both Warren 1995 trials.
- In the combined *in vivo* head and neck squamous cell carcinoma trials, the three Liu 1999 trials start with the same initial conditions, hence the teal curve represents the combined fitting to all three data sets.
- In the combined *in vitro* hepatocellular carcinoma trials, the Huynh 2008 trials share an initial condition, so the green curve represents the fitting to both data sets.

- In the combined *in vivo* hepatocellular carcinoma trials, the Liu 2005 data sets have the same initial condition, so the teal curve indicates the fitting to both data sets.
- In the individual *in vitro* lung cancer trials, Fig. 4D from Fabbri 2005 was cropped from the graph because it was two orders of magnitude higher than the next largest tumor, making the other 12 trials impossible to distinguish. Despite its exclusion here, it was used in the fitting analysis.
- In the combined *in vitro* lung cancer trials, not only is Fig. 4D from Fabbri 2005 excluded, but several trials from the same study have the same initial conditions (*i.e.*, the four visible Fabbri 2005 trials, SW-900 and A549 from Esquela-Kerscher, and all three Fujiwara trials.) For this figure, the seafoam green curve is the fit for all 4 visible Fabbri 2005 trials, the SW-900 and A549 trials from Esquela-Kerscher are both represented by the yellow curve, and all three Fujiwara trials are represented by the purple curve. Additionally, for the Von Bertalanffy fitting, the data sets from Fujiwara 1993 and Takahashi 1992 are hidden by Fig. 3 from Tsubouchi 2000, presumably because their initial conditions are sufficiently close to each other.
- In the *in vivo* melanoma trials, the Boucherke 1989 trial is difficult to see because of its relatively low order of magnitude, but is visible along the bottom of the graphs.
- In the combined *in vitro* ovarian cancer trials, the A2780 and SKOV-3 trials have the same initial condition, and the IGROV-1 and HCT-116 trials have the same initial condition. As a result, the green curve represents the fitting to the first two trials, and the purple curve is the fitting to the last two trials.

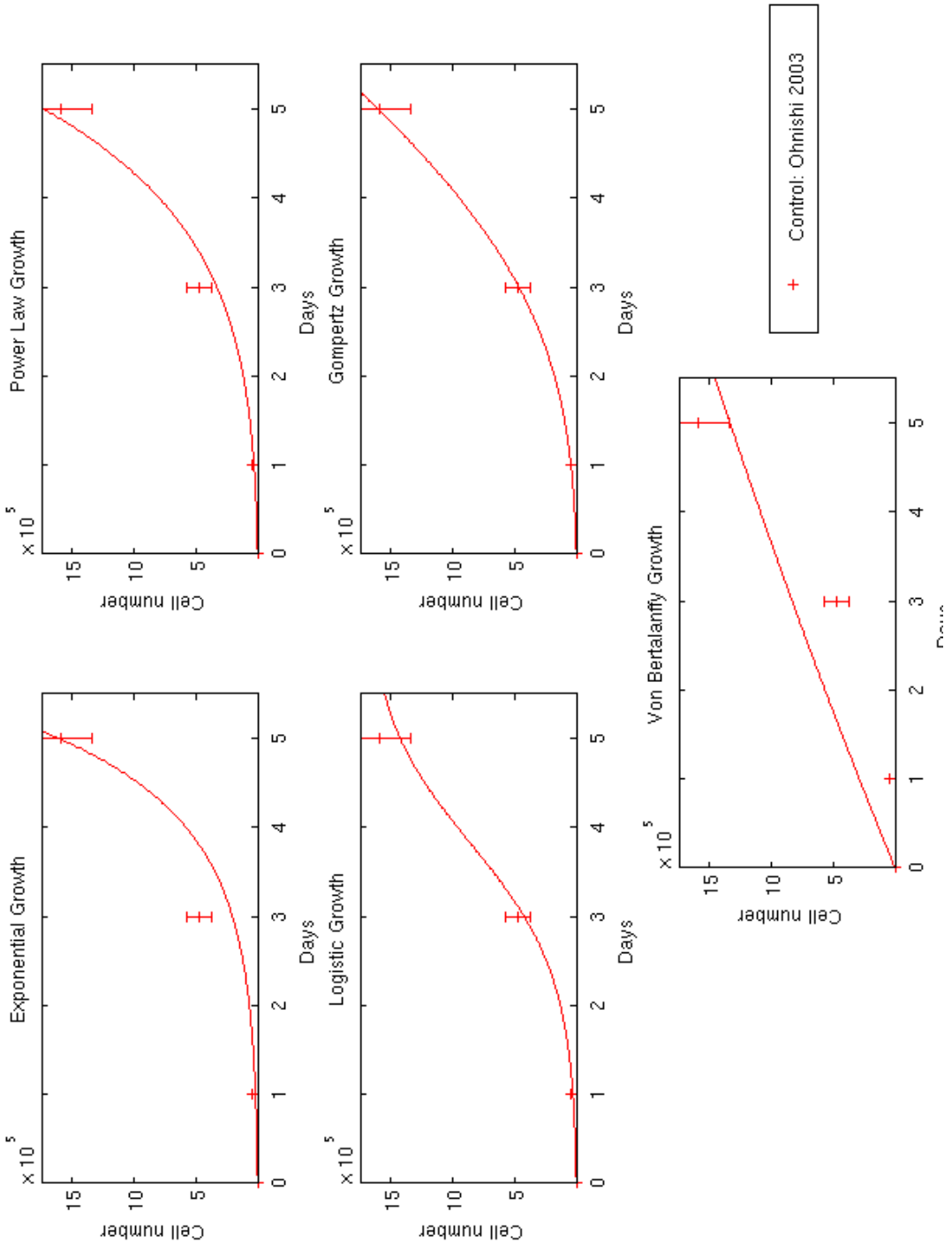

Figure A.1 Parameter Fittings to *In Vitro* Bladder Cancer Trials

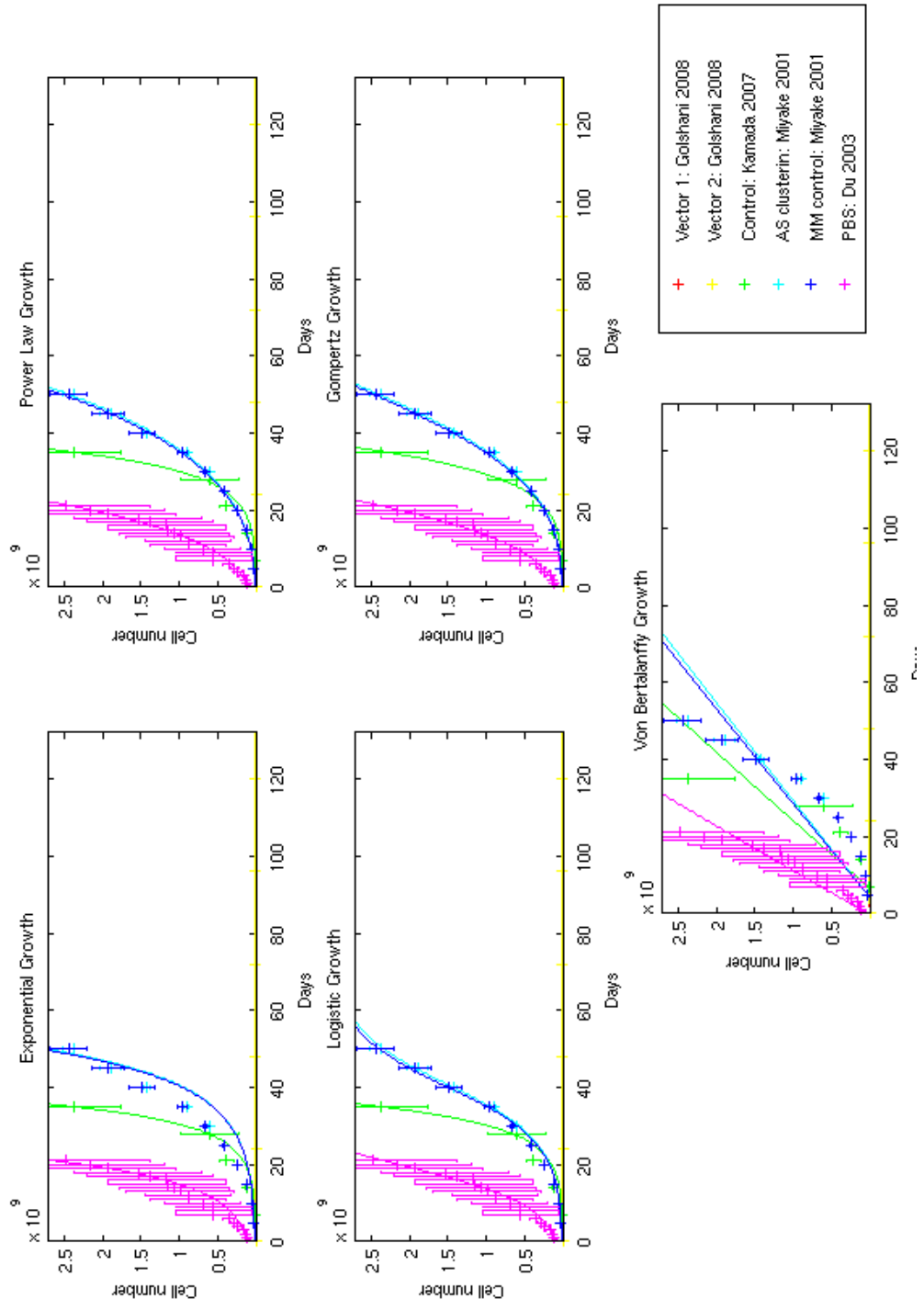

Figure A.2 Parameter Fittings to Individual *In Vivo* Bladder Cancer Trials

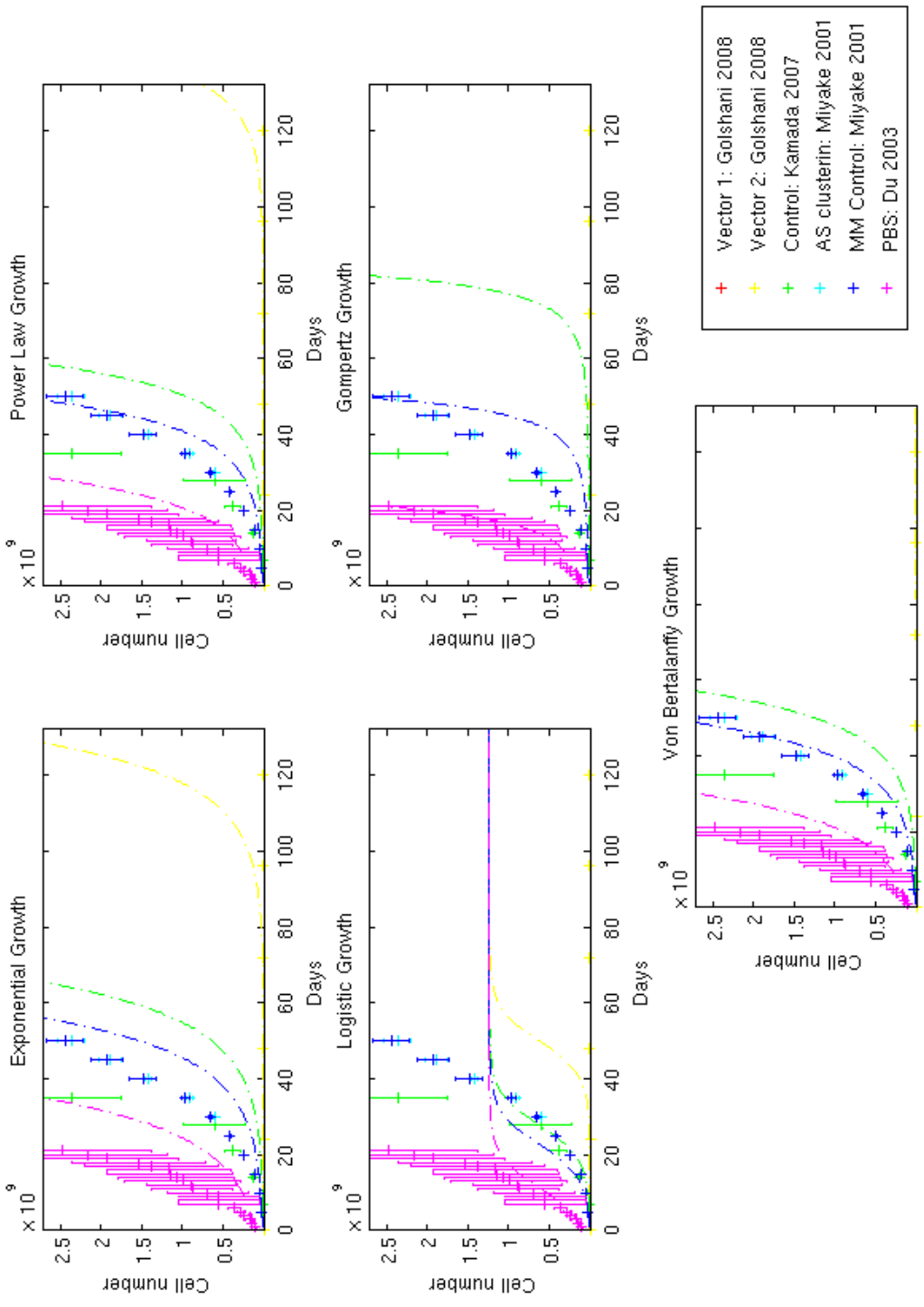

Figure A.3 Parameter Fitting to Combined *In Vivo* Bladder Cancer Trials

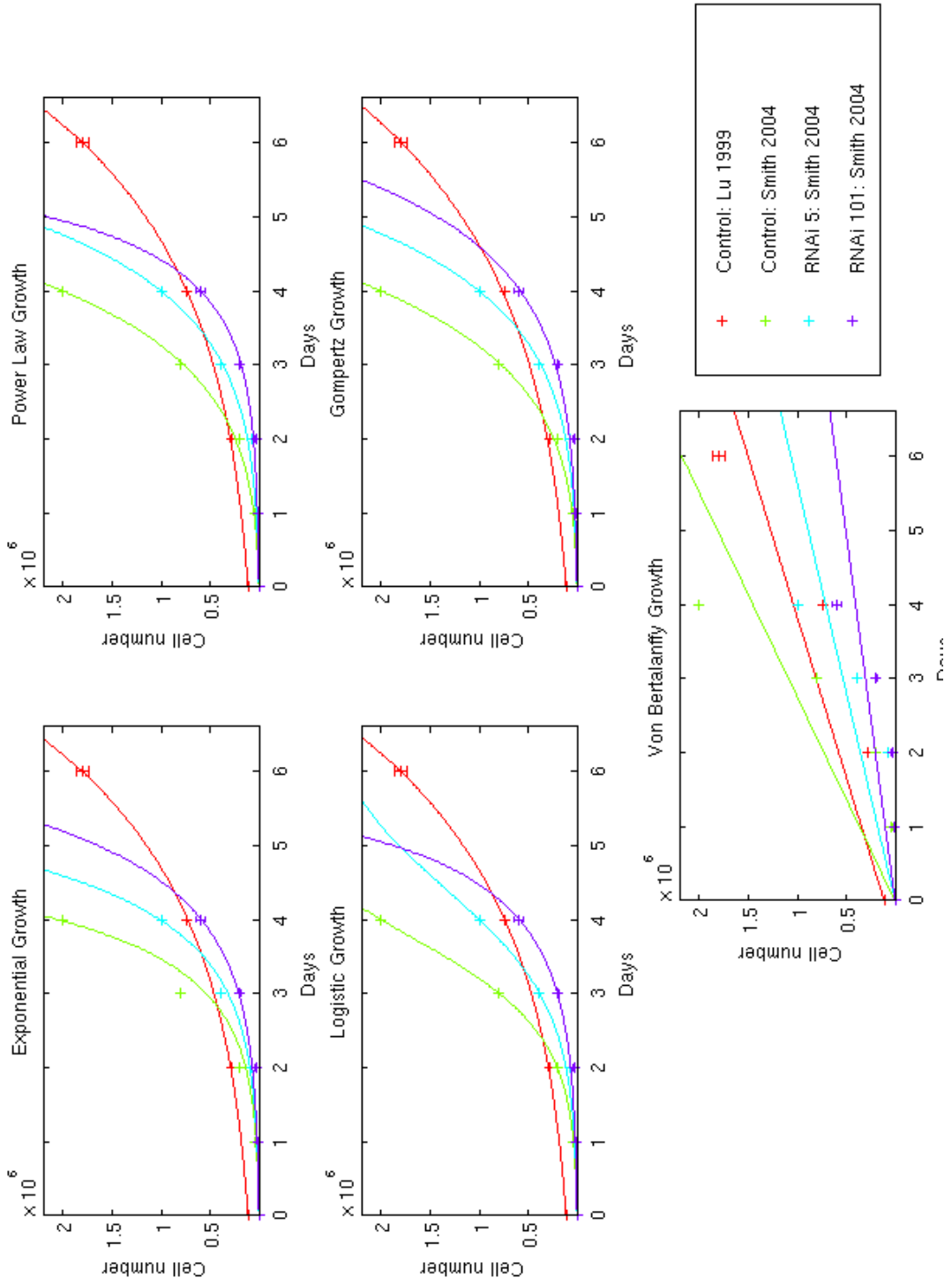

Figure A.4 Parameter Fittings to Individual *In Vitro* Breast Cancer Trials

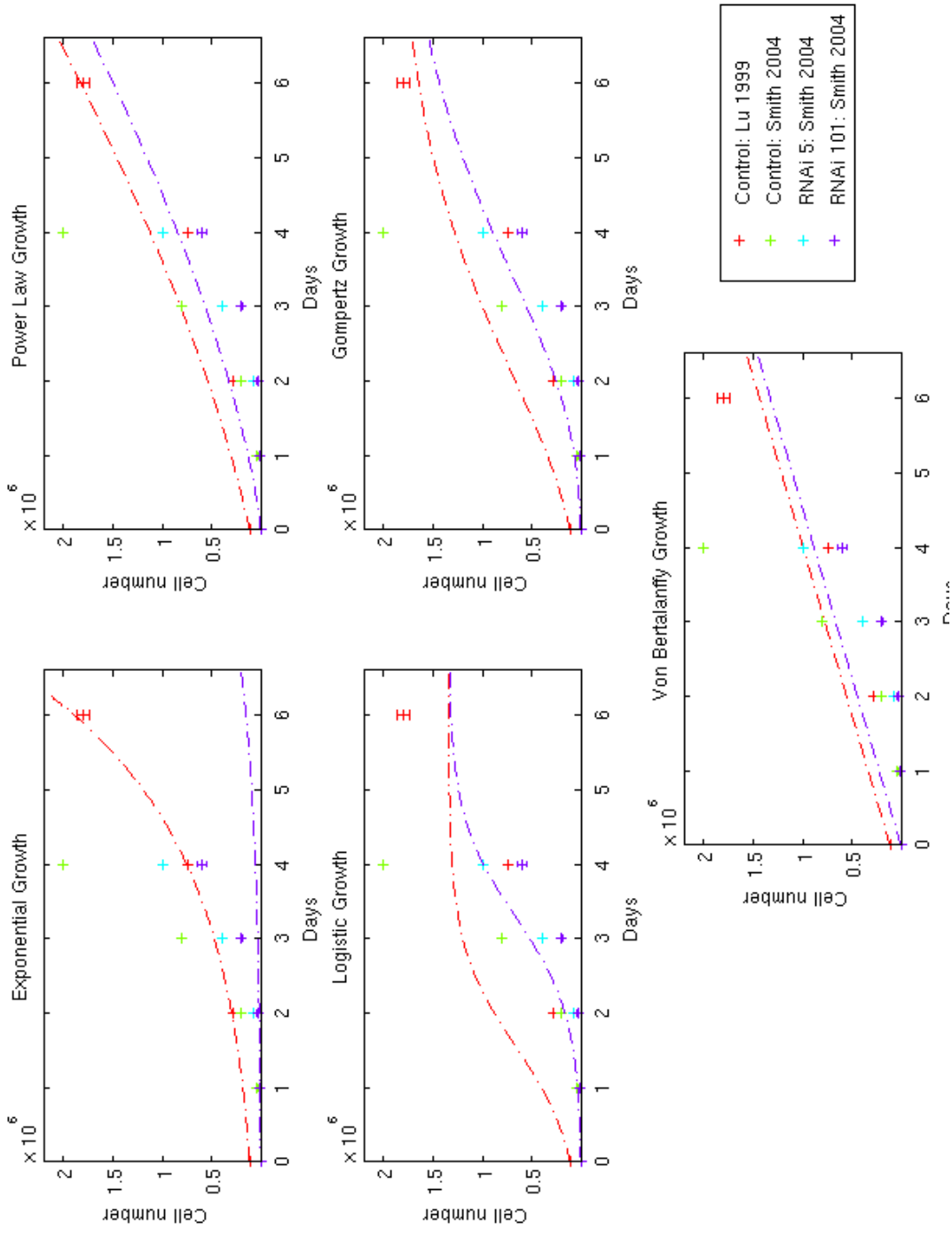

Figure A.5 Parameter Fitting to Combined *In Vitro* Breast Cancer Trials

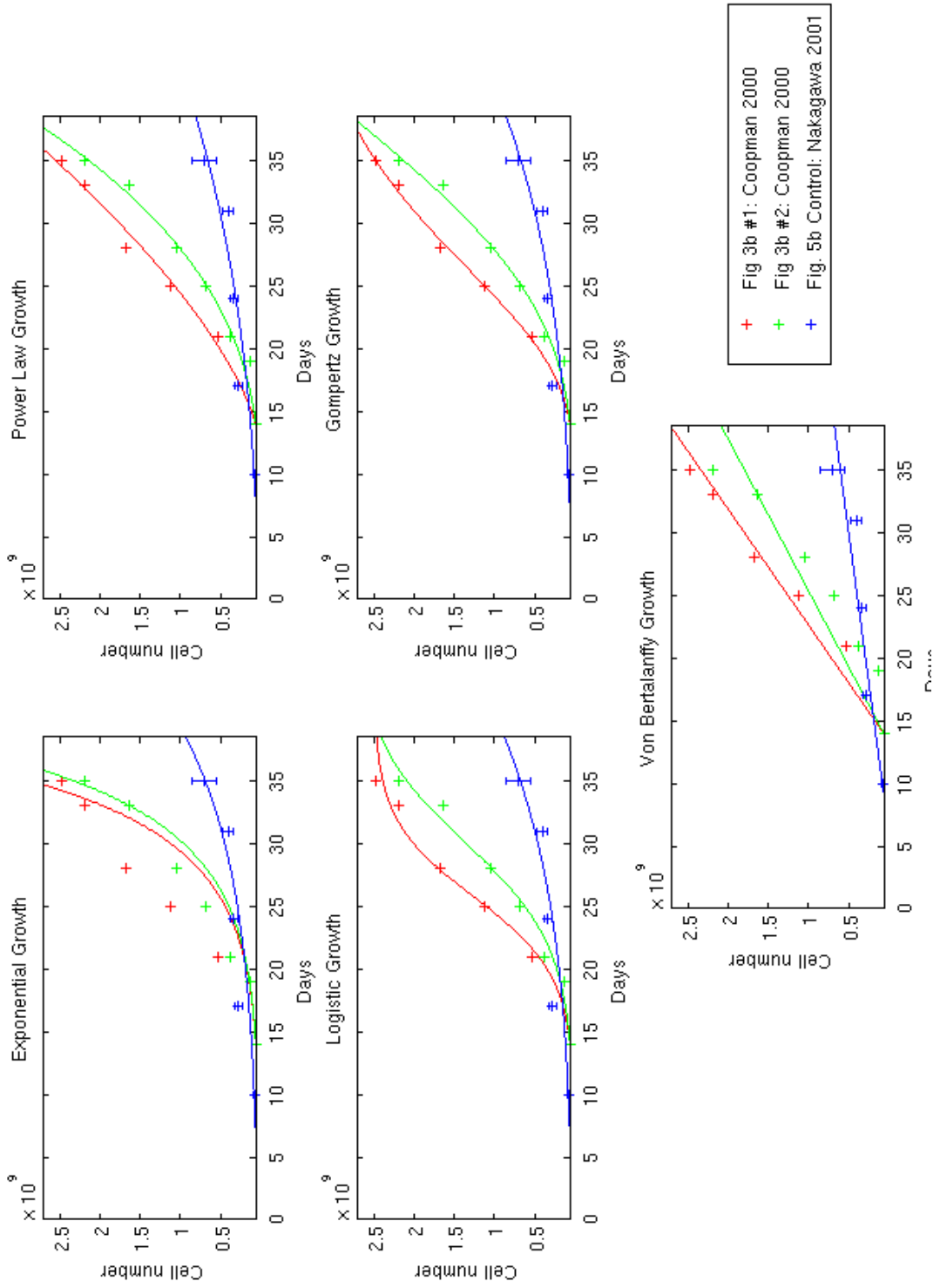

Figure A.6 Parameter Fittings to Individual *In Vivo* Breast Cancer Trials

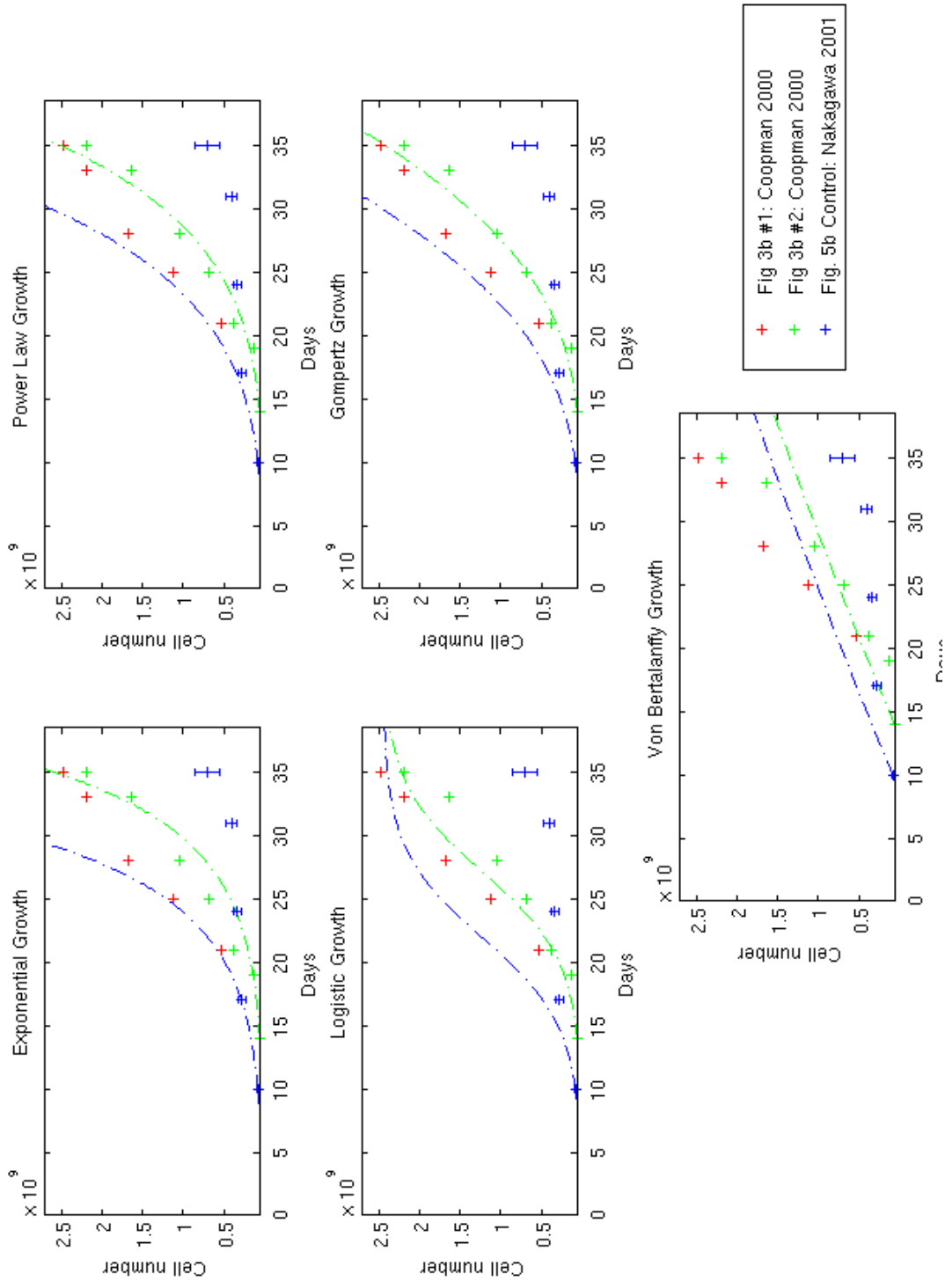

Figure A.7 Parameter Fitting to Combined *In Vivo* Breast Cancer Trials

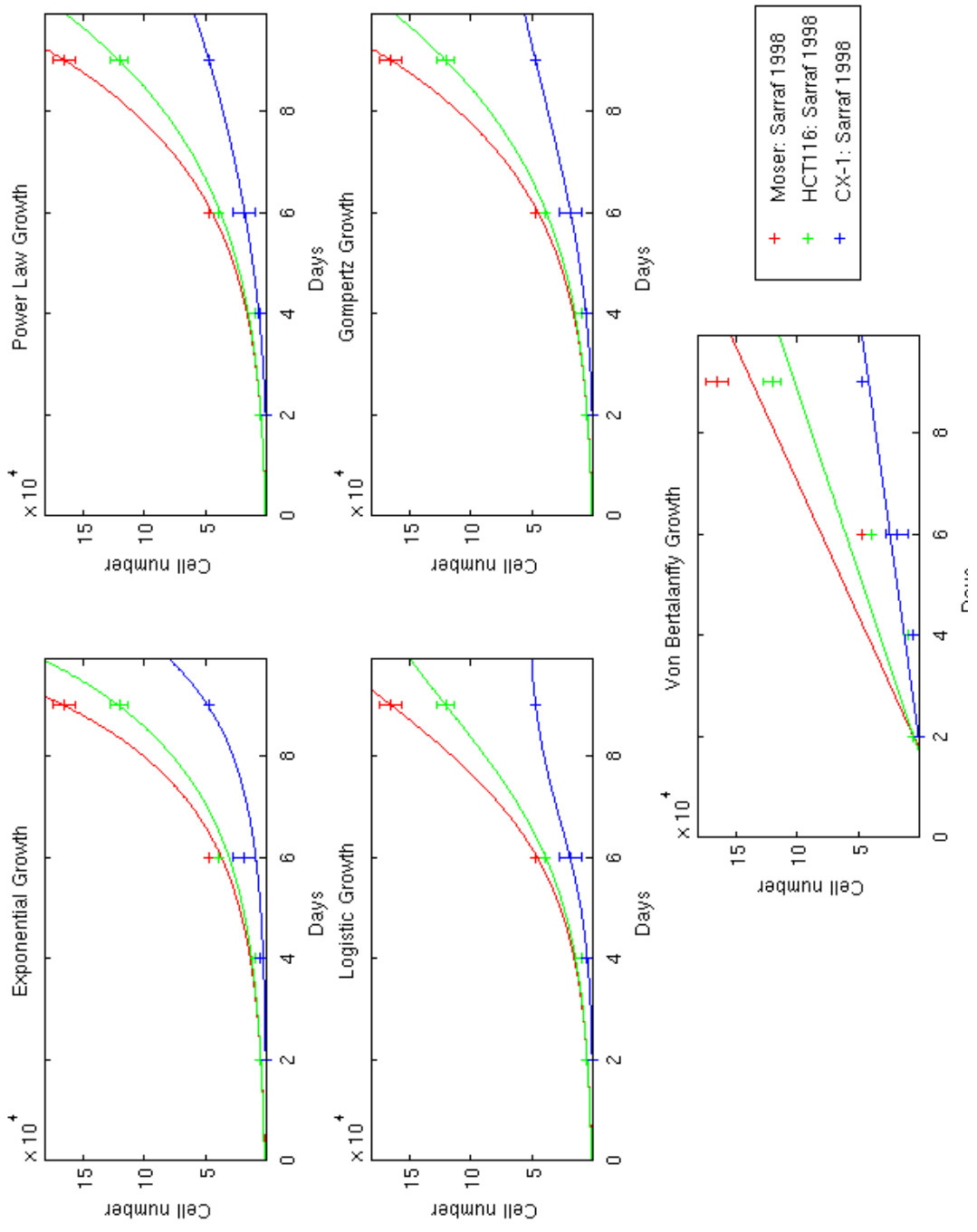

Figure A.8 Parameter Fittings to Individual *In Vitro* Colon Cancer Trials

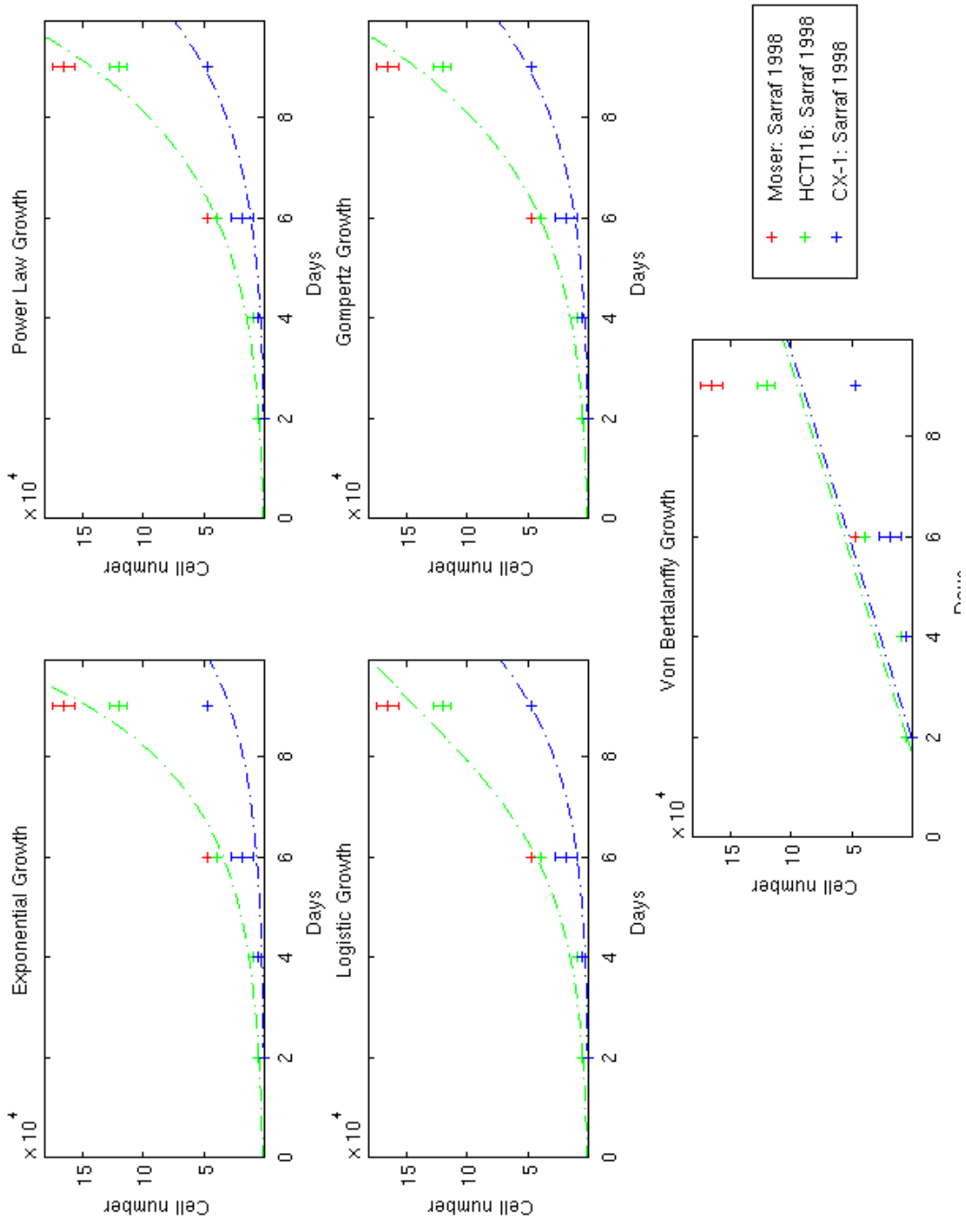

Figure A.9 Parameter Fitting to Combined *In Vitro* Colon Cancer Trials

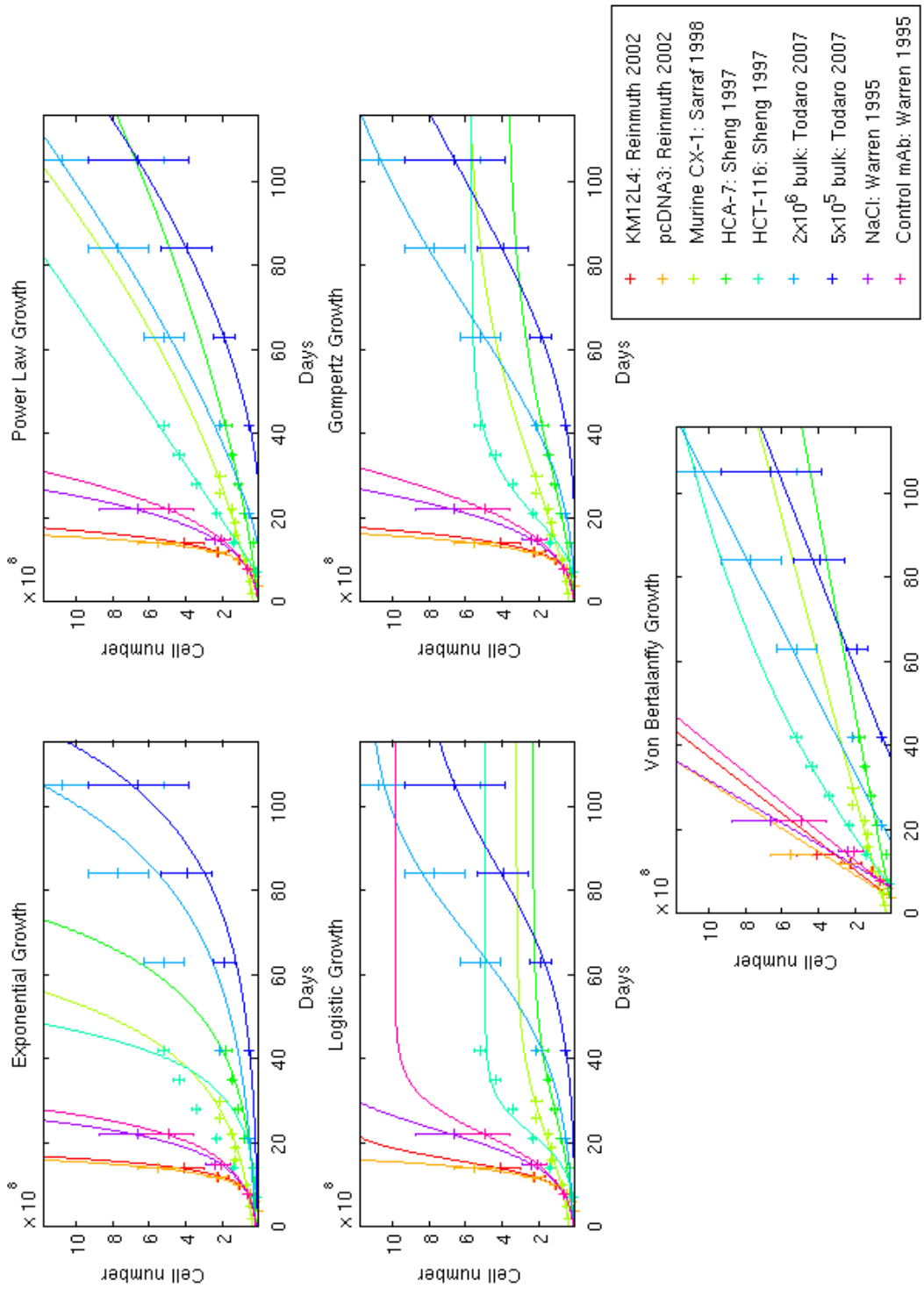

Figure A.10 Parameter Fittings to Individual *In Vivo* Colon Cancer Trials

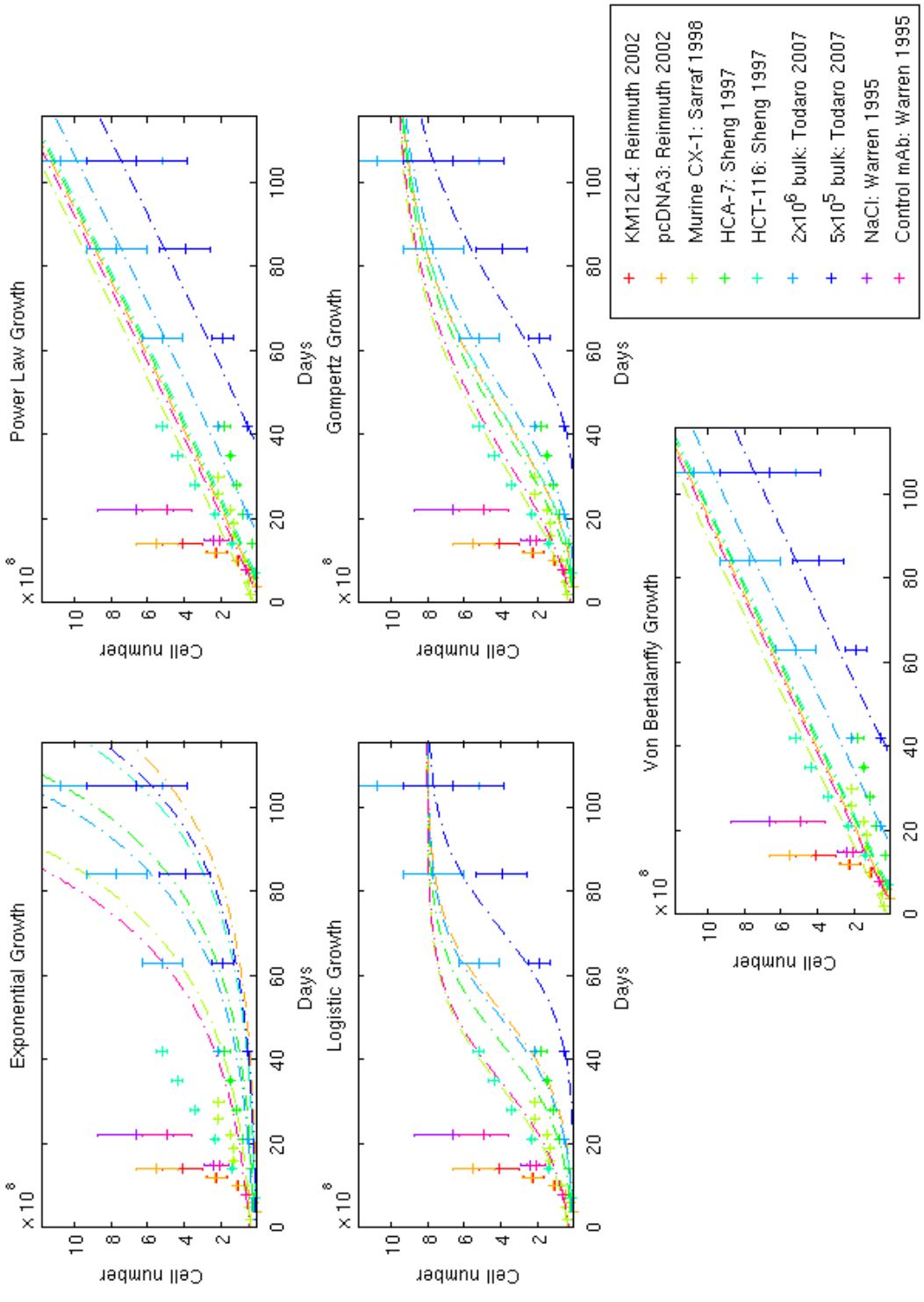

Figure A.11 Parameter Fitting to Combined *In Vivo* Colon Cancer Trials

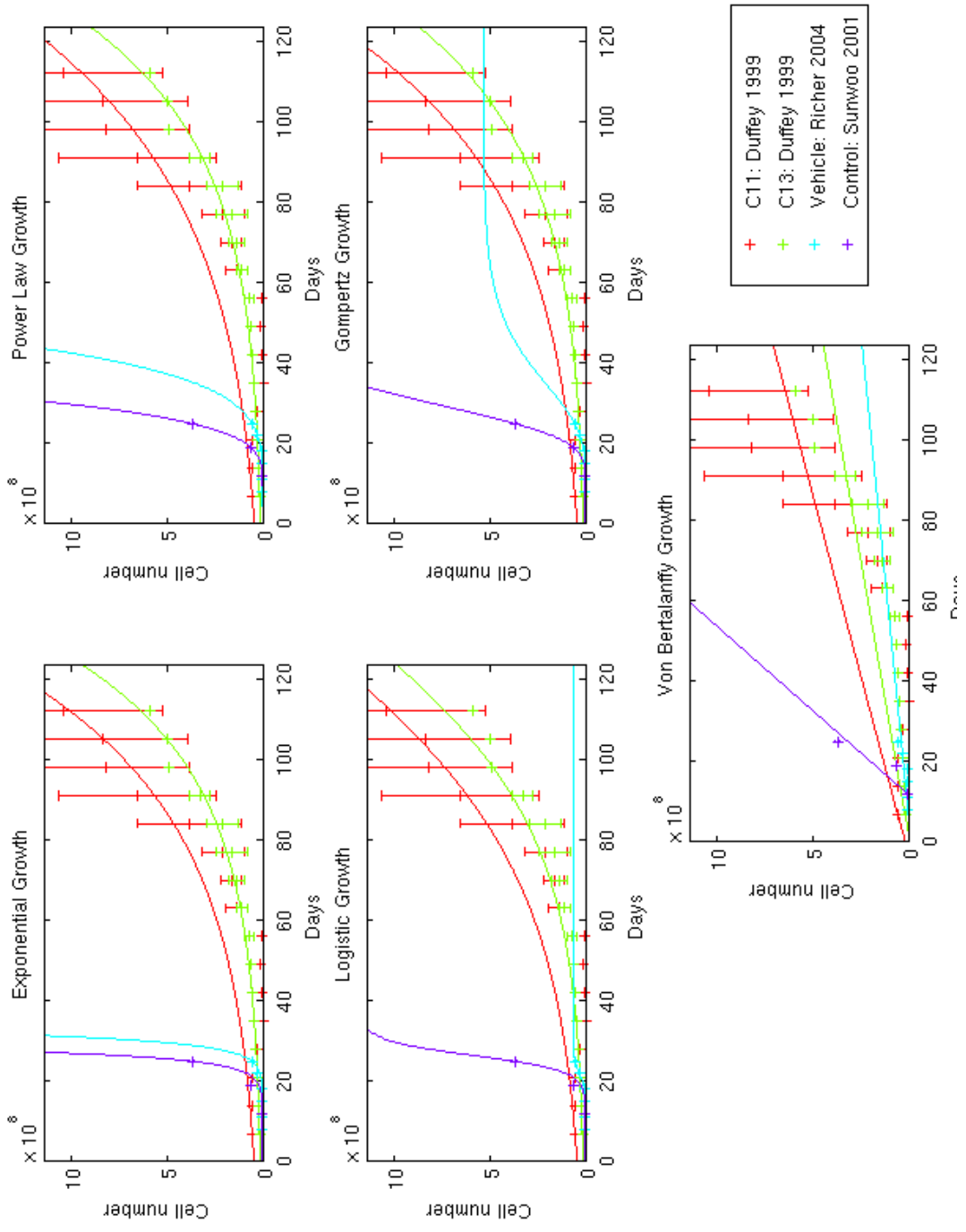

Figure A.12 Parameter Fittings to Individual *In Vitro* Head and Neck Squamous Cell Carcinoma Trials

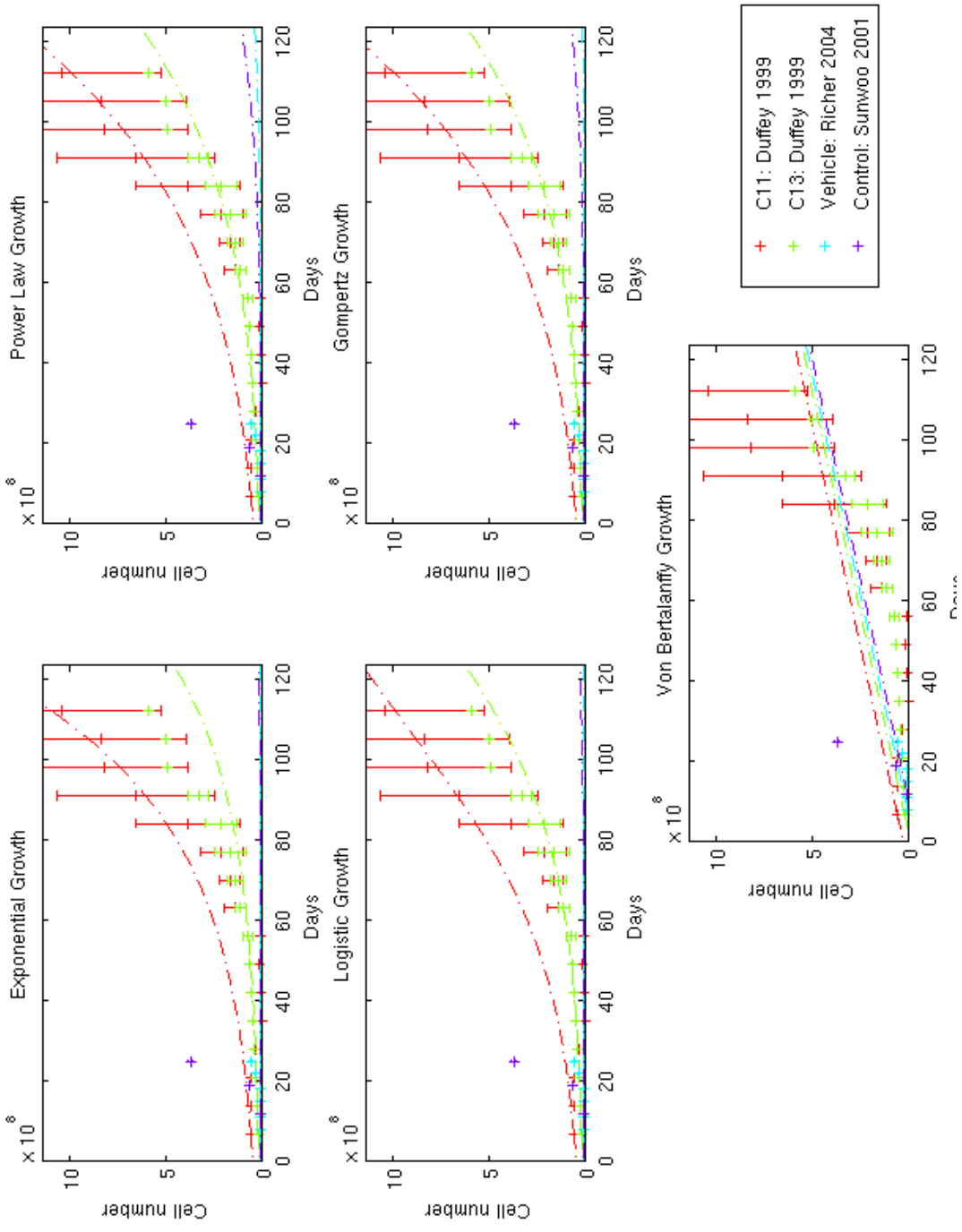

Figure A.13 Parameter Fitting to Combined *In Vitro* Head and Neck Squamous Cell Carcinoma Trials

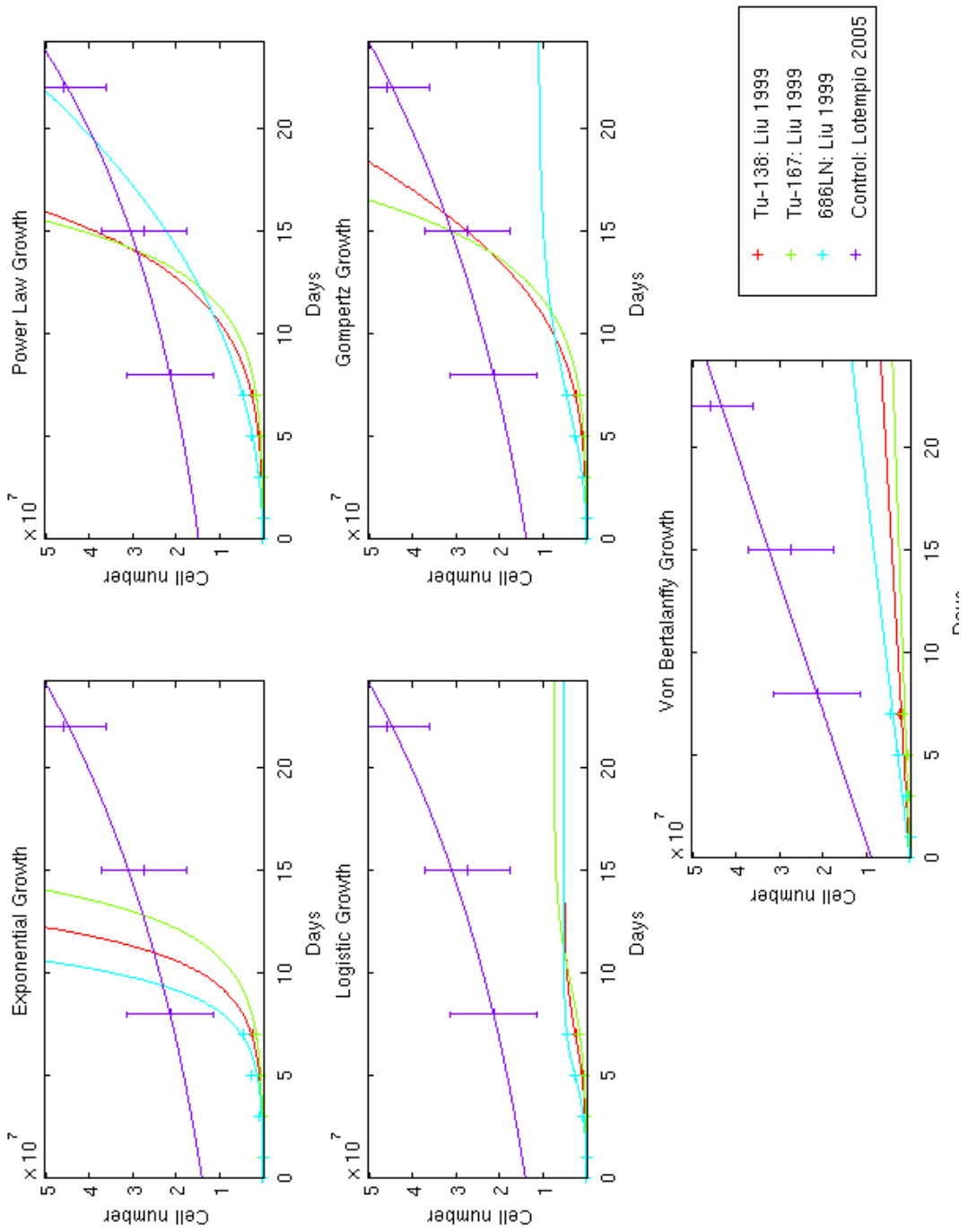

Figure A.14 Parameter Fittings to Individual *In Vivo* Head and Neck Squamous Cell Carcinoma Trials

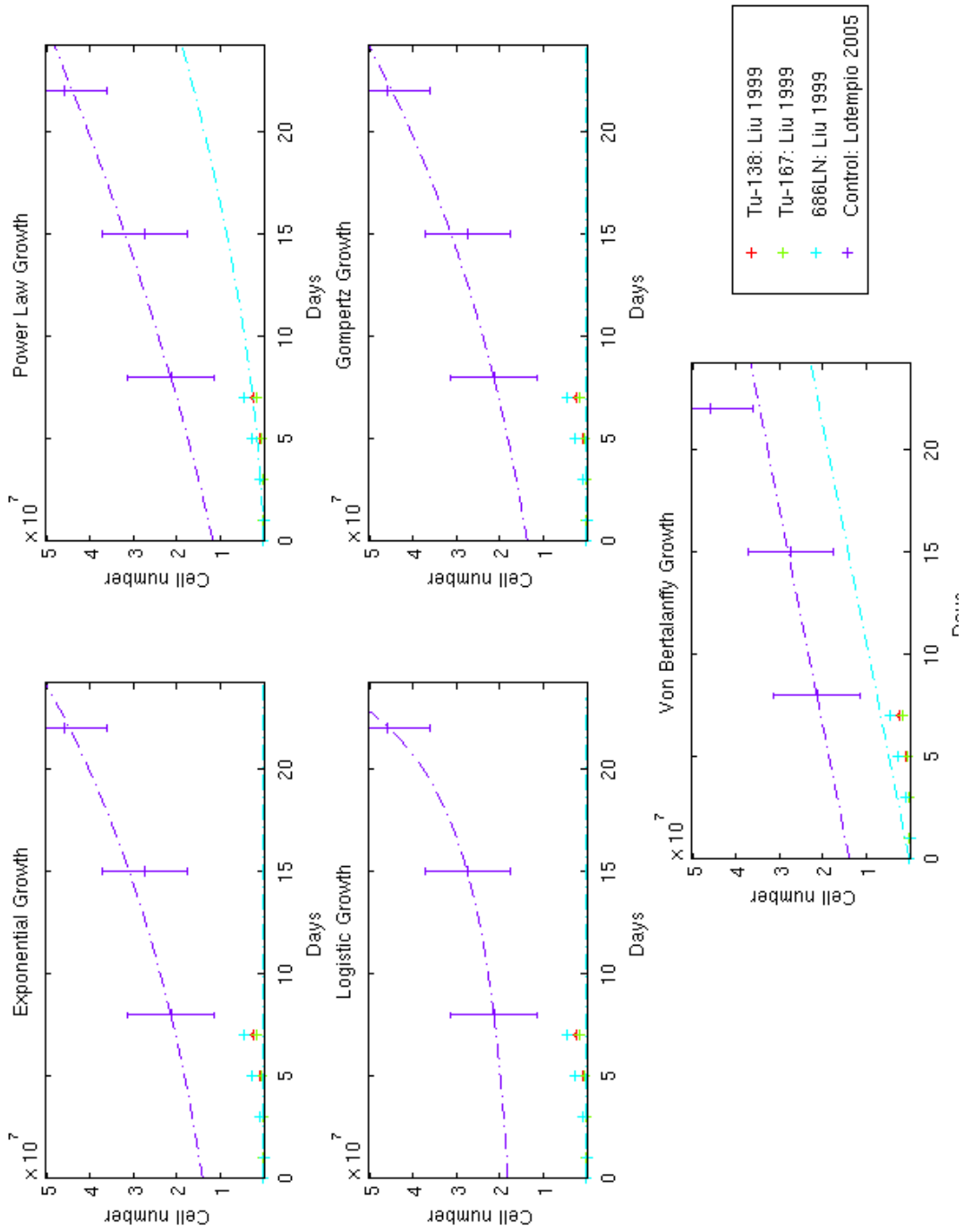

Figure A.15 Parameter Fitting to Combined *In Vivo* Head and Neck Squamous Cell Carcinoma Trials

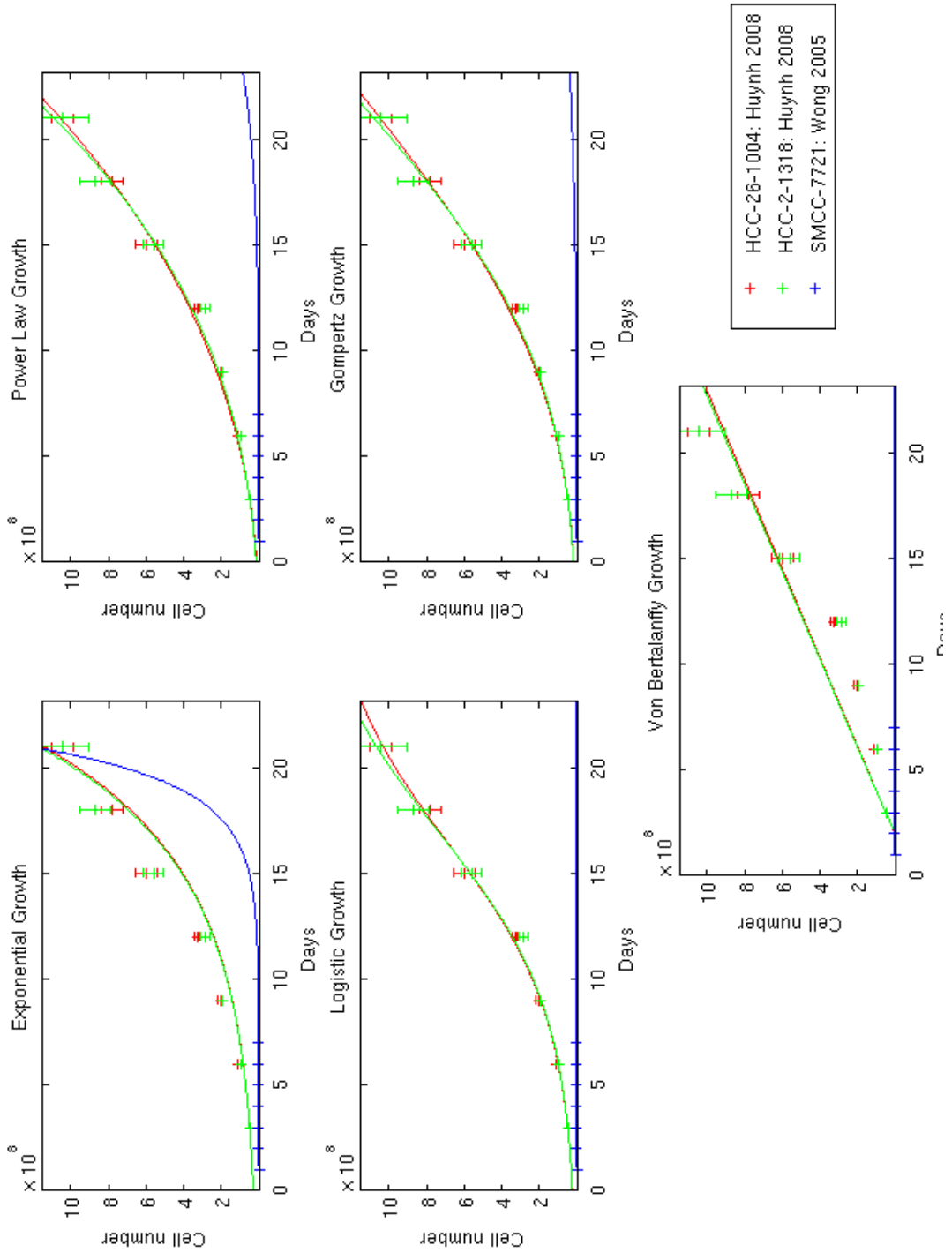

Figure A.16 Parameter Fittings to Individual *In Vitro* Hepatocellular Carcinoma Trials

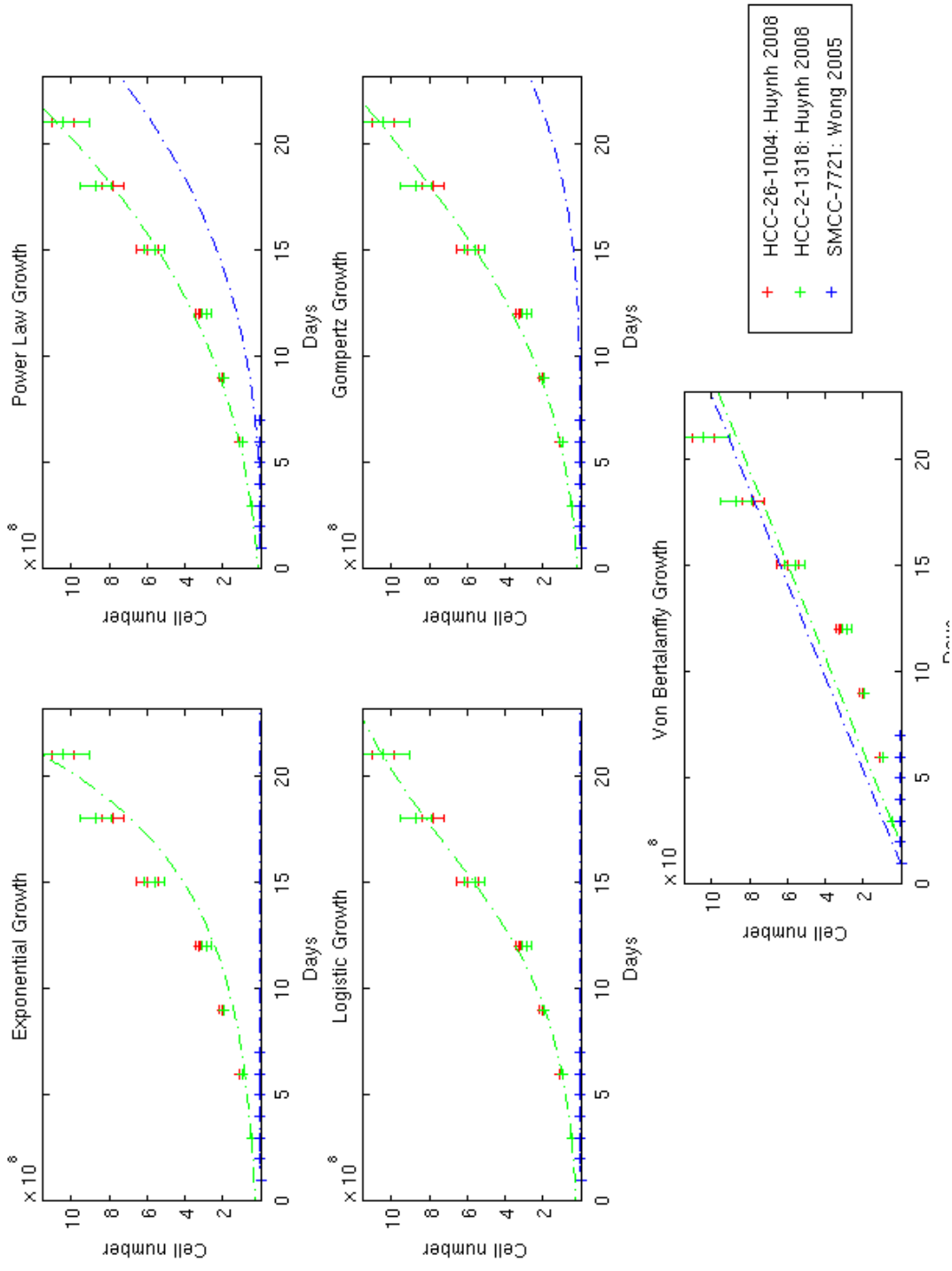

Figure A.17 Parameter Fitting to Combined *In Vitro* Hepatocellular Carcinoma Trials

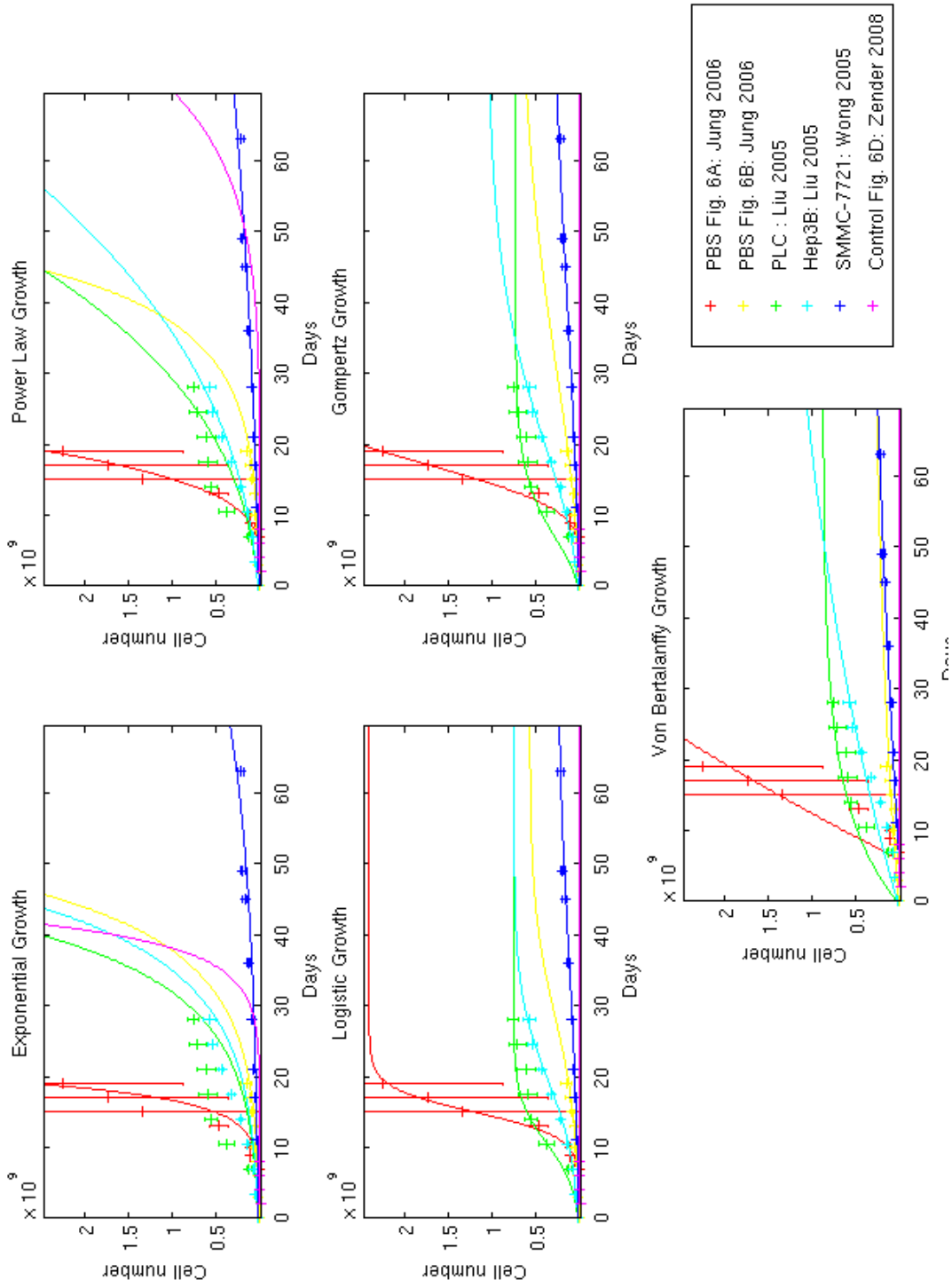

Figure A.18 Parameter Fittings to Individual *In Vivo* Hepatocellular Carcinoma Trials

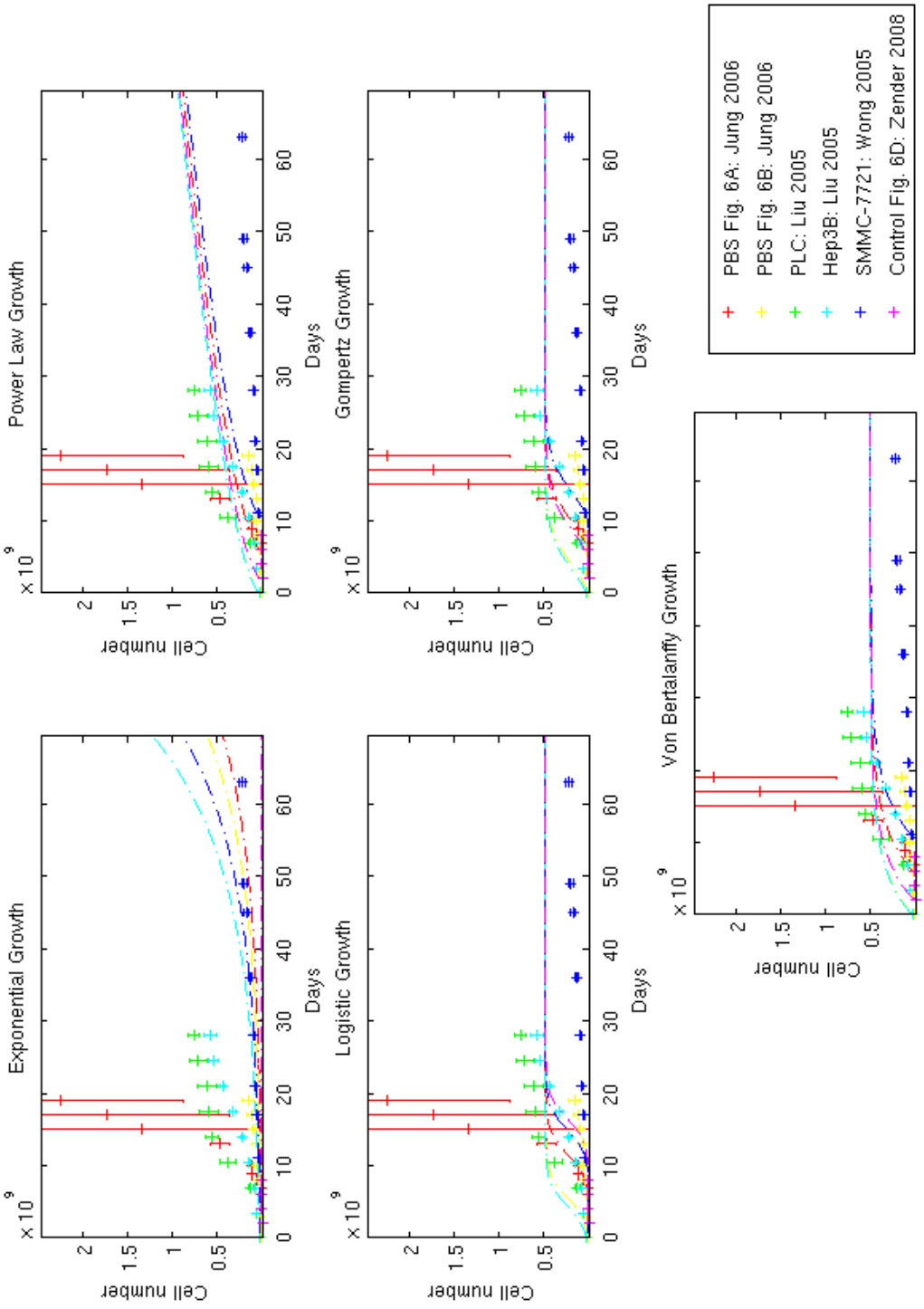

Figure A.19 Parameter Fitting to Combined *In Vivo* Hepatocellular Carcinoma Trials

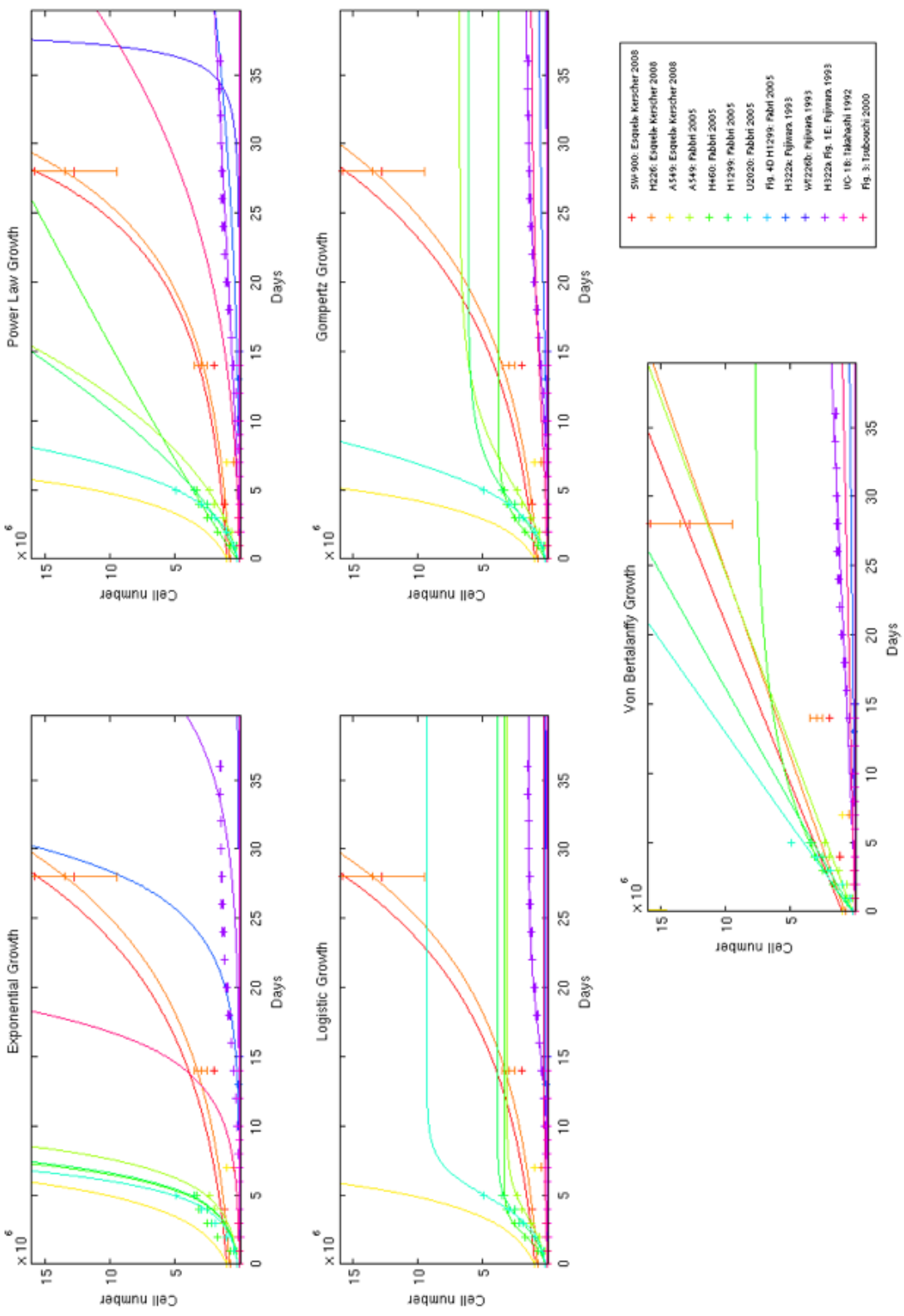

Figure A.20 Parameter Fittings to Individual *In Vitro* Lung Cancer Trials

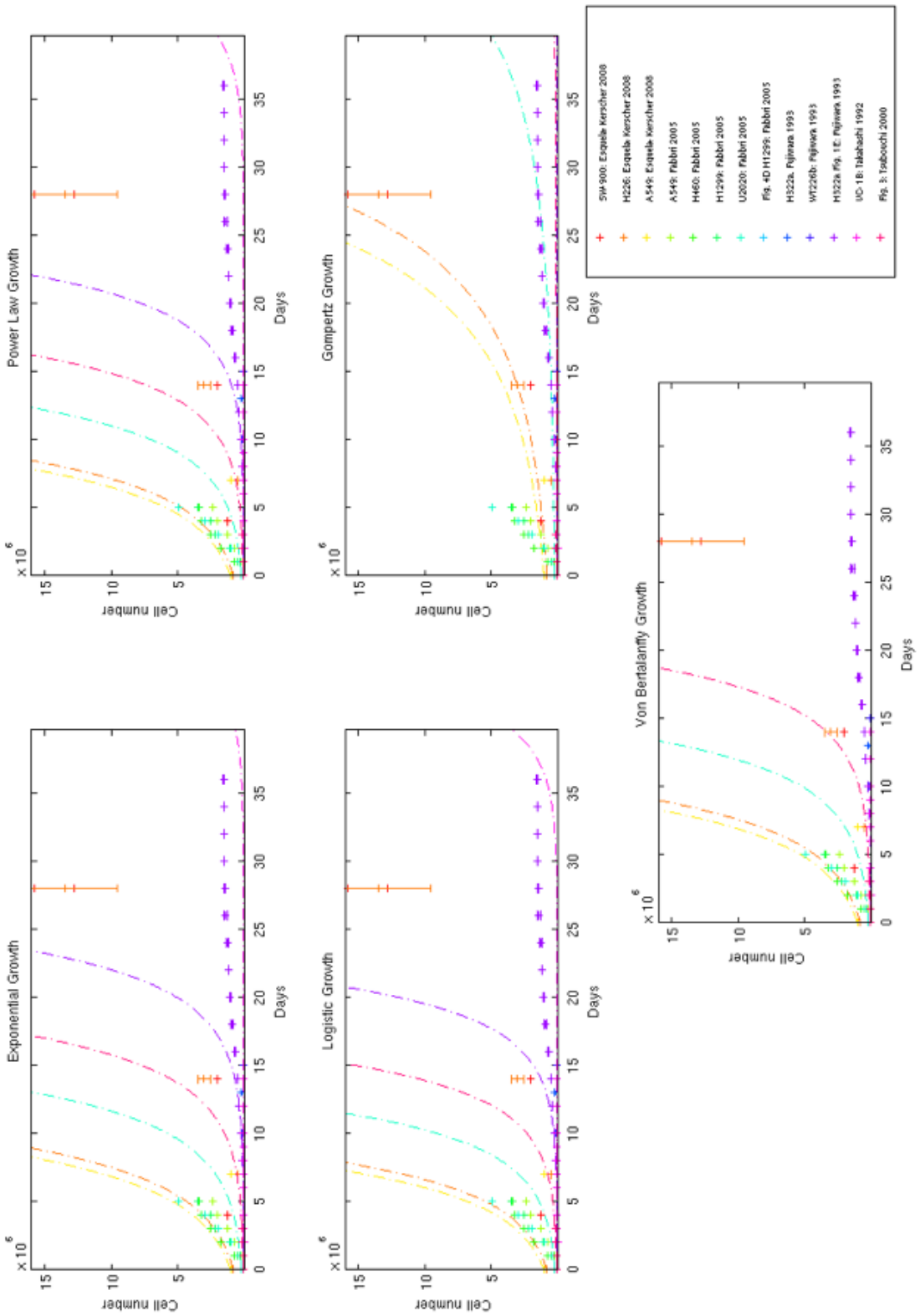

Figure A.21 Parameter Fitting to Combined *In Vitro* Lung Cancer Trials

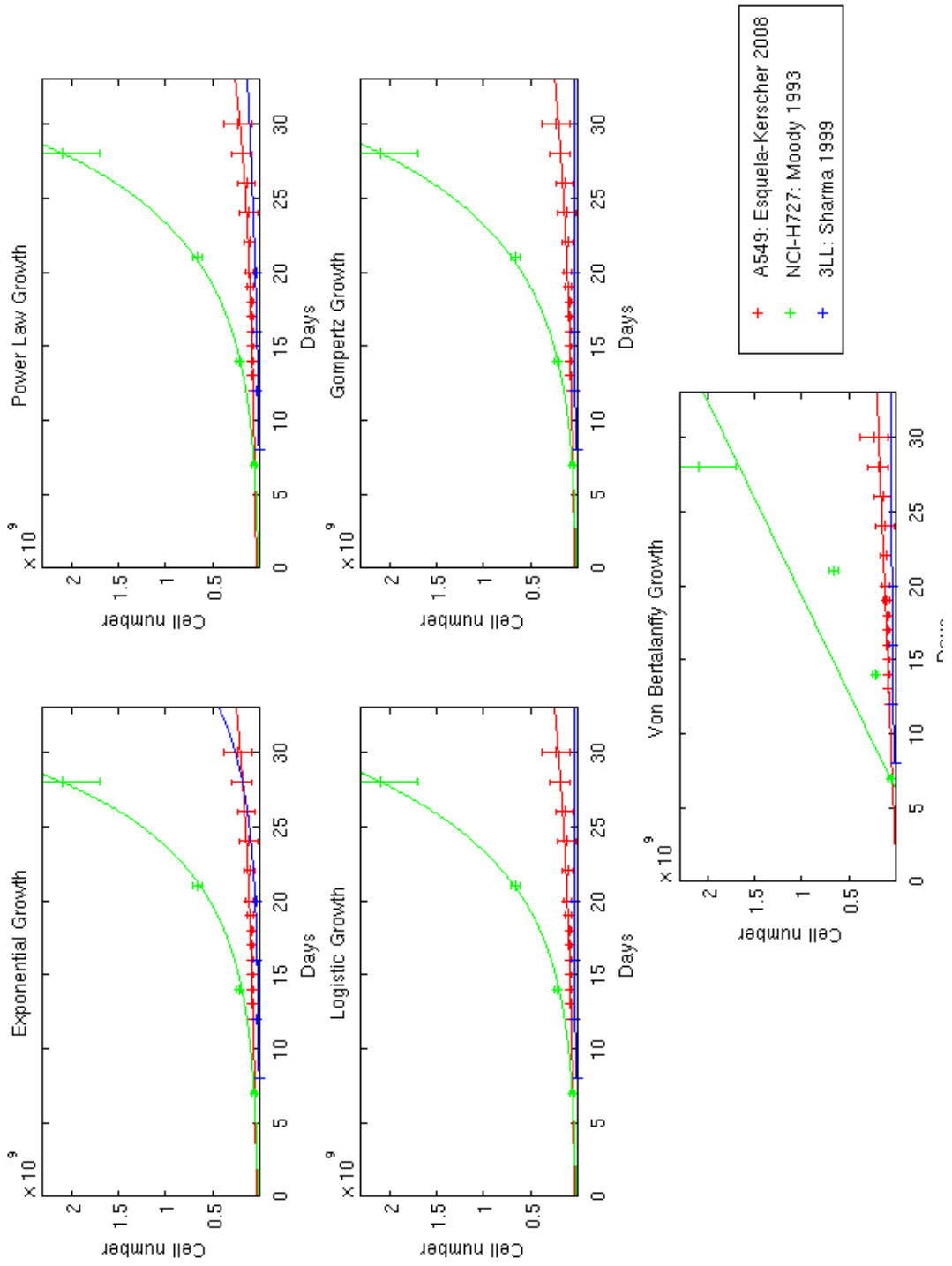

Figure A.22 Parameter Fittings to Individual *In Vivo* Lung Cancer Trials

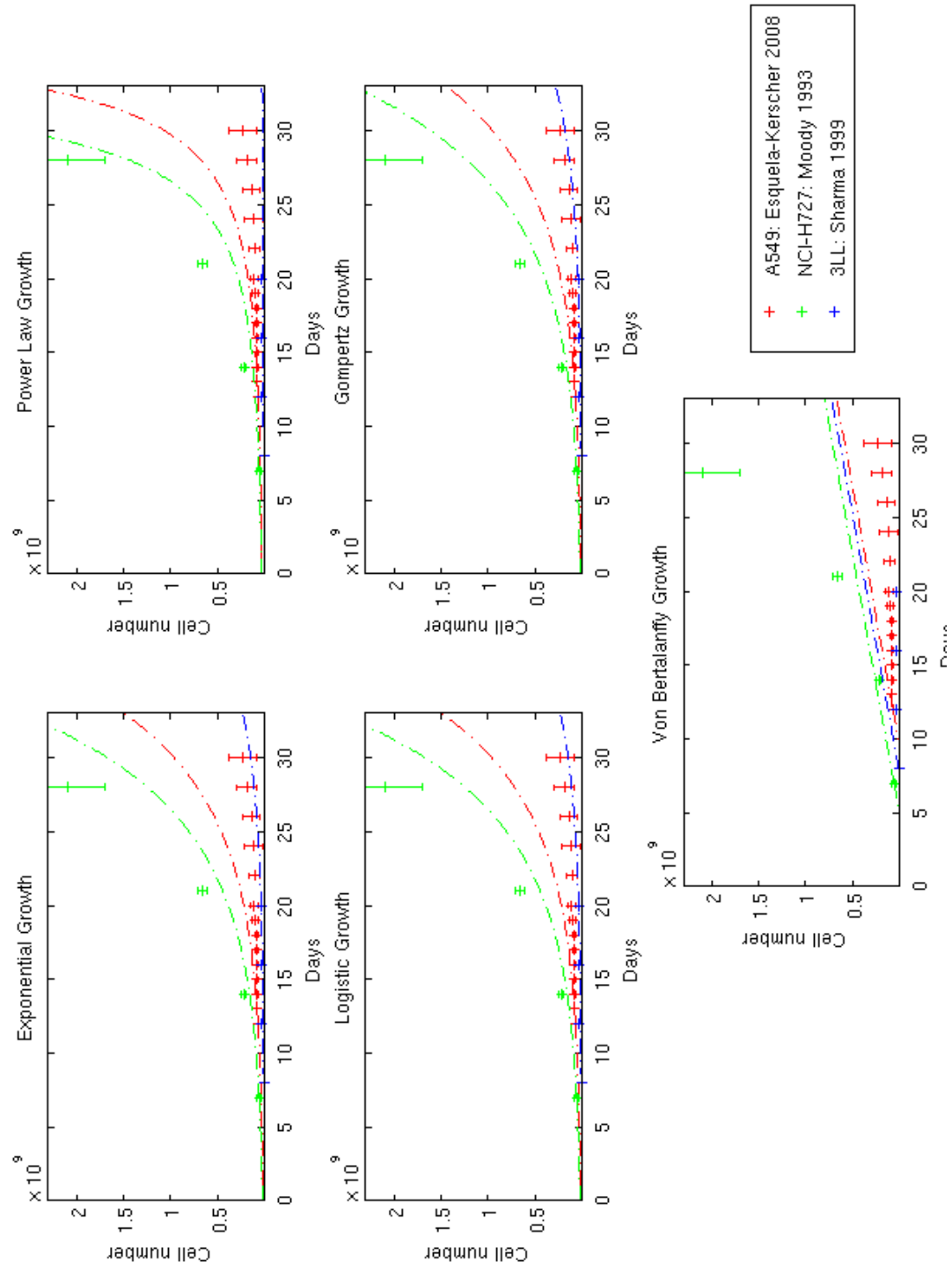

Figure A.23 Parameter Fitting to Combined *In Vivo* Lung Cancer Trials

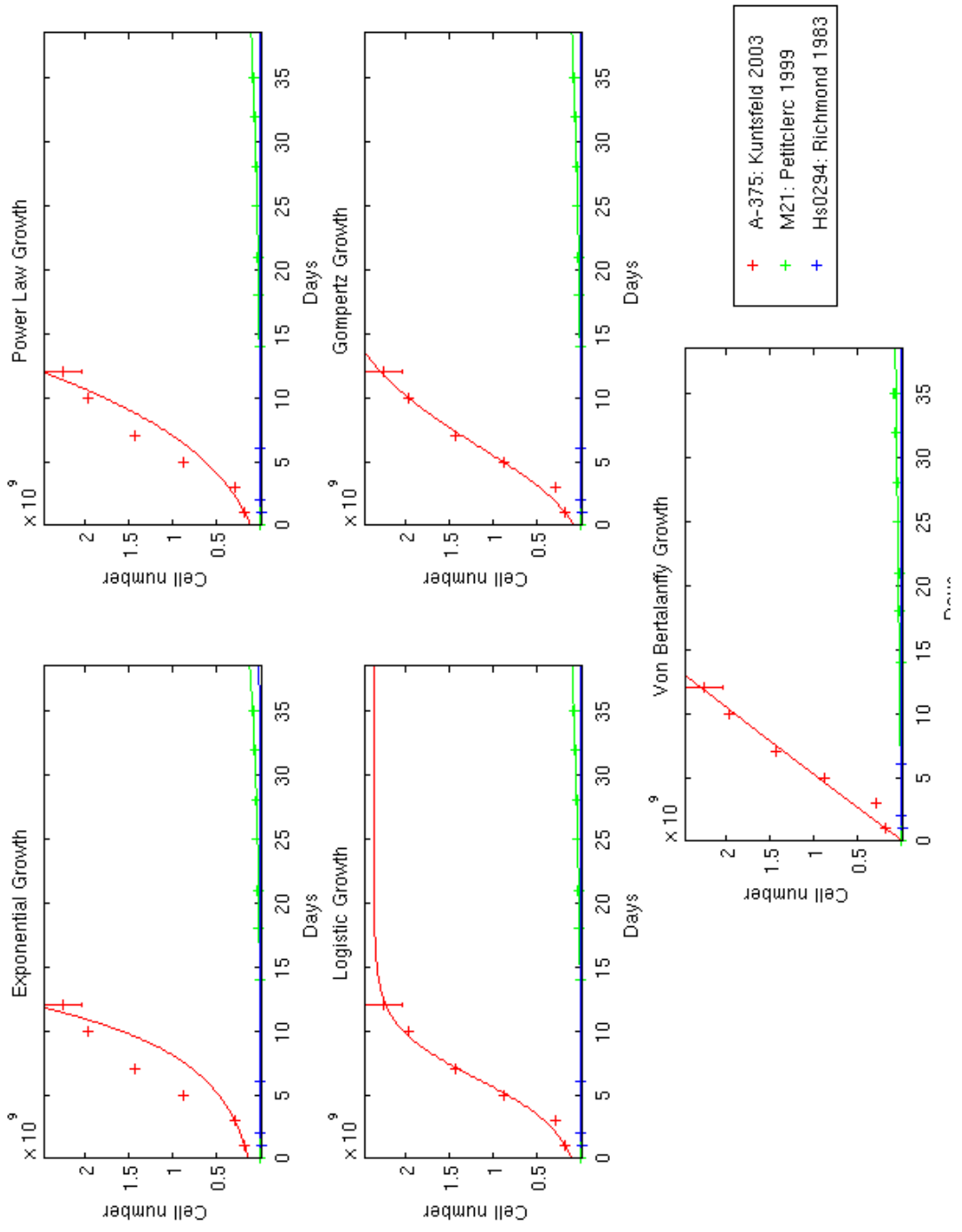

Figure A.24 Parameter Fittings to Individual *In Vitro* Melanoma Trials

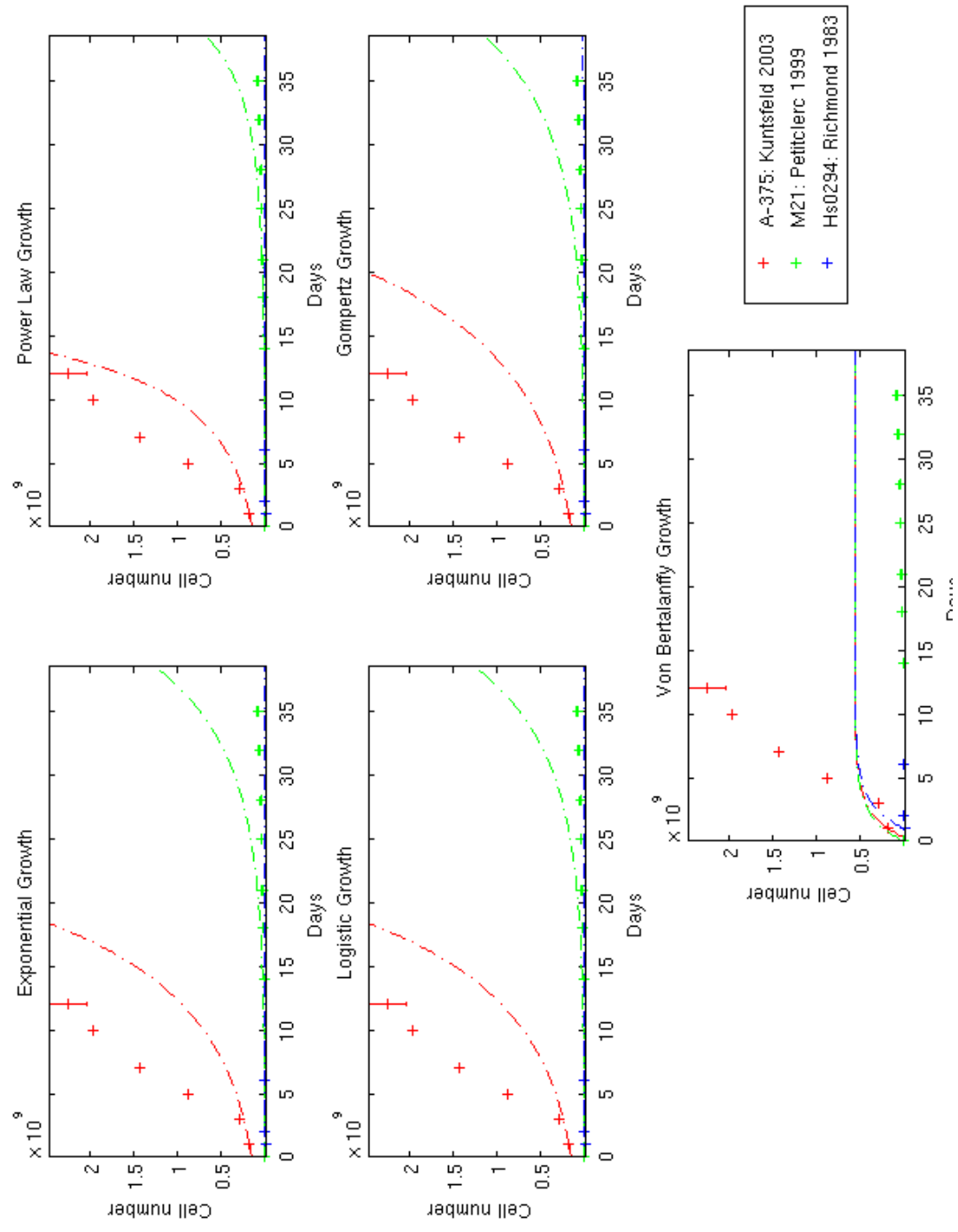

Figure A.25 Parameter Fitting to Combined *In Vitro* Melanoma Trials

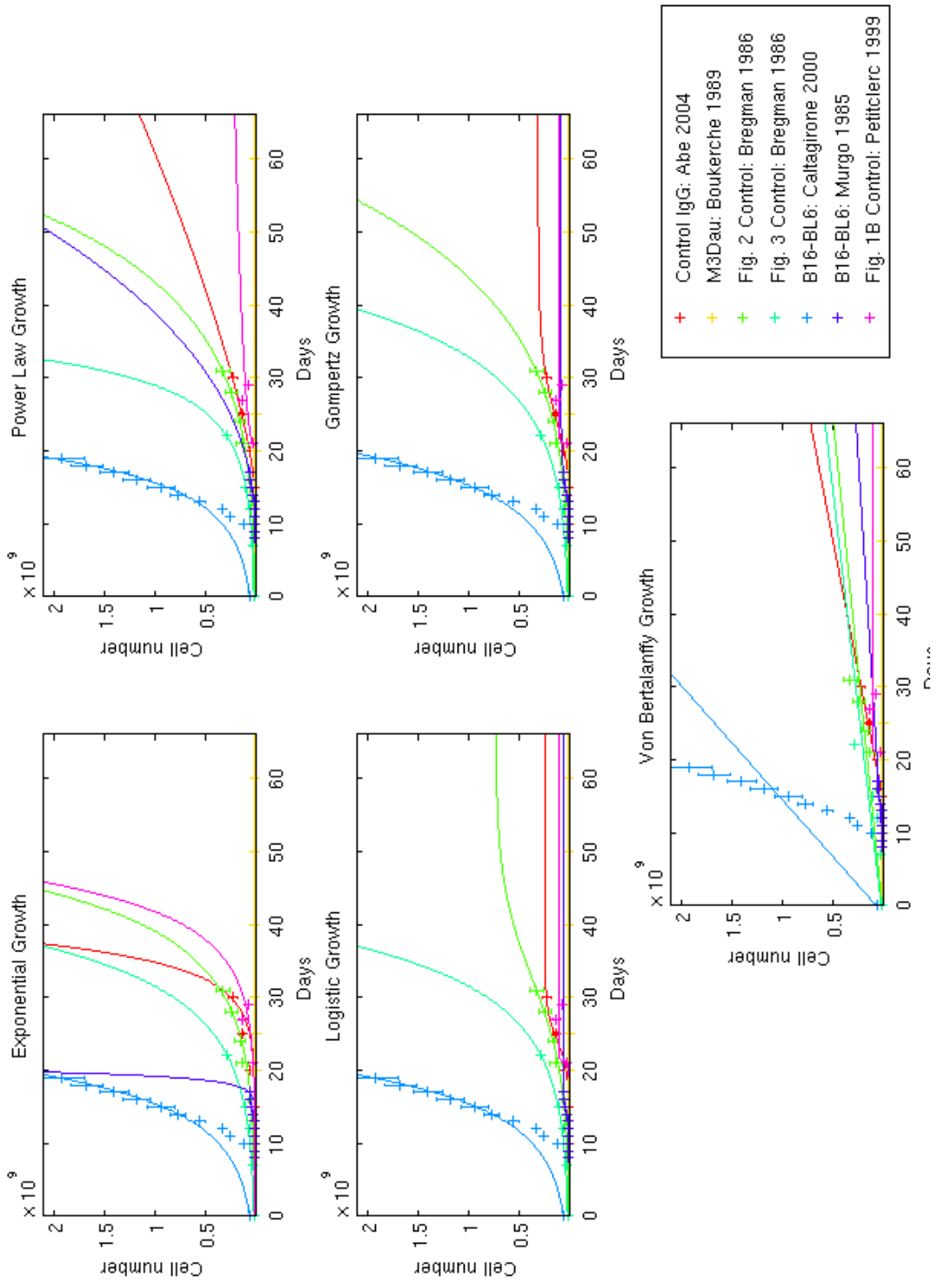

Figure A.26 Parameter Fittings to Individual *In Vivo* Melanoma Trials

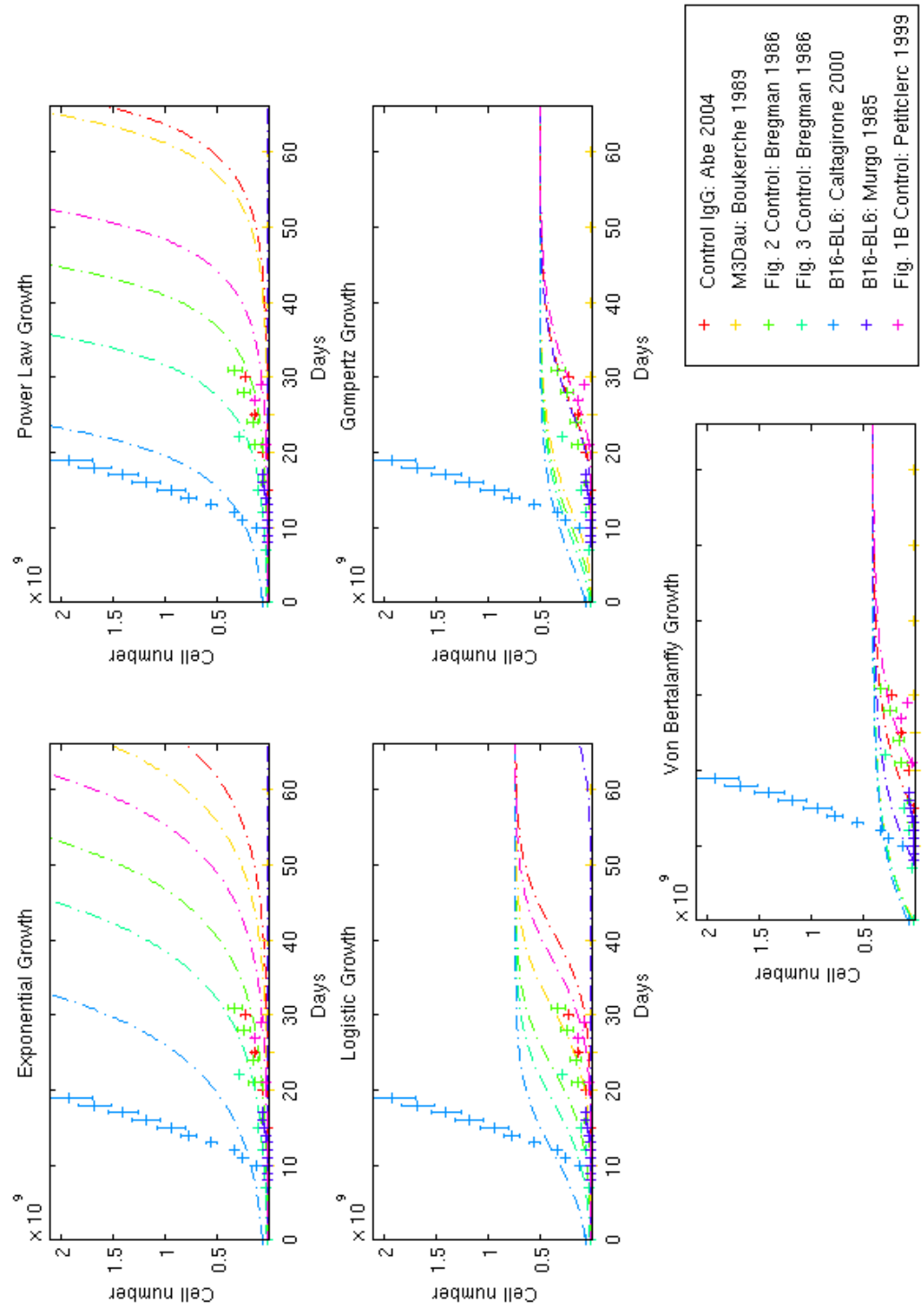

Figure A.27 Parameter Fitting to Combined *In Vivo* Melanoma Trials

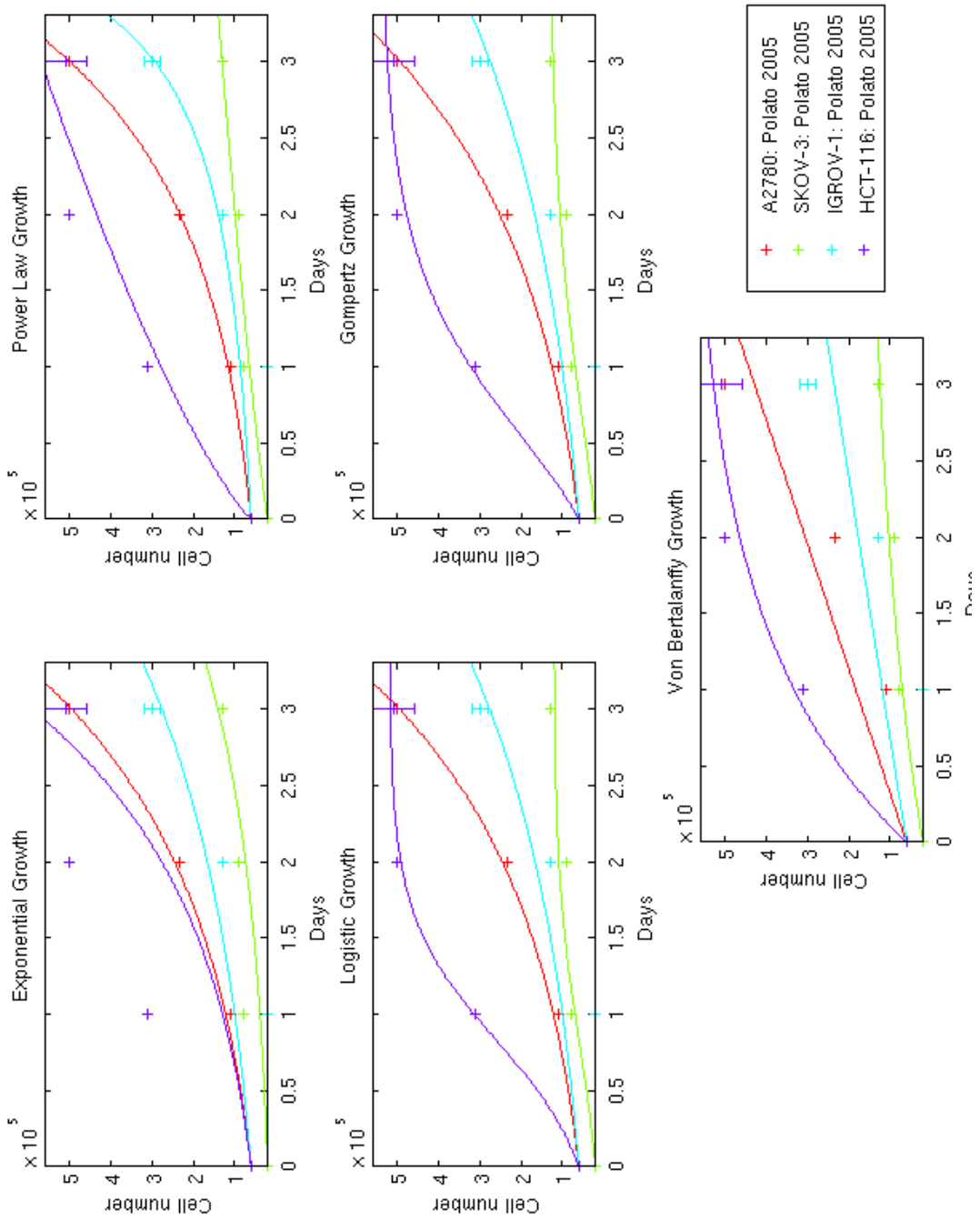

Figure A.28 Parameter Fittings to Individual *In Vitro* Ovarian Cancer Trials

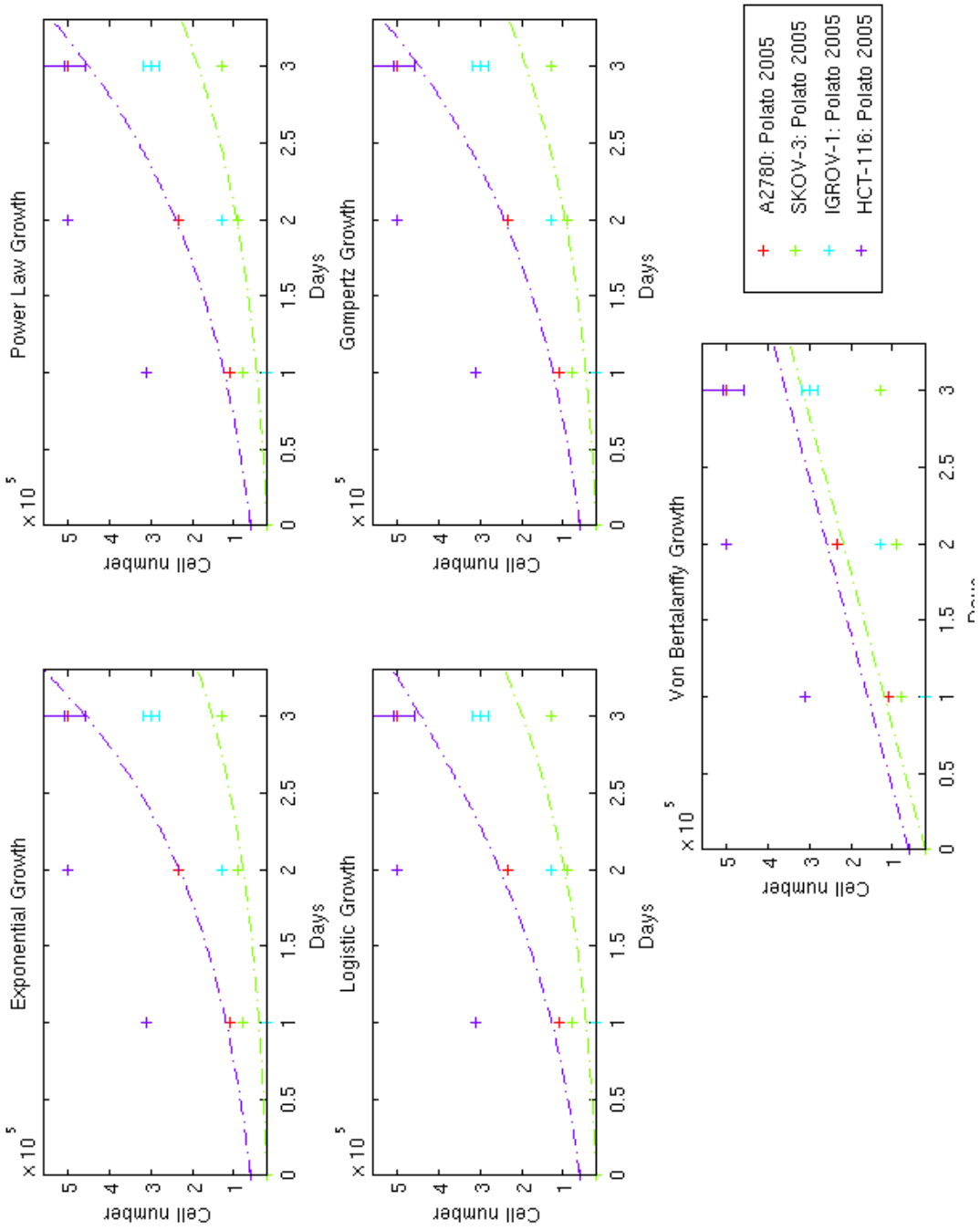

Figure A.29 Parameter Fitting to Combined *In Vitro* Ovarian Cancer Trials

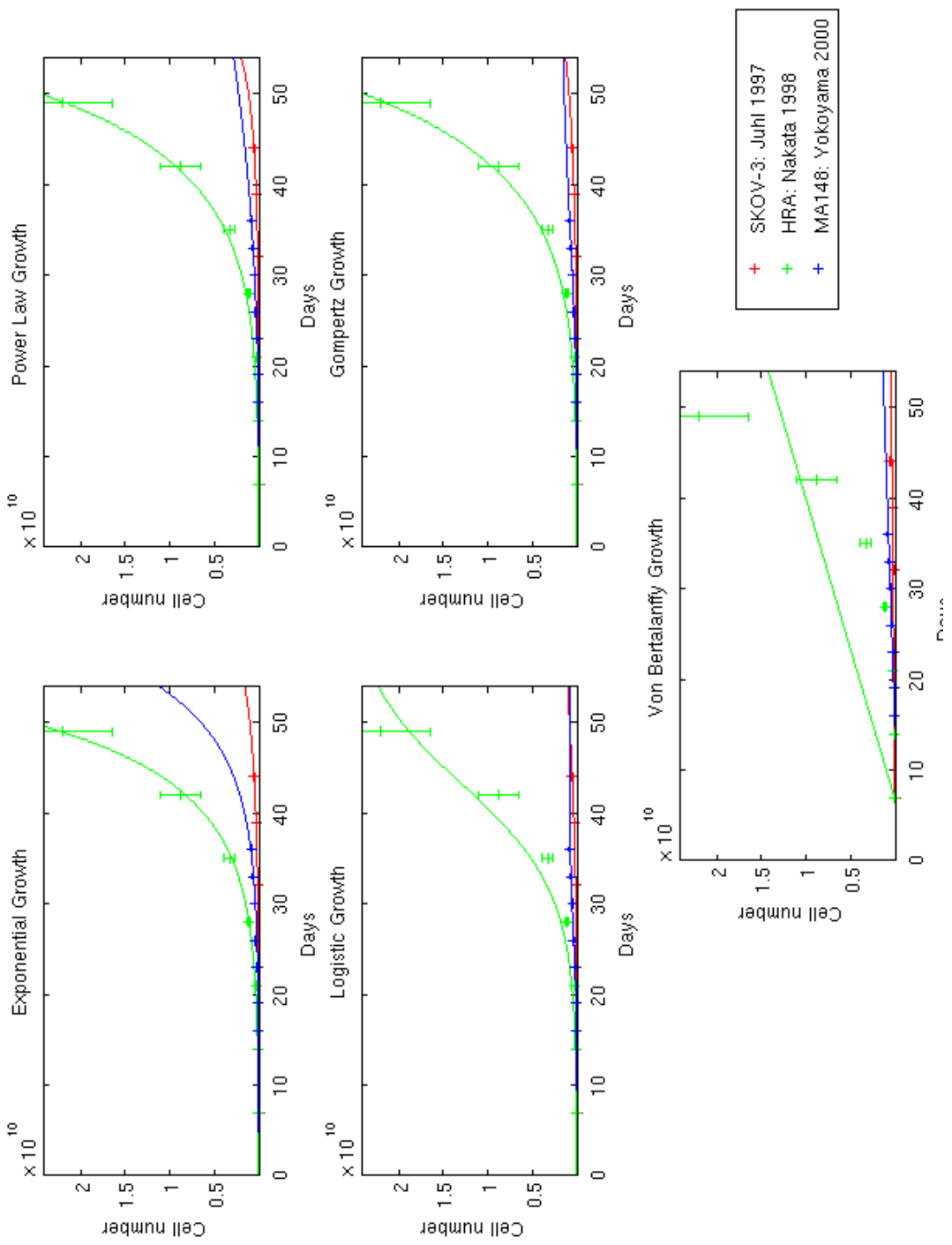

Figure A.30 Parameter Fittings to Individual *In Vivo* Ovarian Cancer Trials

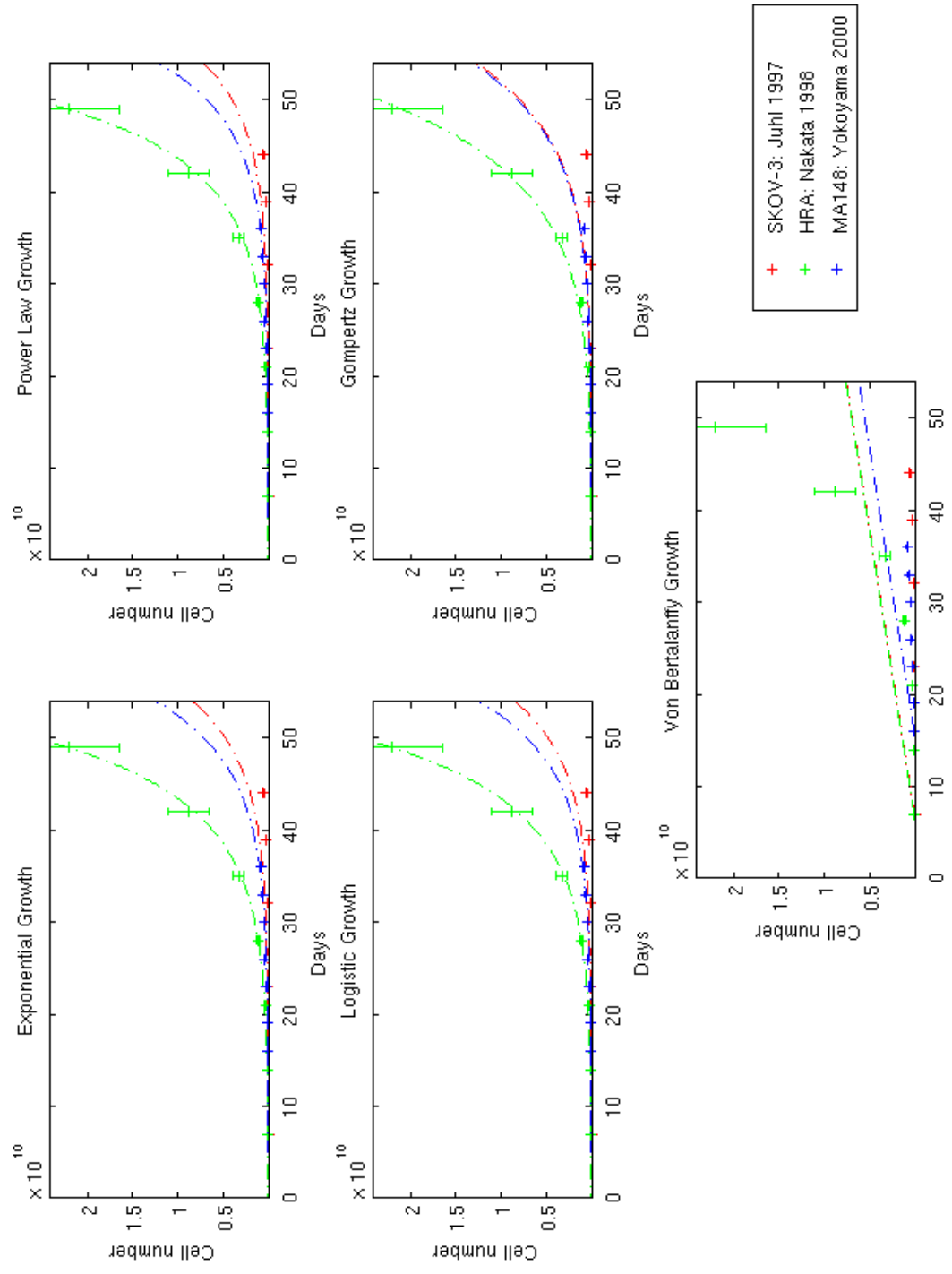

Figure A.31 Parameter Fitting to Combined *In Vivo* Ovarian Cancer Trials

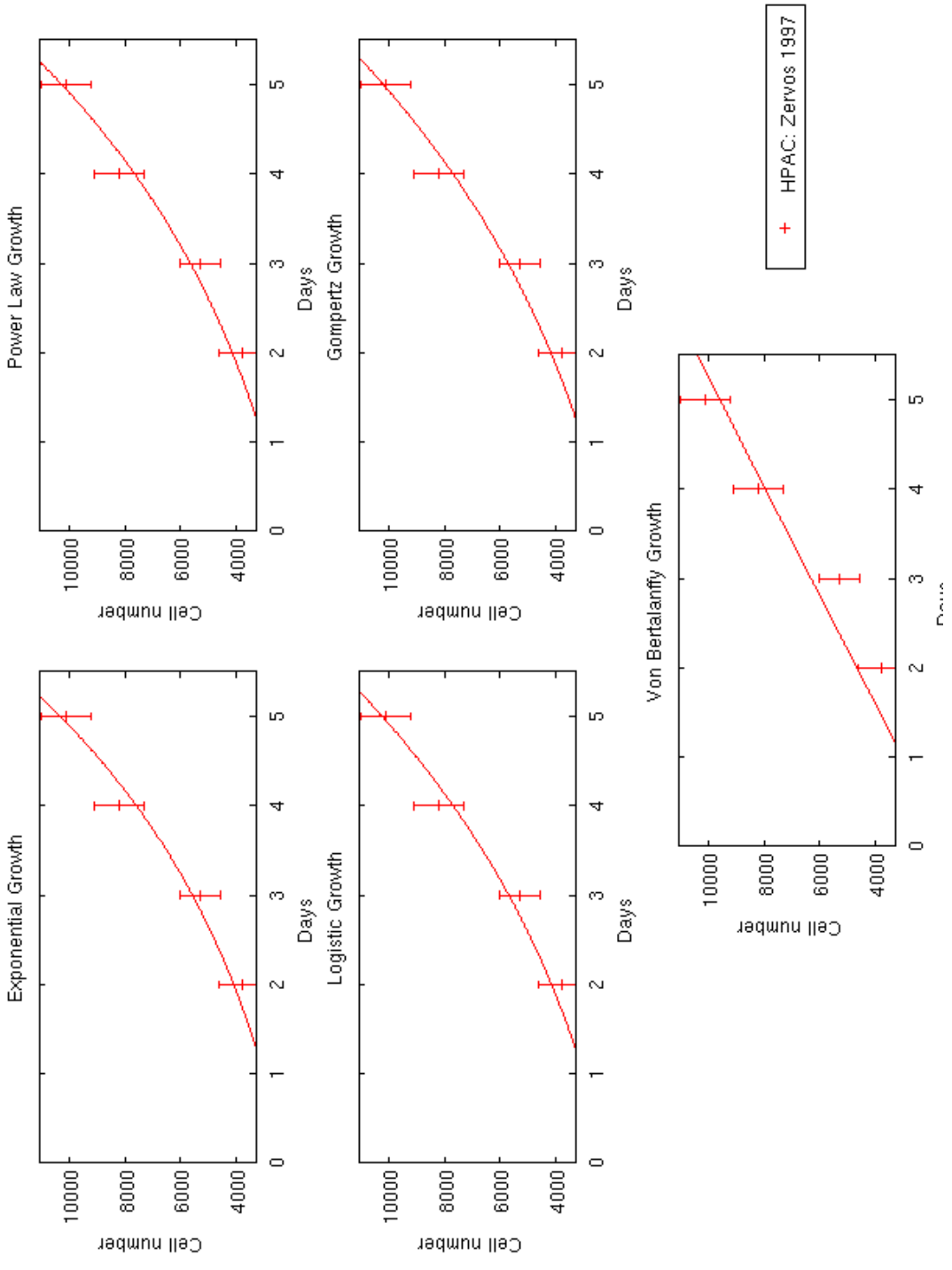

Figure A.32 Parameter Fittings to *In Vitro* Pancreatic Cancer Trials

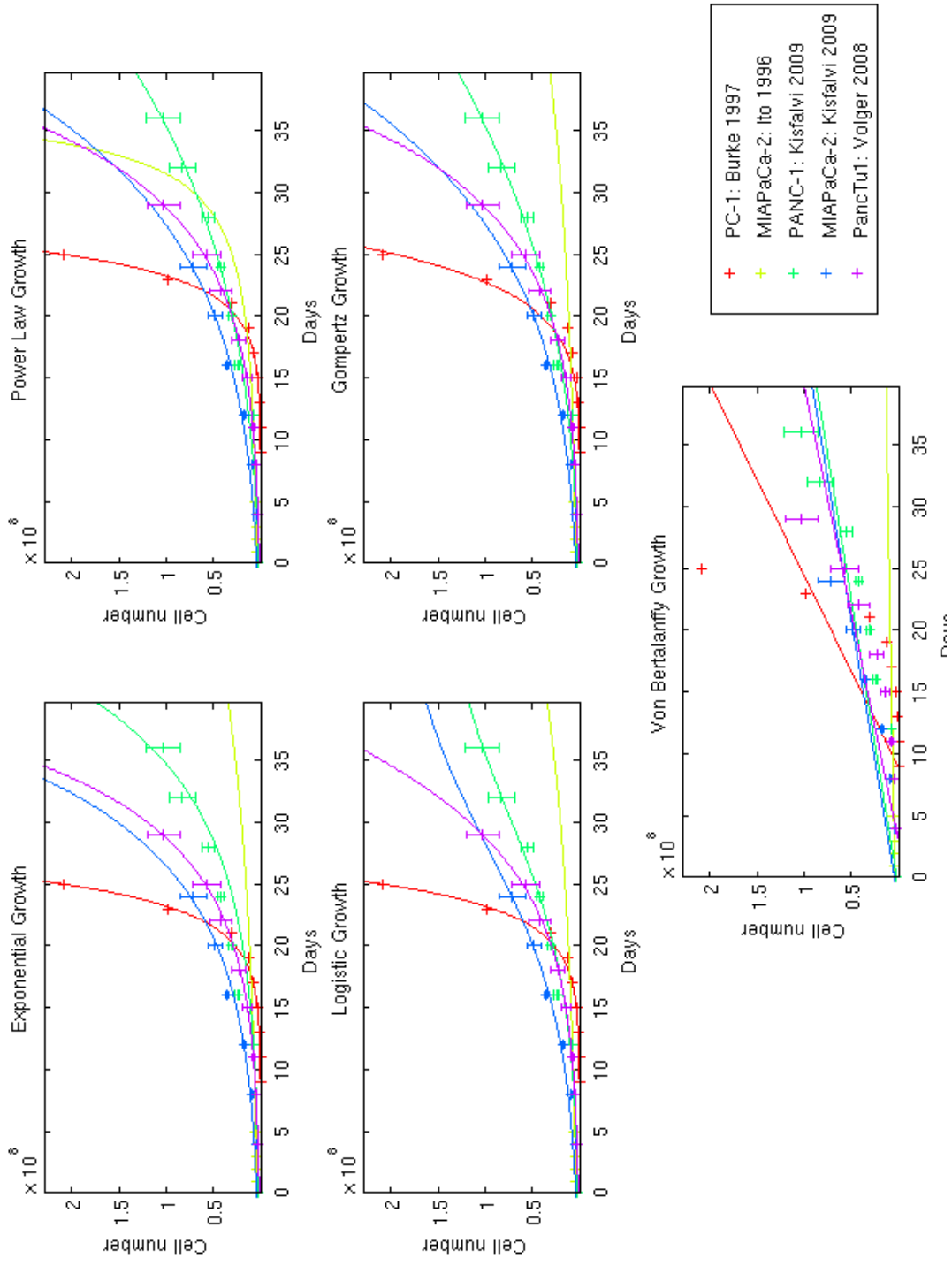

Figure A.33 Parameter Fittings to Individual *In Vivo* Pancreatic Cancer Trials

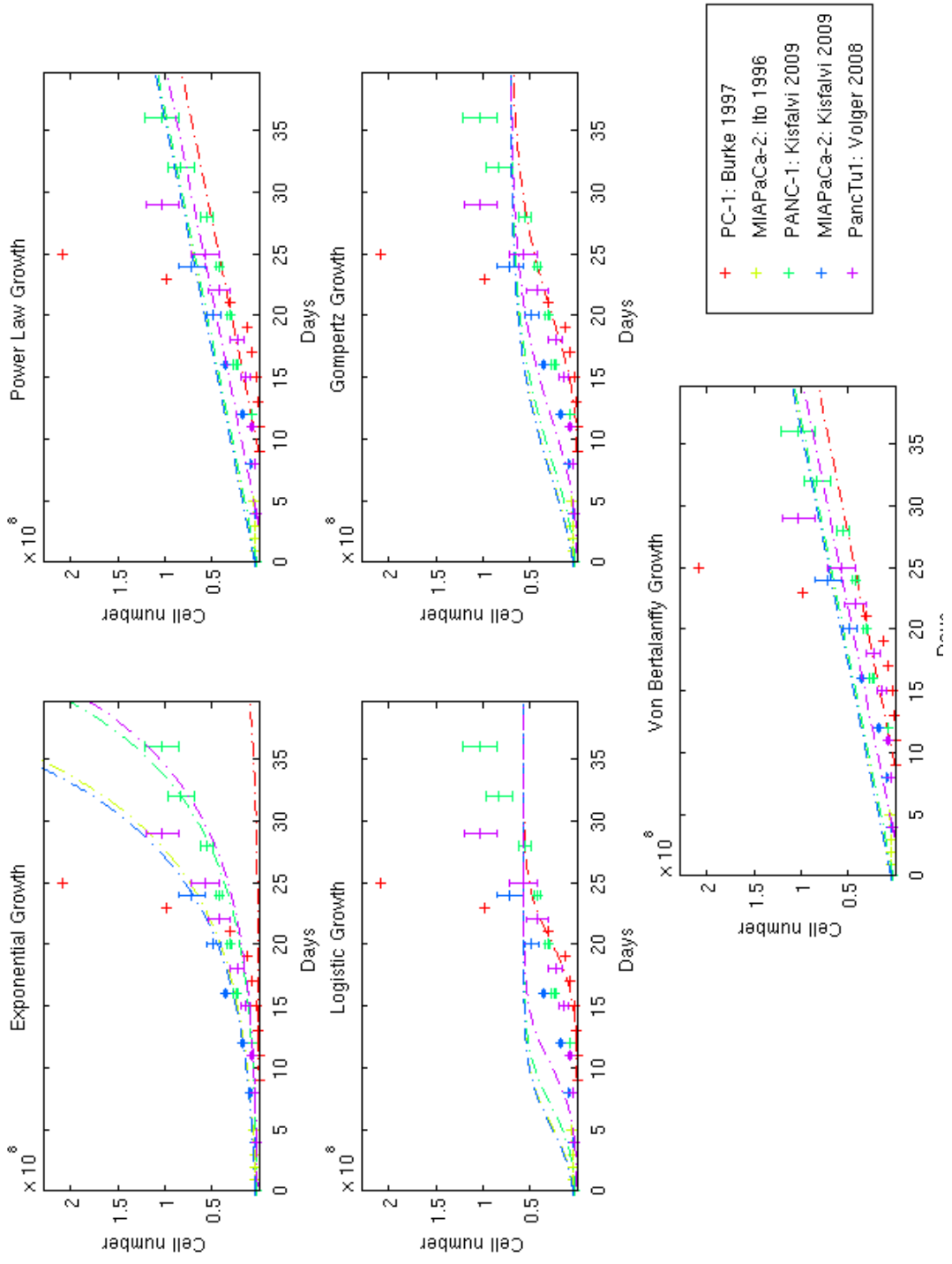

Figure A.34 Parameter Fitting to Combined *In Vivo* Pancreatic Cancer Trials

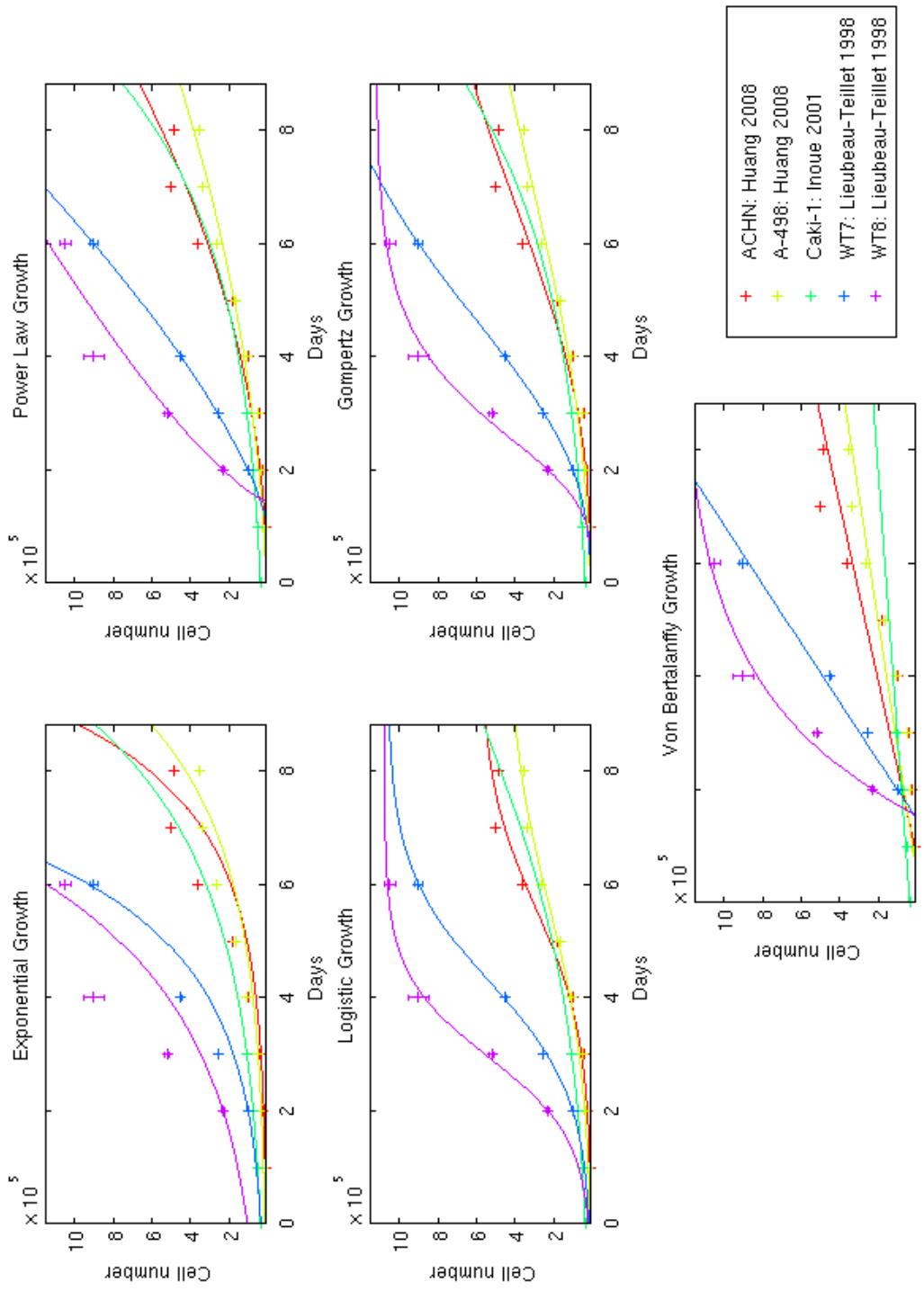

Figure A.35 Parameter Fittings to Individual *In Vitro* Renal Cell Carcinoma Trials

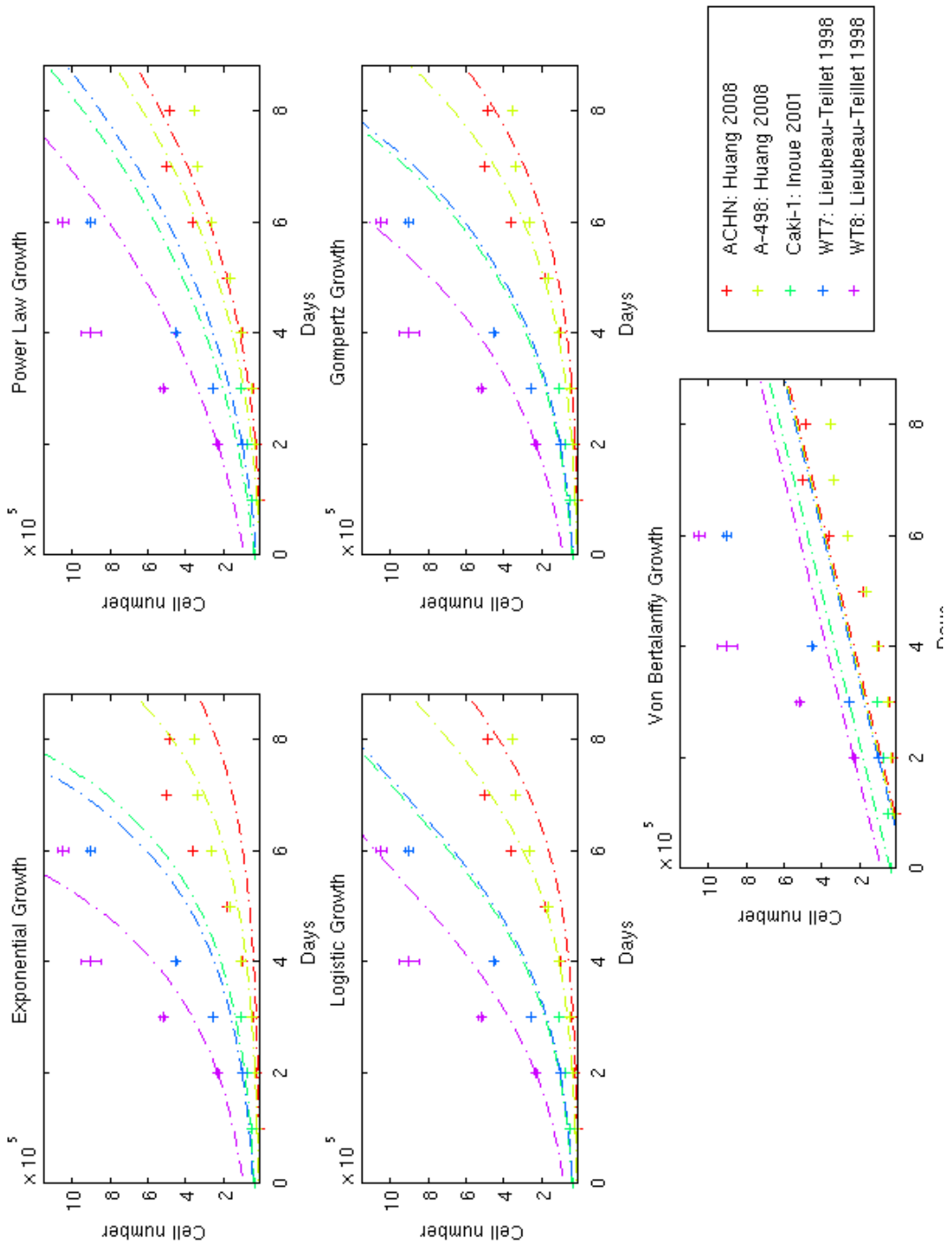

Figure A.36 Parameter Fitting to Combined *In Vitro* Renal Cell Carcinoma Trials

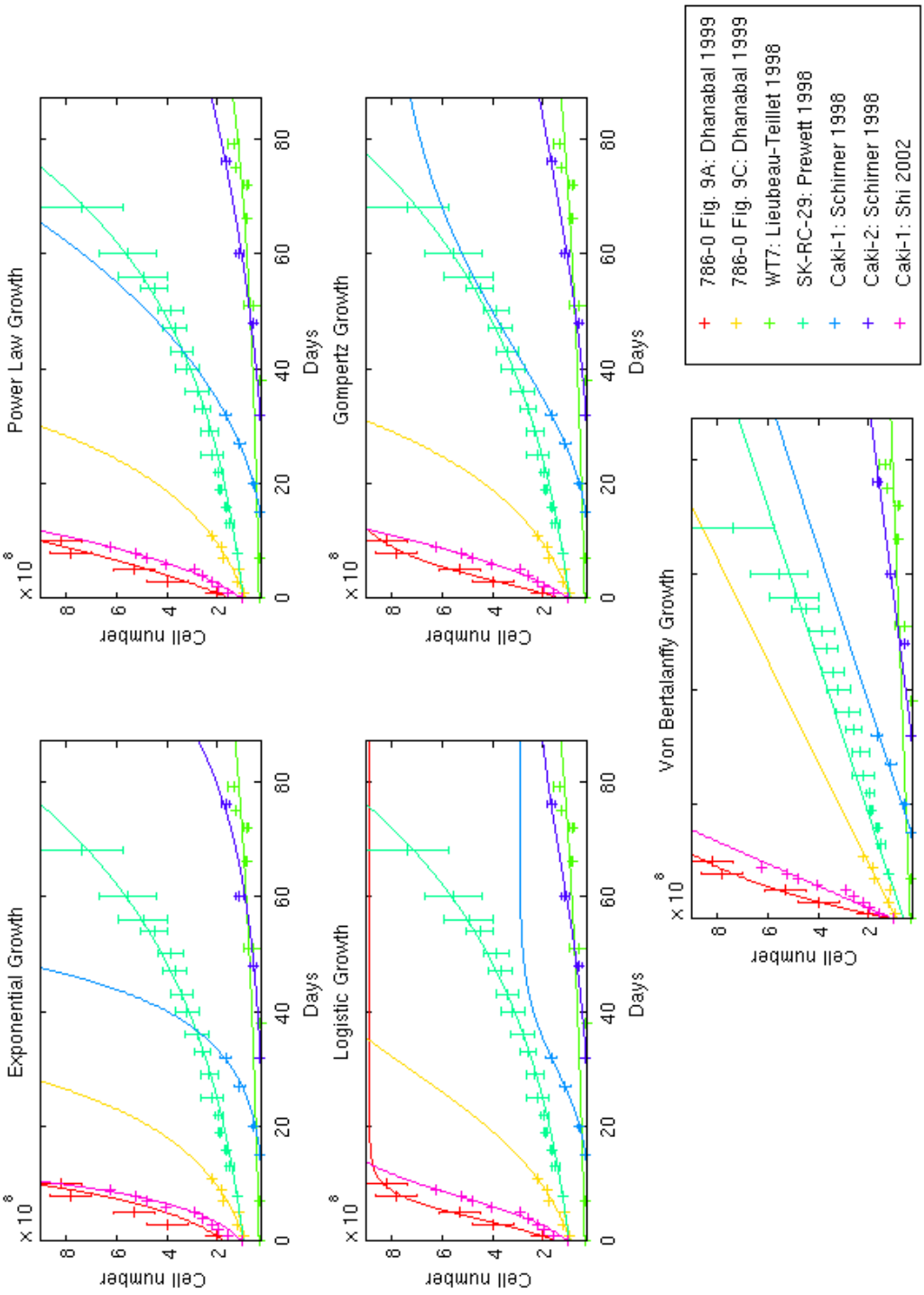

Figure A.37 Parameter Fittings to Individual *In Vivo* Renal Cell Carcinoma Trials

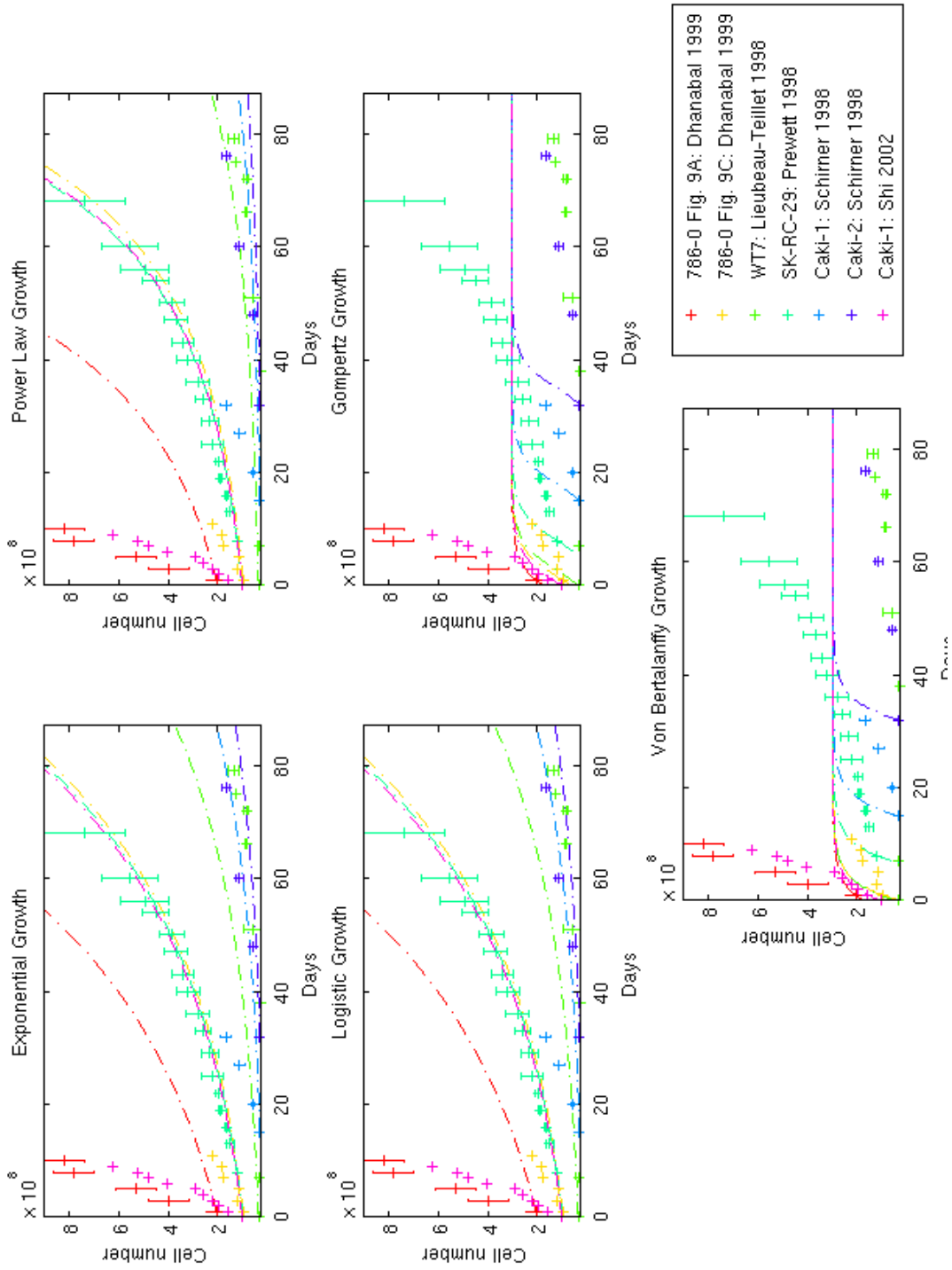

Figure A.38 Parameter Fitting to Combined *In Vivo* Renal Cell Carcinoma Trials

Bibliography

Abe, Riichiro, Tadamichi Shimizu, Hiroshi Sugawara, Hirokazu Watanabe, Hideki Nakamura, Hiroshi Choei, Nobuyuki Sasaki, Sho-ichi Yamagishi, Masayoshi Takeuchi, and Hiroshi Shimizu. 2004. Regulation of Human Melanoma Growth and Metastasis by AGE-AGE Receptor Interactions. *Journal of Investigative Dermatology* 122:461–467.

Ahonen, Merja H., Ya-Hua Zhuang, Risto Aine, Timo Ylikomi, and Pentti Tuohimaa. 2000. Androgen receptor and vitamin D receptor in human ovarian cancer: Growth stimulation and inhibition by ligands. *International Journal of Cancer* 86:40–46.

Aroesty, J., T. Lincoln, N. Shapiro, and G. Boccia. 1973. Tumor growth and chemotherapy: Mathematical methods, computer simulations, and experimental foundations. *Mathematical Biosciences* 17:243–300.

Ashyraliyev, Maksat, Yves Fomekong-Nanfack, Jaap A. Kaandorp, and Joke G. Joke G. Blom. 2009. Systems biology: parameter estimation for biochemical models. *FEBS Journal* 276:886–902.

B. Edris et al. 2012. Antibody therapy targeting the CD47 protein is effective in a model of aggressive metastatic leiomyosarcoma. *PNAS* 17:6656–6661.

Bastogne, T., A. Samson, P. Vallois, S. Wantz-MŐziŕres, S. Pinel, D. Bechet, and M. Barberi-Heyob. 2010. Phenomenological modeling of tumor diameter growth based on a mixed effects model. *Journal of Theoretical Biology* 262:544–552.

Belizério, José E. 2009. Immunodeficient Mouse Models: An Overview. *The Open Immunology Journal* 2.

Boukerche, H, O Berthier-Vergnes, M Bailly, JF Dore, LL Leung, and JL McGregor. 1989. A monoclonal antibody (LYP18) directed against the blood

platelet glycoprotein IIb/IIIa complex inhibits human melanoma growth in vivo. *Blood* 74:909–912.

Bregman, Marvin D., Carole Funk, and Masanori Fukushima. 1986. Inhibition of Human Melanoma Growth by Prostaglandin A, D, and J Analogues. *Cancer Research* 46:2740–2744.

Brooks, Steve, Andrew Gelman, Galin L. Jones, and Xiao-Li Meng. 2011. *Handbook of Markov Chain Monte Carlo*. Chapman & Hall/CRC, 1st ed.

Burke, Yvette D., M. Jennifer Stark, Steven L. Roach, Stephanie E. Sen, and Pamela L. Crowell. 1997. Inhibition of Pancreatic Cancer Growth by the Dietary Isoprenoids Farnesol and Geraniol. *Lipids* 32(2):151–156.

Byrne, H.M., T Alarcon, M.R. Owen, S.D. Webb, and P.K. Maini. 2006. Modelling aspects of cancer dynamics: a review. *Phil Trans R Soc* 10.

Byrne, H.M. and Cox, S.M. and Kelly, C.E. 2004. Macrophage-tumor interactions: *in vivo* dynamics. *Discrete and Continuous Dynamical Systems* 4(1):81–98.

Caltagirone, Sara, Cosmo Rossi, Andreina Poggi, Franco O. Ranelletti, Pier Giorgio Natali, Mauro Brunetti, Francesca B. Aiello, and Mauro Piantelli. 2000. Flavonoids apigenin and quercetin inhibit melanoma growth and metastatic potential. *International Journal of Cancer* 87:595–600.

Chen, Z. Z., S. Y. Zhang, Q. S. Liu, P. F. Xiao, X. Y. Guo, and Z. H. Lu. 2005. The CD47-signal regulatory protein alpha (SIRPα) interaction is a therapeutic target for human solid tumors. In *Proceedings of the 2005 IEEE*, 7497–7500. IEEE.

Coopman, Peter J. P., Michael T. H. Do, Mara Barth, Emma T. Bowden, Andrew J. Hayes, Eugenia Basyuk, Jan K. Blancatok, Phyllis R. Vezza, Sandra W. McLeskey, Paul H. Mangeat, and Susette C. Mueller. 2000. The Syk tyrosine kinase suppresses malignant growth of human breast cancer cells. *Nature* 406:742–747.

de Pillis, L.G., and A.E. Radunskaya. 2006. Some Promising Approaches to Tumor-Immune Modeling. *Contemporary Mathematics* 410:89–105.

de Pillis, Lisette, Trevor Caldwell, Elizabeth Sarapata, and Heather Williams. 2013a. Mathematical Modeling of Regulatory T Cell Effects on Renal Cell Carcinoma Treatment. *AIMS* 18(4):915–943.

de Pillis, Lisette, Renee Fister, , Weiqing Gu, Craig Collins, Michael Daub, David Gross, James Moore, and Benjamin Preskill. 2009. Mathematical Model Creation for Cancer Chemo-Immunotherapy. *Computational and Mathematical Methods in Medicine* 10(3):165–184.

de Pillis, Lisette, Angela Gallegos, and Ami Radunskaya. 2013b. A Model of Dendritic Cell Therapy for Melanoma. *Frontiers in Molecular and Cellular Oncology* 3.

de Pillis, Lisette, Ami Radunskaya, and Charles Wiseman. 2005. A Validated Mathematical Model of Cell-Mediated Immune Response to Tumor Growth. *Journal of Cancer Research* 65:7950–7958.

Dennis, John E. Jr, and Daniel J. Woods. 1987. *New Computing Environments: Microcomputers in Large-Scale Scientific Computing*, chap. Optimization on Microcomputers: The Nelder-Mead Simplex Algorithm. SIAM.

Dhanabal, Mohanraj, Ramani Ramchandran, and Ruediger Volk. 1999. Endostatin : Yeast Production, Mutants, and Antitumor Effect in Renal Cell Carcinoma. *Cancer Research* 59:189–197.

Du, Zhijun, and Shukun Hou. 2003. The Anti-Angiogenic Activity of Human Endostatin Inhibits Bladder Cancer Growth and Its Mechanism. *The Journal of Urology* 170:2000–2003.

Duffey, Dianne C., Zhong Chen, and Gang Dong. 1999. Expression of a Dominant-Negative Mutant Inhibitor-κBα of Nuclear Factor- κB in Human Head and Neck Squamous Cell Carcinoma Inhibits Survival, Proinflammatory Cytokine Expression, and Tumor Growth in Vivo. *Cancer Research* 59:3468–3474.

Elishmereni, Moran, Yuri Kheifetz, Henrik Söndergaard, Rune Viig Overgaard, and Zvia Agur. 2011. An Integrated Disease/Pharmacokinetic/Pharmacodynamic Model Suggests Improved Interleukin-21 Regimens Validated Prospectively for Mouse Solid Cancers. *PLoS Computational Biology* 7.

Esquela-Kerscher, Aurora, Phong Trang, Jason F. Wiggins, Lubna Patrawala, Angie Cheng, Lance Ford, Joanne B. Weidhaas, David Brown, Andreas G. Bader, and Frank J. Slack. 2008. The let-7 microRNA reduces tumor growth in mouse models of lung cancer. *Cell Cycle* 7:759–764.

Fabbri, Muller, Dimitrios Iliopoulos, Francesco Trapasso, Rami I. Aqeilan, Amelia Cimmino, Nicola Zanesi, Sai Yendamuri, Shuang-Yin Han, Dino Amadori, Kay Huebner, and Carlo M. Croce. 2005. WWOX gene restoration prevents lung cancer growth in vitro and in vivo. *PNAS* 102:15,611–15,616.

Fujimoto, Naohiro, Atsuo Sugita, Yoshio Terasawa, and Masakazu Kato. 1995. Observations on the Growth Rate of Renal Cell Carcinoma. *International Journal of Urology* 2:71–76.

Fujiwara, Toshiyoshi, Elizabeth A. Grimm, and Tapas Mukhopadhyay. 1993. A Retroviral Wild-type p53 Expression Vector Penetrates Human Lung Cancer Spheroids and Inhibits Growth by Inducing Apoptosis. *Cancer Research* 53:4129–4133.

Gilks, W. Walter R., Sylvia Richardson, and David J. Spiegelhalter. 1996. *Markov Chain Monte Carlo in Practice: Interdisciplinary Statistics*. Chapman & Hall/CRC, 1st ed.

Golshani, Roozbeh, Luis Lopez, and Veronica Estrella. 2008. Hyaluronic Acid Synthase-1 Expression Regulates Bladder Cancer Growth, Invasion, and Angiogenesis through CD44. *Cancer Research* 68:483–491.

Gomero, Boloye. 2012. Latin Hypercube Sampling and Partial Rank Correlation Coefficient Analysis Applied to an Optimal Control Problem. *Master's Thesis, University of Tennessee* .

Guiot, Caterina, Piero Giorgio Degiorgis, Pier Paolo Delsanto, Pietro Gabriele, and Thomas S. Deisboeck. 2003. Does tumor growth follow a "universal law"? *Journal of Theoretical Biology* 225:147–151.

Hart, D, E Shochat, and Z Agur. 1998. The growth law of primary breast cancer as inferred from mammography screening trials data. *British Journal of Cancer* 78:382–387.

Heuser, Louis, John S. Spratt, and Hiram C Jr. Polk. 1979. Growth Rates of Primary Breast Cancers. *Cancer* 43:1888–1894.

Huang, Dan, Yan Ding, and Wang-Mei Luo. 2008. Inhibition of MAPK Kinase Signaling Pathways Suppressed Renal Cell Carcinoma Growth and Angiogenesis In vivo. *Cancer Research* 68:81–88.

Huynh, Hung, Pierce K.H. Chow, Nallasivam Palanisamy, and Manuel Salto-Tellez. 2008. Bevacizumab and rapamycin induce growth suppression in mouse models of hepatocellular carcinoma. *Journal of Hepatology* 49:52–60.

Inoue, Ken-ichiro, Yutaka Kawahito, Yasunori Tsubouchi, Masataka Kohno, Rikio Yoshimura, Toshikazu Yoshikawa, and Hajime Sano. 2001. Expression of Peroxisome Proliferator-Activated Receptor γ in Renal Cell Carcinoma and Growth Inhibition by Its Agonists. *Biochemical and Biophysical Research Communications* 287:727–732.

Ito, Toshio, Sumio Kawata, Shinji Tamura, Takumi Igura, Toshihiko Nagase, Jun-ichiro Miyagawa, Eiji Yamazaki, Hiroshi Ishiguro, and Yuji Matsuzawa. 1996. Suppression of Human Pancreatic Cancer Growth in BALB/c Nude Mice by Manumycin, a Farnesyl:protein Transferase Inhibitor. *Cancer Science* 87(2):113–116.

Jackson, Trachette L., and Helen M. Byrne. 2000. A mathematical model to study the effects of drug resistance and vasculature on the response of solid tumors to chemotherapy. *Mathematical Biosciences* 164:17–38.

Jane E. Visvader. 2011. Cells of Origin in Cancer. *Nature* 469:314–322.

Juhl, Hartmut, Sean G. Downing, Anton Wellstein, and Frank Czubayko. 1997. HER-2/neu Is Rate-limiting for Ovarian Cancer Growth. *Journal of Biological Chemistry* 272(47):29,482–29,486.

Jung, Cho-Rok, Jinsang Yoo, Ye Jin Jang, Sangsoo Kim, In-Sun Chu, Young Il Yeom, Jong Young Choi, and Dong-Soo Im. 2006. Adenovirus-Mediated Transfer of siRNA Against PTTG1 Inhibits Liver Cancer Cell Growth In Vitro and In Vivo. *Journal of Hepatology* 43:1042–1052.

Kamada, Masayuki, Alan So, and Mototsugu Muramaki. 2007. Hsp27 knockdown using nucleotide-based therapies inhibit tumor growth and enhance chemotherapy in human bladder cancer cells. *Molecular Cancer Therapeutics* 6:299–308.

Kisfalvi, Krisztina, Guido Eibl, and James Sinnett-Smith. 2009. Metformin Disrupts Crosstalk between G ProteinâĹŠCoupled Receptor and Insulin Receptor Signaling Systems and Inhibits Pancreatic Cancer Growth. *Cancer Research* 69:6539–6545.

Koch, Ulrike, Mechthild Krause, and Michael Baumann. 2010. Cancer stem cells at the crossroads of current cancer therapy failuresï£¡ a Radiation oncology perspective. *Seminars in Cancer Biology* 20.

Kunstfeld, Rainer, Georg Wickenhauser, Uwe Michaelis, Michael Teifel, Wolfgang Umek, Kurt Naujoks, Klaus Wolsh, and Peter Petzelbauer. 2003. Paclitaxel Encapsulated in Cationic Liposomes Diminishes Tumor Angiogenesis and Melanoma Growth in a âĂŸâĂŸHumanizedâĂŹâĂŹ SCID Mouse Model. *Journal of Investigative Dermatology* 120:476–482.

Lagarias, Jeffrey C., James A. Reed, Margaret H. Wright, and Paul E. Wright. 1998. Convergence Properties of the Nelder-Mead Simplex Method in Low Dimensions. *SIAM Journal on Optimization* 9:112–147.

Lieubeau-Teillet, Blandine, Janusz Rak, and Serge Jothy. 1998. von Hippel-Lindau Gene-mediated Growth Suppression and Induction of Differentiation in Renal Cell Carcinoma Cells Grown as Multicellular Tumor Spheroids. *Cancer Research* 58:4957–4962.

Liu, Ta-Jen, Mary Wang, Randall L. Breau, Ying Henderson, Adel K. El-Naggar, Kimberly D. Steck, Michael W. Sicard, and Gary L. Clayman. 1999. Apoptosis induction by E2F-1 via adenoviral-mediated gene transfer results in growth suppression of head and neck squamous cell carcinoma cell lines. *Cancer Gene Therapy* 6:163–172.

Liu, Yuqing, Ronnie T. Poon, and Qinyu Li. 2005. Both Antiangiogenesis- and Angiogenesis-Independent Effects Are Responsible for Hepatocellular Carcinoma Growth Arrest by Tyrosine Kinase Inhibitor PTK787/ZK222584. *Cancer Research* 65:3691–3699.

López, S. et al. 2004. Statistical evaluation of mathematical models for microbial growth. *International Journal of Food Microbiology* 96:289–300.

LoTempio, Maria M., Mysore S. Veena, and Helen L. Steele. 2005. Curcumin Suppresses Growth of Head and Neck Squamous Cell Carcinoma. *Clinical Cancer Research* 11:6994–7002.

Lu, Runqing, and Ginette Serrero. 1999. Resveratrol, a Natural Product Derived From Grape, Exhibits Antiestrogenic Activity and Inhibits the Growth of Human Breast Cancer Cells. *Journal of Cellular Physiology* 179:297–304.

Martin, Sarah A., Nuala McCabe, Michelle Mullarkey, Robert Cummins, Darren J. Burgess, Yusaku Nakabeppu, Sugako Oka, Elaine Kay, Christopher J. Lord, and Alan Ashworth. 2010. DNA Polymerases as Potential Therapeutic Targets for Cancers Defcient in the DNA Mismatch Repair Proteins MSH2 or MLH1. *Cancer Cell* 17:235–248.

Miyake, Hideaki, Isao Hara, and Sadao Kamidono. 2001. Synergistic Chemsensitization and Inhibition of Tumor Growth and Metastasis by the Antisense Oligodeoxynucleotide Targeting Clusterin Gene in a Human Bladder Cancer Model. *Clinical Cancer Research* 7:4245–4252.

Moody, Terry W., Farah Zia, Muriel Draoui, Douglas E. Brenneman, Mati Fridkin, Ariane Davidson, and Illiana Gozes. 1993. A vasoactive intestinal peptide antagonist inhibits non-small cell lung cancer growth. *Biochemistry* 90:4345–4349.

Mummert, Anna. 2010. Parameter sensitivity analysis for mathematical modeling. Presented at the Math department research seminar at Marshall University.

Murgo, Anthony J. 1985. Inhibition of B16-BL6 Melanoma Growth in Mice by Methionine-Enkephalin. *Journal of the National Cancer Institute* 75:476–482.

Nagl, Sylvia, and Manish Patel. 2006. *Cancer Bioinformatics: From Therapy Design to Treatment*, chap. Mathematical Models of Cancer. John Wiley & Sons, Ltd, Chichester, UK.

Nakagawa, Hiroyuki, Koji Tsuta, Katsuji Kiuchi, Hideto Senzaki, Kanji Tanaka, Koshiro Hioki, and Airo Tsubura. 2001. Growth inhibitory effects of diallyl disuliňĄde on human breast cancer cell lines. *Carcinogenesis* 22:891–897.

Nakata, Hideyuki, Yoshihiro Kikuchi, Takehiko Tode, Junko Hirata, Tsunekazu Kita, Kenji Ishii, Kazuya Kudoh, Ichiro Nagata, and Nariyoshi Shinomiya. 1998. Inhibitory Effects of Ginsenoside Rh_2 on Tumor Growth in Nude Mice Bearing Human Ovarian Cancer Cells. *Japanese Journal of Cancer Research* 89:733–740.

Norton, Larry. 1988. A Gompertzian Model of Human Breast Cancer Growth. *Cancer Research* 48:7067–7071.

Ohnishi, Shunsuke, Sumiko Ohnami, Friedrich Laub, Kazunori Aoki, Koichi Suzuki, Yae Kanai, Kazunori Haga, Masahiro Asaka, Francesco Ramirez, and Teruhiko Yoshida. 2003. Downregulation and growth inhibitory eïňĂect of epithelial-type Krüppel-like transcription factor KLF4, but not KLF5, in bladder cancer. *Biochemical and Biophysical Research Communications* 308:251–256.

Okegawa, Takatsugu, Rey-Chen Pong, and Yingming Li. 2001. The Mechanism of the Growth-inhibitory Effect of Coxsackie and Adenovirus Receptor (CAR) on Human Bladder Cancer: A Functional Analysis of CAR Protein Structure. *Cancer Research* 61:6592–6600.

Paquin, Dana, Peter S. Kim, Peter P. Lee, and Doron Levy. 2010. Strategic Treatment Interruptions During Imatinib Treatment of Chronic Myelogenous Leukemia. *Bull Math Biol* 73:1082–1100.

Petitclerc, Eric, Staffan Strömblad, and Tami L. von Schalscha. 1999. Integrin $\alpha_V\beta_3$ Promotes M21 Melanoma Growth in Human Skin by Regulating Tumor Cell Survival. *Cancer Research* 59:2724–2730.

Polato, Federica, Annamaria Codegoni, and Robert Fruscio. 2005. PRL-3 Phosphatase Is Implicated in Ovarian Cancer Growth. *Clinical Cancer Research* 11:6835–6839.

Prewett, M, M Rothman, and H Waksal. 1998. Mouse-human chimeric anti-epidermal growth factor receptor antibody C225 inhibits the growth of human renal cell carcinoma xenografts in nude mice. *Clinical Cancer Research* 4:2957–2966.

Priestley, M.B. 1981. *Spectral Analysis and Time Series*. Academic Press.

Reinmuth, Niels, Fan Fan, Wenbiao Liu, Alexander A. Parikh, Oliver Stoeltzing, Young D. Jung, Corazon D. Bucana, Robert Radinsky, Gary E. Gallick, and Lee M. Ellis. 2002. Impact of Insulin-Like Growth Factor Receptor-I Function on Angiogenesis, Growth, and Metastasis of Colon Cancer. *Laboratory Investigation* 82:1377–1389.

Richmond, Ann, David H. Lawson, and Daniel W. Nixon. 1983. Extraction of a Melanoma Growth-stimulatory Activity from Culture Medium Conditioned by the Hs0294 Human Melanoma Cell Line. *Cancer Research* 43:2106–2112.

Ricker, Justin L., Zhong Chen, and Xin Ping Yang. 2004. 2-Methoxyestradiol Inhibits Hypoxia-Inducible Factor 1α, Tumor Growth, and Angiogenesis and Augments Paclitaxel Efficacy in Head and Neck Squamous Cell Carcinoma. *Clinical Cancer Research* 10:8665–8673.

Robertson-Tessi, Mark, Ardith El-Kareh, and Alain Goriely. 2012. A mathematical model of tumor-autoimmune interactions. *Journal of Theoretical Biology* 294:56–73.

Roose, Tiina, S. Jonathan Chapman, and Philip K. Maini. 2007. Mathematical Models of Avascular Tumor Growth. *Journal of Theoretical Biology* 49:179–208.

Sanga, Sandeep, John P Sinek, Hermann B Frieboes, Mauro Ferrari, John P Fruehauf, and Vittorio Cristini. 2006. Mathematical modeling of cancer progression and response to chemotherapy. *Expert Rev Anticancer Ther* 6:1361–1376.

Sarraf, Pasha, Elisabetta Mueller, Daniel Jones, Frederick J. King, Daniel J. DeAngelo, Jeffrey B. Partridge, Sylvia A. Holden, Lan Bo Chen, Samuel Singer, Christopher Fletcher, and Bruce M. Spiegelman. 1998. Differentiation and reversal of malignant changes in colon cancer through PPAR$_\gamma$. *Nature Medicine* 4:1046–1052.

Schirner, M, J Hoffmann, and A Menrad. 1998. Antiangiogenic chemotherapeutic agents: characterization in comparison to their tumor growth inhibition in human renal cell carcinoma models. *Clinical Cancer Research* 4:1331–1336.

Sharma, Sherven, Marina Stolina, Ying Lin, Brian Gardner, Patrice W. Miller, Mitchell Kronenberg, and Steven M. Dubinett. 1999. T Cell-Derived IL-10 Promotes Lung Cancer Growth by Suppressing Both T Cell and APC Function. *Journal of Immunology* 163:5020–5028.

Sheng, Hongmiao, Jinyi Shao, Susan C. Kirkland, Peter Isakson, Robert J. Coffey, Jason Morrow, R. Daniel Beauchamp, and Raymond N. DuBois. 1997. Inhibition of Human Colon Cancer Cell Growth by Selective Inhibition of Cyclooxygenase-2. *The Journal of Clinical Investigation* 99:2254–2259.

Shi, W, and DW Siemann. 2002. Inhibition of renal cell carcinoma angiogenesis and growth by antisense oligonucleotides targeting vascular endothelial growth factor. *British Journal of Cancer* 87:119–126.

Slezak, Diego FernĞndez, Cecilia SuĞrez, Guillermo A. Cecchi, Guillermo Marshall, and Gustavo Stolovitzky. 2010. When the Optimal Is Not the Best: Parameter Estimation in Complex Biological Models. *PLoS* 5.

Smith, Matthew C. P., Kathryn E. Luker, and Joel R. Garbow. 2004. CXCR4 Regulates Growth of Both Primary and Metastatic Breast Cancer. *Cancer Research* 64:8604–8612.

Sunwoo, John B., Zhong Chen, and Gang Dong. 2001. Novel Proteasome Inhibitor PS-341 Inhibits Activation of Nuclear Factor- κB, Cell Survival, Tumor Growth, and Angiogenesis in Squamous Cell Carcinoma. *Clinical Cancer Research* 7:1419–1428.

Takahashi, Takashi, David Carbone, and Toshitada Takahashi. 1992. Wild-type but not Mutant p53 Suppresses the Growth of Human Lung Cancer Cells Bearing Multiple Genetic Lesions. *Cancer Research* 52:2340–2343.

Tan, Daniel S.-W., Marco Gerlinger, Bin-Tean Teh, and Charles Swanton. 2010. Anti-cancer drug resistance: Understanding the mechanisms through the use of integrative genomics and functional RNA interference. *European Journal of Cancer* 46:2166–2177.

Todaro, Matilde, Mileidys Perez Alea, Anna B. Di Stefano, Patrizia Cammareri, Louis Vermeulen, Flora Iovino, Claudio Tripodo, Antonio Russo, Gaspare Gulotta, Jan Paul Medema, and Giorgio Stassi. 2007. Colon Cancer Stem Cells Dictate Tumor Growth and Resist Cell Death by Production of Interleukin-4. *Cell Stem Cell* 1:389–402.

Tsubouchi, Yasunori, Hajime Sano, Yutaka Kawahito, Shigehiko Mukai, Ryoji Yamada, Masataka Kohno, Ken-ichiro Inoue, Timothy Hla, and Motoharu Kondo. 2000. Inhibition of Human Lung Cancer Cell Growth by the Peroxisome Proliferator-Activated Receptor-γ Agonists through Induction of Apoptosis. *Biochemical and Biophysical Research Communications* 270:400–405.

Vogler, Meike, Henning Walczak, and Dominic Stadel. 2009. Targeting XIAP Bypasses Bcl-2 Mediated Resistance to TRAIL and Cooperates with TRAIL to Suppress Pancreatic Cancer Growth In vitro and In vivo. *Cancer Research* 68(19):7956–7965.

Warren, Robert S., Hui Yuan, Mary R. Matli, Nancy A. Gillett, and Napoleone Ferrara. 1995. Regulation by Vascular Endothelial Growth Fac-

tor of Human Colon Cancer Tumorigenesis in a Mouse Model of Experimental Liver Metastasis. *Journal of Clinical Investigation* 95:1789–1797.

Willingham, Stephen B. et al. 2012. The CD47-signal regulatory protein alpha (SIRPα) interaction is a therapeutic target for human solid tumors. *PNAS* 10.

Winkler, Gerhard. 2003. *Image Analysis, Random Fields and Markov Chain Monte Carlo Methods*. Springer-Verlag Berlin Heidelberg New York, 2nd ed.

Wong, Chun-Ming, Judy Wai-Ping Yam, and Yick-Pang Ching. 2005. Rho GTPase-Activating Protein Deleted in Liver Cancer Suppresses Cell Proliferation and Invasion in Hepatocellular Carcinoma. *Cancer Research* 65:8861–8868.

Yokoyama, Yumi, Mohanraj Dhanabal, and Arjan W. Griffioen. 2000. Synergy between Angiostatin and Endostatin: Inhibition of Ovarian Cancer Growth. *Cancer Research* 60:2190–2196.

Zender, Lars, Mona S. Spector, Wen Xue, Peer Flemming, Carlos Cordon-Cardo, John Silke, Sheung-Tat Fan, John M. Luk, Michael Wigler, Gregory J. Hannon, David Mu, Robert Lucito, Scott Powers, and Scott W. Lowe. 2006. IdentiiňĄcation and Validation of Oncogenes in Liver Cancer Using an Integrative Oncogenomic Approach. *Cell* 125:1253–1267.

Zender, Lars, Wen Xue, Johannes Zuber, Camile P. Semighini, Alexander Krasnitz, Beicong Ma, Peggy Zender, Stefan Kubicka, John M. Luk, Peter Schirmacher, W. Richard McCombie, Michael Wigler, James Hicks, Gregory J. Hannon, Scott Powers, and Scott W. Lowe. 2008. An Oncogenomics-Based In Vivo RNAi Screen Identifes Tumor Suppressors in Liver Cancer. *Cell* 135:852–864.

Zervos, Emmanuel E., James G. Norman, William R. Gower, Michael G. Franz, and Alexander S. Rosemurgy. 1997. Matrix Metalloproteinase Inhibition Attenuates Human Pancreatic Cancer Growth in Vitro and Decreases Mortality and Tumorigenesis in Vivo. *Journal of Surgical Research* 69(2):367–371.

Zhang, Ling, Xiaoyang Ren, Eckhard Alt, Xiaowen Bai, Shaoyi Huang, Zhengming Xu, Patrick M. Lynch, Mary P. Moyer, Xian-Feng Wen, and Xiangwei Wu. 2010. Chemoprevention of colorectal cancer by targeting APC-deficient cells for apoptosis. *Nature* 464:1058–1063.